JAERI-M
84-042

ASSESSMENT OF TRAC-PF1 PREDICTIVE CAPABILITY FOR THE THERMAL HYDRAULIC BEHAVIOR ALONG A PRIMARY LOOP DURING THE REFLOOD PHASE OF A PWR LOCA

March 1984

Hajime AKIMOTO

日本原子力研究所
Japan Atomic Energy Research Institute

JAERI-Mレポートは，日本原子力研究所が不定期に公刊している研究報告書です。
入手の問合わせは，日本原子力研究所技術情報部情報資料課（〒319-11茨城県那珂郡東海村）あて，お申しこしください。なお，このほかに財団法人原子力弘済会資料センター（〒319-11 茨城県那珂郡東海村日本原子力研究所内）で複写による実費頒布をおこなっております。

JAERI-M reports are issued irregularly.
Inquiries about availability of the reports should be addressed to Information Section, Division of Technical Information, Japan Atomic Energy Research Institute, Tokai-mura, Naka-gun, Ibaraki-ken 319-11, Japan.

編集兼発行　日本原子力研究所
印　　刷　㈱高野高速印刷

JAERI-M 84-042

Assessment of TRAC-PF1 predictive capability for the thermal hydraulic behavior along a primary loop during the reflood phase of a PWR LOCA

Hajime AKIMOTO
Department of Nuclear Safety Research
Tokai Research Establishment, JAERI
(Received January 31, 1984)

In order to identify the reason for the problems in the previous TRAC calculations for the estimation of the loop flow resistance coefficient and the heat transfer at the steam generator, and to assess the capability of the TRAC code for the prediction of the thermal hydraulic behavior along a primary loop during the reflood phase of a PWR LOCA, a parametric study was performed with TRAC-PF1 code using the data from the CCTF test C1-19(Run 38) as the initial and boundary conditions. Through the comparison between CCTF and TRAC results, it was found that the overestimation of the loop flow resistance coefficient and the underestimation of the total energy transfer were caused by the error in the input data of the additive friction factor at the pump simulator and the overestimation of the flow quality through the steam generator, respectively. A review on the following items is recommened for the future improvements of the TRAC-PF1 code: (a) Water accumulation model at the inlet plenum of the steam generator. (b) Heat transfer model at the steam generator, especially for the evaporation rate of incoming water. (c) Critical flow model in the condensing two-phase flow, especially when flowing steam is condensed completely due to the direct contact with the subcooled ECC water.

Keywords: Reactor Safety, Loss-of-coolant, PWR, Reflood, CCTF, TRAC Code, Two-phase Flow, Heat Transfer, Predictive Capability, Comparative Evaluation

---

The work was performed under contract with the Atomic Energy Bureau of Science and Technology of Japan.

JAERI－M 84－042

加圧水型原子炉冷却材喪失事故再冠水期におけるループ部熱水力挙動に対するＴＲＡＣ－ＰＦ１コードの予測性能の評価

日本原子力研究所東海研究所安全工学部
秋本　肇

（１９８４年１月３１日受理）

従来のＴＲＡＣ計算におけるループ流動抵抗評価と蒸気発生器での伝熱量評価に関する問題点の原因を究明するとともに，加圧水型原子炉冷却材喪失事故再冠水時の一次系ループにおける熱水力挙動に対するＴＲＡＣコードの予測性能を評価することを目的として，円筒炉心試験Ｃ１－１９（Run38）の試験結果の一部を境界条件としたＴＲＡＣ－ＰＦ１コードによるパラメータ計算を行った。試験結果と計算結果との比較検討により，従来のＴＲＡＣ計算ではループ流動抵抗の過大評価と伝熱量の過小評価は，それぞれ，ポンプ模擬部での付加摩擦損失係数に対する入力データの誤差により，蒸気発生器を通過する二相流のクォリティの過大評価により，それぞれ生じたことが確かめられた。またＴＲＡＣ－ＰＦ１コードの予測性能を向上するためには今後以下の諸点についてさらに検討する必要のあることがわかった。(a)蒸気発生器入口プレナム部での蓄水モデル　(b)蒸気発生器における熱伝達モデル，特に流入水の蒸発モデル　(c)凝縮二相流中の二相臨界流モデル，特にサブクール状態の非常用炉心冷却水との直接接触により蒸気流が完全に凝縮される場合。

本報告書は，電源開発促進対策特別会計法に基づき，科学技術庁からの受託によって行われた研究の成果である。

Contents

目　　次

List of tables

List of figures

1. Introduction

The core heat transfer during the reflood phase of a loss-of-coolant-accident(LOCA) in a pressurized water reactor(PWR) is strongly dependent on the core inlet mass flow rate, the core pressure and the initial clad surface temperature. The capability of the system to exhaust the steam to the break will affect the core inlet mass flow rate and the core pressure, because the steam flow through the primary loops establishes the back pressure for the coolant flow entering the core. The effect of the back pressure formation is known as steam binding effect. The effect is one of the most important problems in order to confirm the effectiveness of the Emergency Core Cooling System(ECCS) during the reflood phase of a PWR LOCA.

The Cylindrical Core Test Facility(CCTF) was designed to provide information on the thermal hydraulic behavior during refill and reflood phases of a PWR LOCA.[1],[2] The CCTF has full-height core section with about 2000 electrically heated rods arranged in cylindrical configuration and has four primary loops with reactor component simulators. Each loop of the CCTF has a hot leg section, an active steam generator, a loop seal section, a pump simulator, a cold leg section and an Emegency Core Cooling(ECC) water injection port. The vertical dimensions and the flow path length of the components are kept as close to as the reference PWR as possible. The flow area of each component is scaled down in proportion to the scaling factor of the core flow area, that is, 1/21.4. The system integral effects and the core cooling characteristics are being investigated with CCTF to demenstrate the effectiveness of ECCS, to verify computer codes, and to collect information for the improvement of the thermal hydraulic models in analysis codes.

In order to provide advanced best-estimate predictions of a PWR LOCA, the PWR version of the Transient Reactor Analysis Code(TRAC) is being developed at Los Alamos National Laboratory.[3],[4] TRAC is being used to analyze the CCTF test results because of its versatility.[5],[6] The author analyzed one of the posttest calculations with TRAC for CCTF tests.[7] Through the comparison between the CCTF data and TRAC predictions, it was pointed out that TRAC overestimated the flow resistance coefficient through an intact loop by 65 % and underestimated the heat transfer from the secondary side to the primary side of the steam generator. Because the evaluation of the flow resistance through the

primary loop and the heat transfer at steam generator is essential for the accurate prediction of the steam binding effect, it is required to identify why TRAC produced these errors in the calculations for the CCTF tests.

However, the reason for these errors were uncertain in the previous TRAC calculations because of the complexity of the TRAC modeling. The calculations were performed not only with the loop model but also with the pressure vessel model to simulate the integral system of the CCTF. It is considered that some error may be produced by the deficiency of the flow model of the pressure vessel component. It is almost impossible to distinguish the error of the loop model from the error of the pressure vessel component. Additionally, detail comparison between CCTF and TRAC results of the flow behavior along the loop was difficult because the consistency between the CCTF measurements and the TRAC noding was poor in the previous calculations.

The objectives of this study are (1) to identify the reasons for the problems in the previous TRAC calculations for the estimation of the loop flow resistance coefficient and the heat transfer at the steam generator, and (2) to assess the capability of the TRAC code for the prediction of the thermal hydraulic behavior along a primary loop during the reflood phase of a PWR LOCA.

The loop model in the previous TRAC calculations was isolated to eliminate the error from the pressure vessel component and revised to get better consistency between CCTF measurements and TRAC noding. The revised input was checked using the data from the CCTF test C1-19(Run 38). Finally, the thermal-hydraulic behavior along the loop was analyzed with the checked model to assess the integral capability of the TRAC code.

2. TRAC input

Figure 1 shows the TRAC input schematic used for this study. An intact loop of CCTF is modeled by PIPE, STGEN, and TEE components of TRAC-PF1. The boundary ocnditions are specified with a FILL component for mass flow from the upper plenum, another FILL component for ECC injection, and a BREAK component for the pressure boundary condition at the exit of cold leg (that is, at the top of downcomer). Two FILL components are used to close the secondary side of the steam generator with zero velocity. The listing of TRAC input file for this study is shown in Appendix B.

primary loop and the heat transfer at steam generator is essential for the accurate prediction of the steam binding effect, it is required to identify why TRAC produced these errors in the calculations for the CCTF tests.

However, the reason for these errors were uncertain in the previous TRAC calculations because of the complexity of the TRAC modeling. The calculations were performed not only with the loop model but also with the pressure vessel model to simulate the integral system of the CCTF. It is considered that some error may be produced by the deficiency of the flow model of the pressure vessel component. It is almost impossible to distinguish the error of the loop model from the error of the pressure vessel component. Additionally, detail comparison between CCTF and TRAC results of the flow behavior along the loop was difficult because the consistency between the CCTF measurements and the TRAC noding was poor in the previous calculations.

The objectives of this study are (1) to identify the reasons for the problems in the previous TRAC calculations for the estimation of the loop flow resistance coefficient and the heat transfer at the steam generator, and (2) to assess the capability of the TRAC code for the prediction of the thermal hydraulic behavior along a primary loop during the reflood phase of a PWR LOCA.

The loop model in the previous TRAC calculations was isolated to eliminate the error from the pressure vessel component and revised to get better consistency between CCTF measurements and TRAC noding. The revised input was checked using the data from the CCTF test C1-19(Run 38). Finally, the thermal-hydraulic behavior along the loop was analyzed with the checked model to assess the integral capability of the TRAC code.

2. TRAC input

Figure 1 shows the TRAC input schematic used for this study. An intact loop of CCTF is modeled by PIPE, STGEN, and TEE components of TRAC-PF1. The boundary ocnditions are specified with a FILL component for mass flow from the upper plenum, another FILL component for ECC injection, and a BREAK component for the pressure boundary condition at the exit of cold leg (that is, at the top of downcomer). Two FILL components are used to close the secondary side of the steam generator with zero velocity. The listing of TRAC input file for this study is shown in Appendix B.

2.1 Geometry of CCTF intact loop

Figure 2(a) shows the detail of the PIPE component for this study. Figure 2(b) shows the modeling for the previous studies. The revised hot-leg model has more fluid cells than the previous one to be consistent with the experimental measuring locations. In the revised model the first through seventh cells model the hot-leg piping. The eighth through tenth cells model a part of the inlet plenum of the steam generator. The flow area is constant along the hot leg piping and it expands at the inlet plenum of the steam generator.

Figure 3 shows the details of the STGEN component model for this study and for the previous studies. In revising the previous model, the noding was determined to establish better agreement with the measurement locations of the secondary-side fluid temperature. The first and last cells correspond to the reviewing part of the inlet and outlet plenums of the steam generator. Their cell lengths were determined based on the locations of the pressure taps.

Figure 4 shows the detail of the TEE component model for the remainder of the loop. The locations of the pressure taps of the CCTF correspond to the centers of the seventh, nineth, twelveth, fifteenth and twenty-second cells in the revised model, respectively. The pump orifice in the pump simulator corresponds to the cell bounrady between the tenth and eleventh cells in the revised model. The flow area change at the pump simulator of CCTF is simulated in the revised model with five nodes at this section, that is, the nineth through the fifteenth cells.

2.2 Initial and boundary conditions

The boundary conditions for the TRAC calculation were determined based on the measured data from CCTF test C1-19 (Run 38).[8] Figures 5 through 7 show the ECC water flow rate, the ECC water temperature, and the pressure at the top of the downcomer, respectively. The measured data were input as tables to the FILL and BREAK components. The assumed transients in this study are also shown in these figures. The initial water and steam temperatures are assumed at saturation temperature, except for the water temperature of the secondary side of the steam-generator. The measured fluid temperatures were used as the initial temperatures of steam and water at the secondary side of the steam generator.

The total mass flow rate from the upper plenum was determined from the pitot tube data measured at the steam-generator exit. The

water mass flow rate from the upper plenum was determined by an energy balance calculation for the secondary side of the steam generator. The source listing of the energy balance calculation is shown in Appendix A. Finally, the steam flow rate from the upper plenum was calculated by subtracting the water mass flow rate from the total mass flow rate. Figure 8 shows the evaluated water, steam and total mass flow rates.

2.3 Calculation conditions

Four types of parametric calculations were performed in this study. At first, each component of TRAC input model was checked separately:

1. Hot leg study: Study of the thermal-hydraulic behavior in the hot-leg piping and the inlet plenum of the steam generator with the PIPE component shown in Fig. 2(a).

2. Steam generator study: Study of the steam-generator thermal-hydraulic behavior with the STGEN component shown in Fig. 3(a).

3. Cold leg study: Study of the thermal-hydraulic behavior of the loop seal piping, pump simulator, and cold leg with the TEE component shown in Fig. 4(a).

The calculation conditions and indexes are listed in Table 1. In hot leg study (H-1 through H-3), studied are the water accumulation in the inlet plenum of the steam generator and the sensitivity of the pressure loss on the selection of the wall friction model in TRAC-PF1. In steam generator study (S-1 through S-5), studied are the effect of the heat conduction through the tube sheet, the initial temperature profile of the secondary side fluid, the convection in the secondary side and the inlet quality from the hot leg. In cold leg sutdy (C-1 through C-3), studied are the effect of the form loss in the pump simulator and the fluid temperature through the pump orifice plate. After these studies, each component of TRAC input model is combined and a calculation of an intact loop is performed with system schematic as shown in Fig. 1 to assess the integral capability of TRAC-PF1 for the prediction of the loop thermal-hydraulic behavior.

3. Results and discussion

3.1 Check calculation of each component of TRAC input model

3.1.1 Hot leg study

Figure 9 shows the comparison of the void fractions at cells 7 through 10 between the H-1 and H-2 calculations. In calculation H-1 (with the actual geometry of the inlet plenum of the steam generator), the void fraction of cell 9 starts to decrease at 102 s and it saturates at about 340 s with a void fraction of 0.7. The void fraction of cell 10 starts to decrease when the void fraction of cell 9 reaches the saturation value. This void fraction decrease shows the water accumulation in the inlet plenum. On the contrary, no significant water accumulation is found in calculation H-2 where the same flow area was assumed as the hot leg piping for the cells corresponding to the inlet plenum of the steam generator. The water accumulation in calculation H-1 is due to the reduced steam velocity from flow expansion at this part.

Figure 10 shows the overall mass balance for the PIPE component in calculations H-1 and H-2. Almost no water accumulated in calculation H-2. About 50 % of total water from the upper plenum (UP) accumulated inside the PIPE component (hot leg piping and the inlet plenum of the steam generator) in calculation H-1. The mass of accumulated water was about 50 kg at 600 s. The total mass for three intact loops and one broken loop would be about 200 kg at 600 s. This amount is about the same as that accumulated in the upper plenum. To study the de-entrainment effect on the steam binding during the reflood phase, the water accumulation inside the inlet plenum of the steam generator should be considered as well as that in the upper plenum. More study is recommended on water accumulation in the inlet plenum of the steam generator.

Figures 11 and 12 show the comparisons of the differential pressure between TRAC and CCTF results. The calculated results are lower than the measured data. Apparently, more water flowed during the test than assumed in this calculation through the hot leg piping. The assumed water flow for the calculation is the water mass flow rate through the heat exchange piping of the steam generator. The water mass accumulated in the inlet plenum of the steam generator was not accounted for in this calculation. No significant difference was found in the predicted differential pressures between the homogeneous or the annular flow models for the wall friction as shown in Figs. 11 and 12.

3.1.2 Steam generator study

In this steam generator study (calculations S-1 through S-5), the inlet and outlet plenums were modeled by the cells having the same flow area as the total area of the heat exchanging pipe of the steam generator.

Figure 13 shows the TRAC input schematic and the boundary conditions assumed for calculation S1 (base case) of the steam generator study. The assumed boundary conditions for the steam generator study show good agreement with the measured results of the CCTF test C1-19 (Run 38).

Figure 14 shows the comparison of the differential pressure through the steam generator between CCTF and TRAC results. The calculated result shows good agreement with the measured result. Figure 15 shows the comparison of the calculated differential pressures from S-1, S-2, S-3, and S-4. This figure shows that heat conduction through the tube sheet, the friction factor in the secondary side of the steam generator, and the low liquid temperature at the bottom of the secondary side of the steam generator have little effect on the differential pressure through the steam generator under the conditions close to those of the CCTF test C1-19 (Run 38).

Figure 16 shows the comparison of S-1 and S-5 calculations for the pressure profile along the heat exchange pipe of the steam generator at 200 s. The steam and water flows are 0.881 kg/s and 0.068 kg/s at this time in the S-1 calculation, respectively. The water is evaporated completely by 2.75 m from the inlet plenum. The calculated differential pressure in the S-1 calculation is identical with that in the S-5 calculation (single-phase steam at the inlet) between 5 and 16.2 m from the inlet plenum. The S-1 case predicts a little higher pressure drop between 0 and 2.75 m than the S-5 calculation because of the two-phase multiplier in the estimation of the friction loss. The total differential pressure through the steam generator in the S-1 calculation is only 3 % higher than that in the S-5 calculation (single-phase steam at the inlet). Thus, the most significant factor for the differential presusre through the steam generator is the friction loss arising from the single-phase flow; the acceleration loss due to the evaporation of the water and the increase of the friction loss coming from the two-phase multiplier have secondary importance in the CCTF test C1-19 (Run 38).

Figure 17 shows the comparison of the fluid temperature at the outlet plenum of the steam generator between the CCTF and the TRAC calculations (S-1). The calculated quality was unity during the transient.

The calculated liquid temperature corresponded to the saturation temperature. The calculated steam temperature was at least 20 K higher than the CCTF results. The CCTF results show that the fluid temperature is close to saturation after 300 s. This may indicate that the thermocouples are wetted by the saturated water in the outlet plenum of the steam generator. The water seems to come through the tube of the steam generator.

Figure 18 shows the comparison of the calculated steam temperature at the outlet plenum among the calculations S-1 through S-4. It shows that the heat conduction through the tube sheet and the friction factor of the secondary side of the steam generator have little effect on the steam temperature at the outlet plenum of the steam generator.

Figure 19 shows the comparison of the total energy transfer from the secondary side to the primary side of the steam generator between CCTF and TRAC results. The energy is shown as the equivalent water mass to evaporating it. The latent heat of 2240 kJ/kg was used to evaluate the mass. Figure 19(a) shows the comparison of the total energy transfer from the secondary side to the primary side of the steam generator, calculated from the temperature drop of the liquid in the secondary side. Between 0 and 100 s, the CCTF result is almost equal to zero. This indicates that the heat loss from the secondary side was practically negligible. The calculated total energy transfer was higher than the CCTF result after 100 s. Thus, TRAC overestimates the total energy heat transfer from the secondary side to the primary side of the steam generator. Figure 19(b) shows the comparison of the energy for evaporating water and for superheating steam. Good agreement is found in the energy for evaporating water. Therefore, one can conclude the overestimation of the total energy transfer is caused by the overestimation of the energy to superheat the steam, or the overestimation of the steam temperature at the outlet plenum of the steam generator.

Even though the total energy transfer is overestimated in the present calculation, it was underestimated in the previous TRAC calculations.[7] In the present calculation, the steam and water mass flow rates through the steam generator was determined by the test data as described in 2.2. The flow quality of the two-phase mixture was evaluated to be about 0.9 from the energy balance calculation. On the other hand, it was almost unity in the previous TRAC calculation.[7] In such a case, the energy for evaporating water is almost equal to zero and the total energy transfer at the steam generator is determined only by the energy to superheat the steam. It is concluded that the

underestimation in the previous TRAC calculations was attributed mainly to the overestimation of the flow quality of the two-phase mixture through the steam generator.

Figure 20 shows the comparisons between the CCTF and TRAC liquid temperatures at various elevations of the secondary side. Figure 21 shows the comparisons of the temperature decrease from the initial liquid temperature at 200, 300, and 400 s. TRAC predicts less temperature decrease in the lower part of the secondary side (below 0.8 m) and more temperature decrease in the upper part of the secondary side (above 1.0 m). In this TRAC calculation (S-1), the heat conduction through the tube sheet and the flow resistance due to the baffle plates were not considered. To check the effect of these factors on the temperature transients of the secondary-side liquid, the calculation results from S-2 (including the heat conduction through tube sheet) and S-4 (assuming high additive friction factor in the secondary side of the steam generator to suppress the convection) calculations are compared with the results from calculation S-1. Figure 22 shows the comparisons of the liquid temperature between S-1 and S-2 calculations. It was expected that the heat conduction through the tube sheet should enhance the heat transfer from the lower part of the secondary side; however, no significant difference was found except in the fluid cell next to the tube sheet. Figure 23 shows the comparisons of the liquid temperature between S-1 and S-4 calculations. The observed discrepancy between CCTF and TRAC results for the temperature decrease could be explained by too much convection in the secondary side because the liquid in the lower part could be heated by mixing with the liquid in the upper part. To determine if the convection effect in the secondary side is significant, calculation S-4 was performed assuming the friction factor of 10^4 in the secondary side to prevent the convection effect. No significant difference is shown between these two calculation in Fig. 23. This shows that the convection effect is negligible in the secondary side.

Figure 24 shows the comparison of the steam temperature along the heat exchange tube at 200 s between S-1 and S-3 calculations (with high initial temperature at the bottom of the secondary side). The water was evaporated completely by 2.75 m from the inlet plenum of the steam generator in both calculations. The discrepancy in the outlet steam temperature arises from the heat transfer near the outlet plenum (in the section bewteen 14 and 15.2 m). In the S-1 calculation, the liquid temperature of the secondary side was about 470 K. The superheated

steam in the primary side transferred energy to the secondary side and was cooled.

Figure 25 shows the comparison of the liquid temperature drop from the initial liquid temperature at 200, 300, and 400 s between CCTF results and S-5 calculations (single-phase water or steam flow). The CCTF test results are very similar to the single-phase water results at the 0.25 m elevation. The CCTF test results approach the single-phase steam results in the upper part of the heat-transfer tube and show good agreement with the single-pahse steam results above 0.8 m. These results show that high heat transfer similar to the single-phase water results occurred at the bottom of the secondary side of the steam tenerator in the CCTF test and suggest that the inside of the heat-exchange tube was covered with a liquid film. Because of the rapid evaporation of the incoming water in the lower part of the steam generator, it seems that single-phase flow or two-phase flow with high quality is established in the upper part of the steam generator. This may be why the CCTF results show good agreement with the single-phase steam result.

3.1.3 Cold leg study

Figure 26 shows the TRAC input schematic and the boundary conditions for the cold-leg study. The hot-leg and steam generator models in Fig. 1 were replaced by a FILL component. The steam flow and temperature were input as tables of the FILL component based on the measured data in the CCTF test C1-19 (Run 38). Reasonable agreement is obtained between the measrued data and the boundary conditions for the TRAC calculations of the cold-leg study.

As the first step of the cold-leg study, a parametric study was performed for the differential pressure through the pump orifice part to determine the appropriate additive friction factor.

In TRAC, the pressure loss ΔP is calculated by

$$\Delta P = \Delta P_F + \Delta P_A \quad , \tag{1}$$

where ΔP_F and ΔP_A indicate the wall shear and form losses, respectively. The form loss is calculated by

$$\Delta P_A = \frac{(\Delta X_j + \Delta X_{j-1})}{2D_{h,j}} (FRIC)_j \rho_m V_m |V_m| \tag{2}$$

where

ΔX : Cell length (m),
D_h : Hydraulic diameter (m),
ρ_m : Mixture density (kg/m^3),
V_m : Mixture velocity (m/s),
FRIC : Additive friction factor, and
j,j-1 : Indexes for cell number.

The additive friction factors are input data and represent the pressure loss due to the abrupt flow area change and bend etc. A parametric study for the additive friction factor was performed to get the proper form loss of the pump orifice part. A study was performed assuming a steady state. Figure 27 shows the result of the parametric study. When FRIC = 0, the calculated pump K-factor is 6.52. This value shows the contribution of the wall shear loss in the whole pressure loss through the pump orifice part. The calculated pump K-factor increased with FRIC linearly. The estimated pump K-factor was about15.9 in the CCTF C1-19 (Run 38). The value of 0.215 was selected as the additive friction factor through the comparison with the measrued data. In the previous TRAC calculations [such as for CCTF TEST C1-19 (Run 38)],[7],[8] the contribution of the wall shear loss to the whole pressure loss through the pump orifice part was not considered and the value of FRIC was calculated from the given measured pump K-factor assuming that the wall shear loss is zero. Therefore, in the previous TRAC calculations, the pump K-factor was overestimated by the wall shear loss. The additive friction factor should be modified by considering the contribution of the wall shear loss through the pump orifice part.

Figure 28 shows the comparison of the differential pressure through the pump orifice part and the pump K-factor for CCTF and TRAC results, respectively. With the value of 0.215 for the additive friction factor of the pump orifice, the TRAC-PF1 prediction gives excellent agreement with the CCTF measured pressure loss through the pump orifice part during LPCI injection. This result shows that TRAC-PF1 can reasonably predict the pressure loss through the pump orifice part if the additive friction factor is determined appropriately. The configuration of the pump orifice of the CCTF is so complicated that it is difficult to get the proper additive friction factor due to the form loss by the combination of the previously developed correlations. In this analysis we fixed the additive friction factor due to the form loss with a known

flow condition at first and applied the obtained value to the whole transients of the test. The good agreement in Fig. 28 shows that this approach is useful to get the appropriate additive friction factor. However, it is still necessary to check whether the selected value of the additive friction factor is appropriate for the other CCTF tests.

To check effect of the steam temperature on the differential pressure through the pump orifice part, a TRAC-PF1 calculation was performed assuming a constant steam temperature. This temperature is almost equal to the initial liquid temperature of the secondary side of the steam generator as in the evaluation calculation for the licencing of PWRs. Figures 29 and 30 show the comparisons of the steam temperature and the calculated differential pressure through the pump orifice part. Higher steam temperature results in the higher differential pressure. The calculated differential pressure with high steam temperature is about 15 % higher than the base-case calculation (C-2) of the cold-leg study.

Figures 31 and 32 show the comparisons of the pump K-factor and the steam density between these two calculations. The steam temperature has little effect on the pump K-factor. Therefore, the higher differential pressure with the steam temperature arises from the lower steam density.

During the accumulator injection period, Fig. 28 shows the poor agreement between TRAC and CCTF results. This is caused by the condensation shock in the TRAC calculation. Figure 33 shows the calculated pressure and void fraction profiles along the cold leg at 115 s. A sharp pressure decrease is predicted at -3.3 m from the cold-leg outlet in the TRAC calculation, which was not observed in the CCTF tests. This decrease is the result of the choke model calculating a limiting velocity less than the input velocity of the FILL. This low velocity for choking was the result of an error in the choke model. Downstream of the pressure decrease (between -3.3 m and 0 m from the cold-leg outlet), the pipe is plugged by the water, while little water flowed backward upstream of the ECC injection nozzle. Upstream of the ECC injection nozzle, steam was accumulated from the FILL component that replaced the steam generator and the pressure increased bewteen the FILL component and the ECC injection nozzle as shown in Fig. 34. The pressure at the cell 17 (adjacent to the ECCS injection nozzle) reached more than 15 bar at the end of the accumulator injection. By the switching from the accumulator to the LPCI at 121 s, the ECC flow rate was decreased and

the plugging water downstream of the ECC injection nozzle was swept to the downcomer. This resulted in the rapid pressure decrease upstream of the ECC injection nozzle as shown in Fig. 34. The application of the choke models should be reviewed during accumulator injection.

3.2 Transient calculation for CCTF test C1-19

A system calculation was performed with the TRAC input shown in Fig. 1 to assess the integral predictive capability of TRAC for the loop flow behavior during the reflood phase. In the calculation, the cells corresponding to the inlet plenum of the steam generator were replaced with the cells modeling the extension of the hot leg pipe for better agreement in the mass flow through the steam generator. The main results of this calculation are shown in the Appendix C.

Figure 35 shows the comparison of CCTF and TRAC mass flow rates through the loop. The assumed mass flow rate shows good agreement with CCTF results at the exit of the steam generator. The calculation results show that no significant water accumulation occurred in the hot leg and the steam generator, but the inlet plenum of the steam generator was not modeled accurately in this calculation and the liquid flow from the vessel may have been too small.

Figure 36 shows the comparison of TRAC and CCTF results for the total differential pressure through the loop. The TRAC result shows high differential pressure during accumulator injection (between 105 and 121 s) from condensation shock at the cold leg as previously mentioned. The calculated differential pressure is about 10 % lower than the CCTF result during the LPCI injection ($t > 130$ s). Table 2 shows the comparisons of TRAC and CCTF for the component-by-component differential pressure at 200 s. For the hot-leg piping (DT12 and DT22H), the calculated differential pressure is 1.07 kPa lower than the CCTF results as well as in the hot-leg study. This discrepancy may be caused by less water flow through the hot leg. For the steam generator (DT21G), the calculated differential pressure is 0.58 kPa lower than the CCTF result even though good agreement was obtained in the steam generator study. This difference is caused by the flow expansion at the outlet plenum of the steam generator in the loop calculation. For the loop seal piping and the pump simulator (DT21L, DT22L, DT23L and DT89), the calculated differential pressure is 1.94 kPa higher than the CCTF result. The calculated steam temperature at the exit of the steam generator was about 25 K higher than the CCTF result at 200 s (see Appendix C). This

results in the higher differential pressure at the loop-seal piping and the pump orifice part as shown in Figs. 29 and 30. For the cold-leg piping (DT9-11), the calculated differential pressure is 2.70 kPa lower than the CCTF result. By improving the loop input model, better agreement was obtained for the differential pressures.

However, the following are recommended for better evaluation of the steam binding effects during the reflood phase of a PWR loss-of-coolant accident. Based on these comparisons with the CCTF test C1-19 results:

1. Review of the water accumulation behavior in the inlet plenum of the steam generator in the experiment and calculation.

2. Review of the heat transfer model in the steam generator.

3. Review of the choke model for condensing two-phase flow, especially during the accumulator injection.

4. Conclusions

In order to assess the predictive capability of the TRAC-PF1 code for the thermal hydraulic behavior along a primary loop during the reflood phase of a PWR LOCA, a parametric study was performed using the data from the CCTF test C1-19(Run 38). The following conclusions were obtained from the present study:

(1) The overestimation of the loop flow resistance in the previous TRAC calculations was caused mainly by the error in the input data of the additive friction factors. With the appropriate additive friction factors, TRAC-PF1 predicted the loop flow resistance within the error of 10 % during the LPCI injection.

(2) The underestimation of the total energy transfer from the secondary side to the primary side of the steam generator was attributed mainly to the overestimation of the flow quality of the two-phase mixture through the steam generator in the previous TRAC calculations.

(3) A review on the following items is recommened for the future improvements of the TRAC-PF1 code:

(a) Water accumulation model at the inlet plenum of the steam generator.

(b) Heat transfer model at the steam generator, especially for the evaporation rate of incoming water.

(c) Critical flow model in the condensing two-phase flow, especially when flowing steam is condensed completely due to the direct contact with the subcooled ECC water.

results in the higher differential pressure at the loop-seal piping and the pump orifice part as shown in Figs. 29 and 30. For the cold-leg piping (DT9-11), the calculated differential pressure is 2.70 kPa lower than the CCTF result. By improving the loop input model, better agreement was obtained for the differential pressures.

However, the following are recommended for better evaluation of the steam binding effects during the reflood phase of a PWR loss-of-coolant accident. Based on these comparisons with the CCTF test C1-19 results:

1. Review of the water accumulation behavior in the inlet plenum of the steam generator in the experiment and calculation.

2. Review of the heat transfer model in the steam generator.

3. Review of the choke model for condensing two-phase flow, especially during the accumulator injection.

4. Conclusions

In order to assess the predictive capability of the TRAC-PF1 code for the thermal hydraulic behavior along a primary loop during the reflood phase of a PWR LOCA, a parametric study was performed using the data from the CCTF test C1-19(Run 38). The following conclusions were obtained from the present study:

(1) The overestimation of the loop flow resistance in the previous TRAC calculations was caused mainly by the error in the input data of the additive friction factors. With the appropriate additive friction factors, TRAC-PF1 predicted the loop flow resistance within the error of 10 % during the LPCI injection.

(2) The underestimation of the total energy transfer from the secondary side to the primary side of the steam generator was attributed mainly to the overestimation of the flow quality of the two-phase mixture through the steam generator in the previous TRAC calculations.

(3) A review on the following items is recommened for the future improvements of the TRAC-PF1 code:

(a) Water accumulation model at the inlet plenum of the steam generator.

(b) Heat transfer model at the steam generator, especially for the evaporation rate of incoming water.

(c) Critical flow model in the condensing two-phase flow, especially when flowing steam is condensed completely due to the direct contact with the subcooled ECC water.

Acknowledgments

This work was performed during the stay at Los Alamos National Laboratory (LANL) where the author was delegated as a resident engineer in the 2D/3D program since February 1982 to March 1983. He would like to thank Dr. K. Williams, Messrs. R. Fujita, F. Motley, M. Cappiello and Mrs. S. Smith of Los Alamos National Laboratory for their helpful advice. Grateful thanks are forwarded to Mr. F. Motley, for providing support and valuable discussions.

He would like to express his thanks to Dr. M. Nozawa, Deputy Director General of Tokai Research Establishment JAERI, Dr. S. Katsuragi, Director of Reactor Safety Research Center of JAERI, Dr. M. Ishikawa, Director of Department of Nuclear Safety Evaluation, Dr. M. Hirata, Director of Department of Nuclear Safety Research, Dr. K. Hirano, Deputy Director of Department of Nuclear Safety Research, and Dr. Y. Murao, General Manager of Reactor Safety Laboratory II, for their guidance and encouragement.

He also appreciates to the members of the CCTF analysis group, Messrs. T. Iguchi, T. Sudoh, J. Sugimoto and T. Okubo for valuable discussions.

References

1. HIRANO, K. and MURAO, Y.: "Large Scale Reflood Test (in Japanese)", J. Atom. Engg. Soc. Japan, 22(10) pp. 680-686, (1980).

2. MURAO, Y.,et al.: "Experimental study of system behavior during reflood of PWR-LOCA using CCTF", J. Nucl. Sci. and Technol., 19(9), pp. 705-719, (1982).

3. LILES, D. et al.: "TRAC-PD2: An Advanced Best-Estimate Computer Program for Pressurized Water Reactor Loss-of-Coolant Accident Analysis", LA-8709-MS, NUREG/CR-2054, (1981).

4. LILES, D., et al.: "TRAC-PF1: An Advanced Best-Estimate Computer Program for Pressurized Water Reactor Analysis", Los Alamos National Laboratory (to be published).

5. KIRCHNER, W. L. and WILLIAMS, K. A.: "FY 1981 2D/3D Analysis Program Annual Report", LA-2D/3D-IN-81-36, (1981).

6. MOTLEY, F.: "Investigation of Radial Power and Temperature Effects in Large-Scale Reflood Experiments", Proceeding of Second International Topical Meeting on Nuclear Thermal Hydraulics", January, (1983).

7. AKIMOTO, H.: "Analysis of TRAC-PD2 results for the Cylindrical Core Test Facility Evaluation-Model Test (Run 38)", JAERI-M 84-041, (1984).

8. MURAO, Y., et al.: "Evaluation Report on CCTF Core-I Reflood Test C1-19 (Run 38)", JAERI-M 83-029, February (1983).

Table 1 Calculation conditions of parametric study

Calculation Index	Conditions
H-1	Hot-leg study using the PIPE component shown in Fig. 2(a). The time-dependent boundary conditions were determined based on the CCTF test C1-19 results.
H-2	Hot-leg study using the modified PIPE component with the homogeneous model of the wall friction. The steam-generator inlet plenum (cells 8 through 10 in Fig. 2(a)) is replaced to the same flow area of the hot-leg piping in the modified model.
H-3	Hot-leg study using the modified PIPE component with the annular flow model of the wall friction.
S-1	Steam-generator study with the STGEN component shown in Fig. 3(a). The time-dependent boundary conditions were determined based on the CCTF test C1-19 results.
S-2	Steam-generator study to check effect of the heat conduction through the tube sheet. Tube sheet model was considered by adding the heat-conduction path from the bottom of the secondary side to the inlet and outlet plenums of the steam generator to the STGEN model shown in Fig. 3(a).
S-3	Steam-generator study to check the effect of the initial temperature profile of the secondary-side fluid. Constant high-temperature profile was assumed instead of the initial temperature profile obtained from CCTF test C1-19.
S-4	Steam-generator study to check the effect of convection in the secondary side. High additive friction factor (1×10^4) was assumed to suppress the convection effect in the secondary side instead of no additive friction factor (0.0).

S-5 Steam-generator study to check the effect of the inlet quality. Two calculations were performed for the single-phase steam or water flow with the same total mass flow that was assumed in calculation S-1.

C-1 Cold-leg study to determine appropriate additive friction factor for the form loss of the orifice plate in the pump simulator. Seven steady-state calculations were performed with various additive friction factors under the same flow conditions.

C-2 Cold-leg study with the selected additive friction factor from calculation C-1. The time-dependent boundary conditions were determined base on the CCTF test C1-19 results.

C-3 Cold-leg study to check the effect of the fluid temperature through the orifice plate. High constant temperature equal to the fluid temperature at the secondary side of the steam generator was assumed as in the calculation for the safety assessment for the PWRs.

L-1 Loop study with the combined loop model shown in Fig. 1. The boundary conditions were determined based on the CCTF test C1-19 results.

Table 2 Comparison of differential pressure at each section of an intact loop between CCTF and TRAC results at 200 s of CCTF test C1-19

Tag-ID	CCTF	TRAC	DIFFERENCE
DPLT2	25.76	23.33	-2.43
DT12	0.89	0.32	0.57
DT22H	0.78	0.28	-0.50
DT21G	3.60	3.02	-0.58
DT21L	1.87	2.22	+0.35
DT22L	0.20	0.24	+0.04
DT23L	15.79	16.61	+0.82
DT89	0.25	0.98	+0.73
DT9-11	2.37	-0.33	-2.70

(*) Note: Unit in kPa

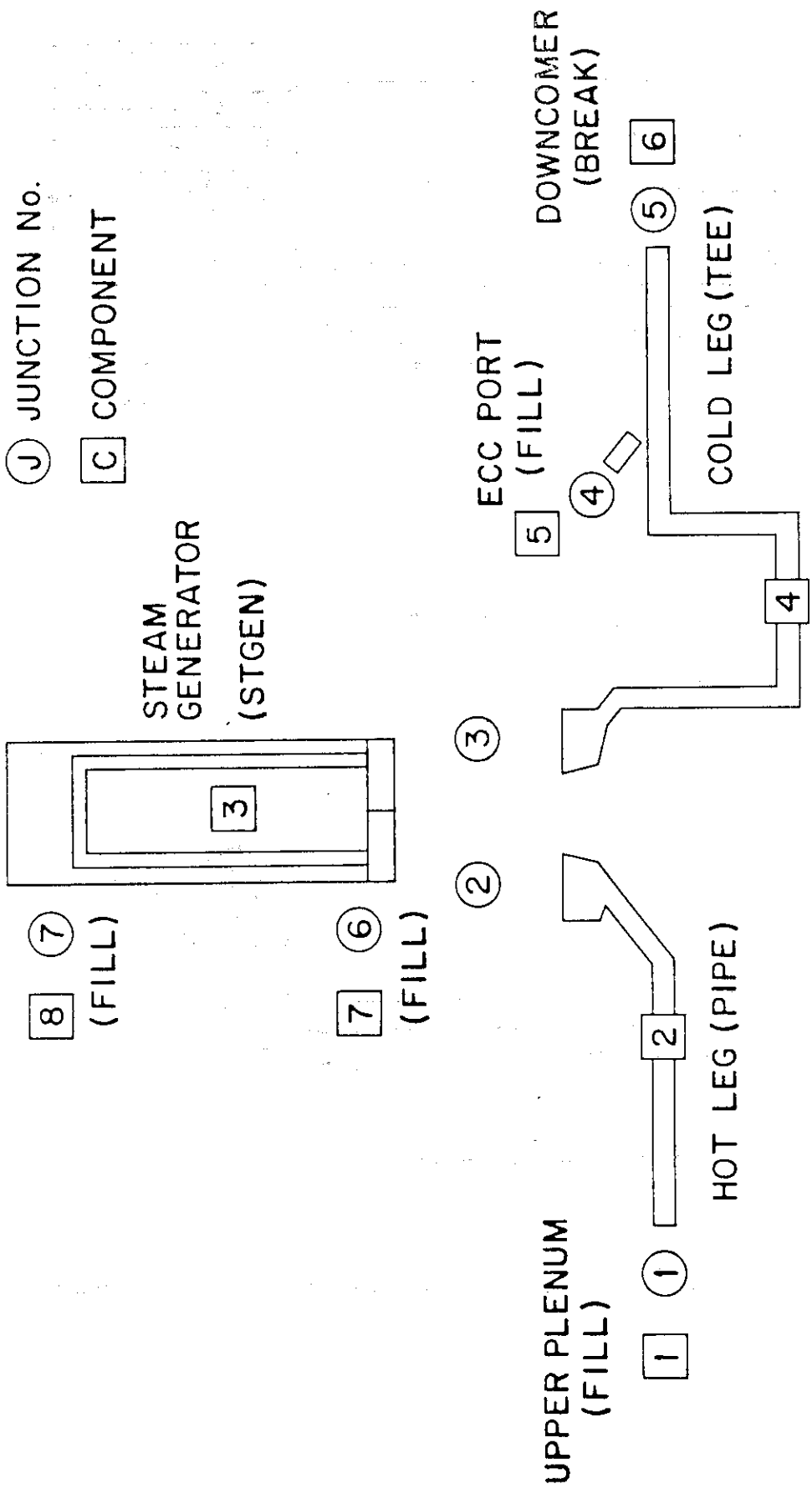

Fig. 1 TRAC input schematic.

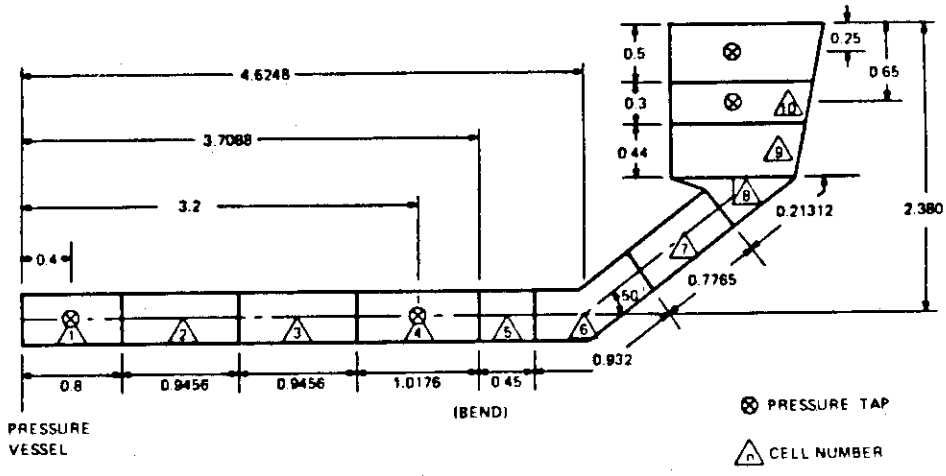

(a)Revised hot leg model.

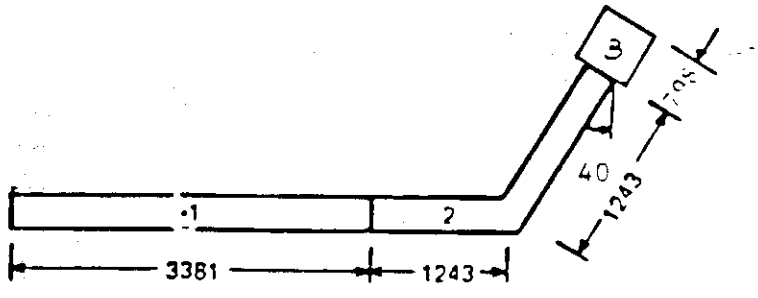

(b)Previous hot leg model.

Fig. 2 Detail of the hot-leg model with a PIPE component.

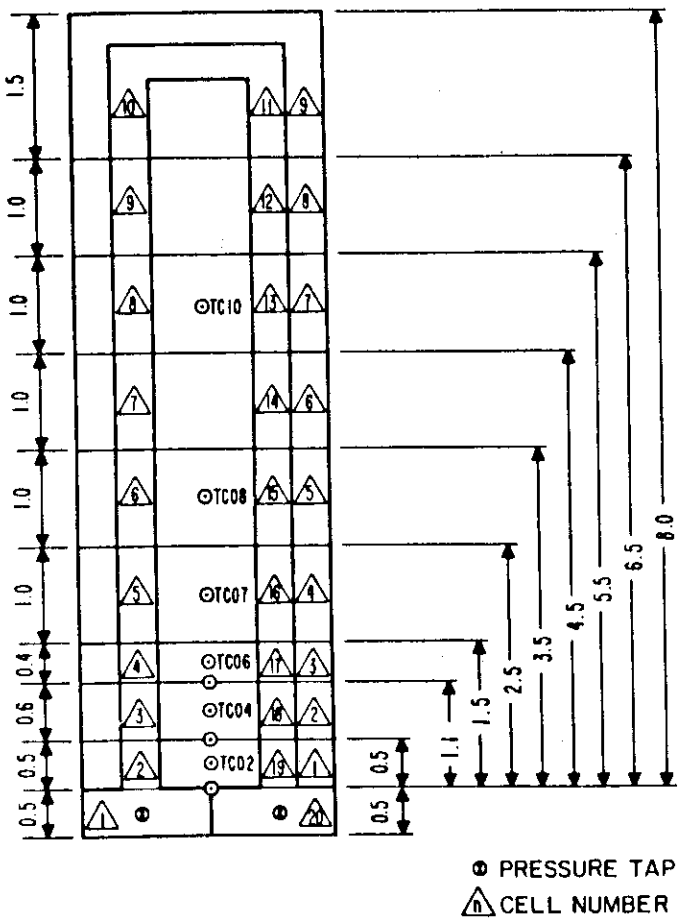

(a)Revised steam generator model.

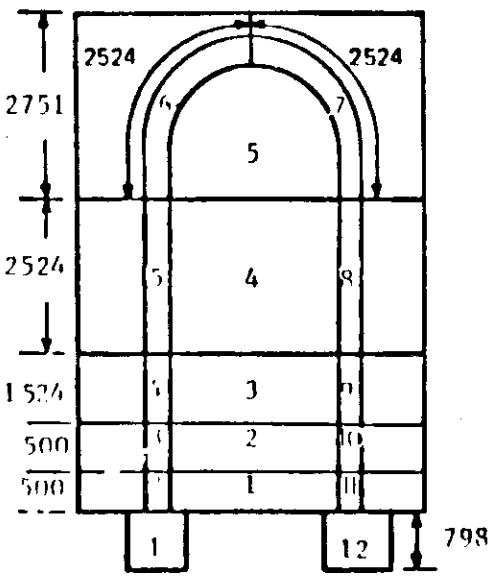

(b)Previous steam generator model.

Fig. 3 Detail of the steam generator model with a STGEN component.

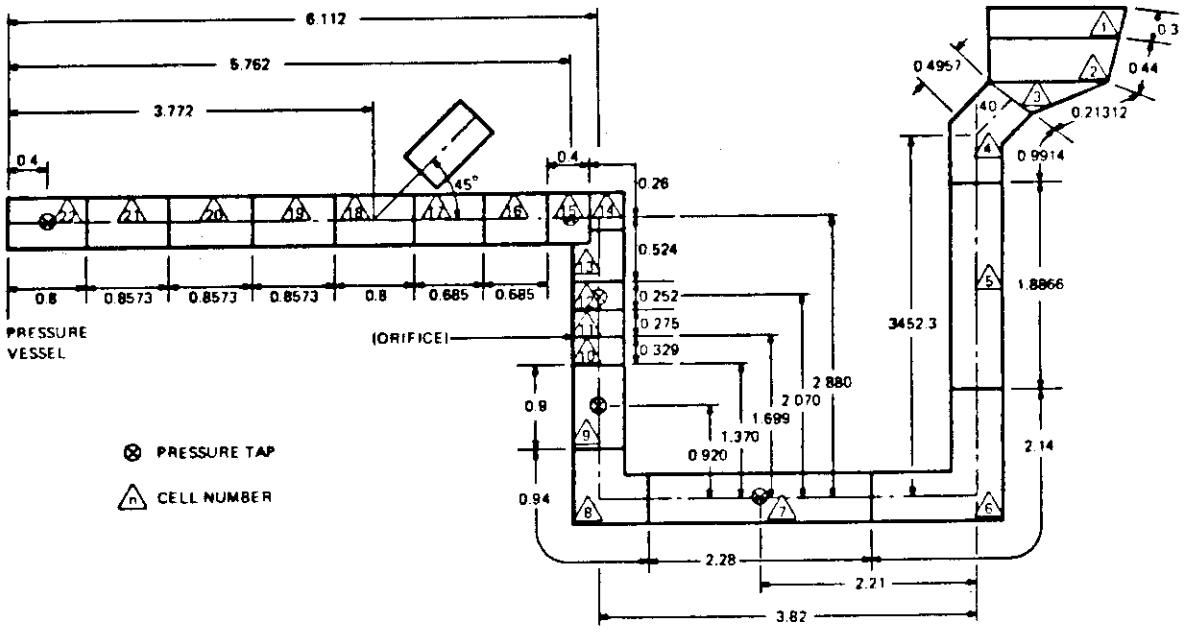

(a)Revised cold leg model.

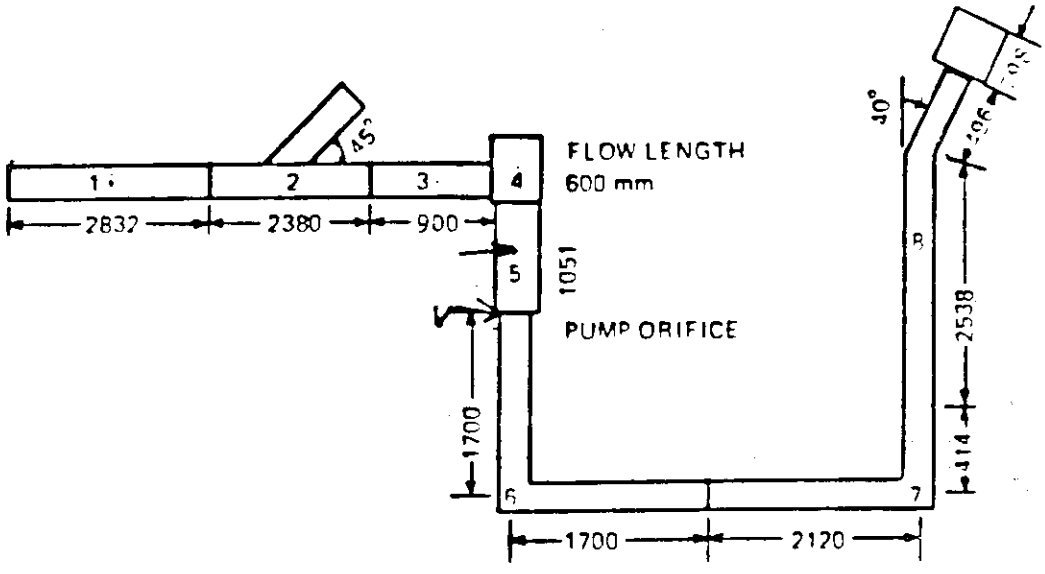

(b)Previous cold leg model.

Fig. 4 Detail of the loop-seal and cold-leg model with a TEE component.

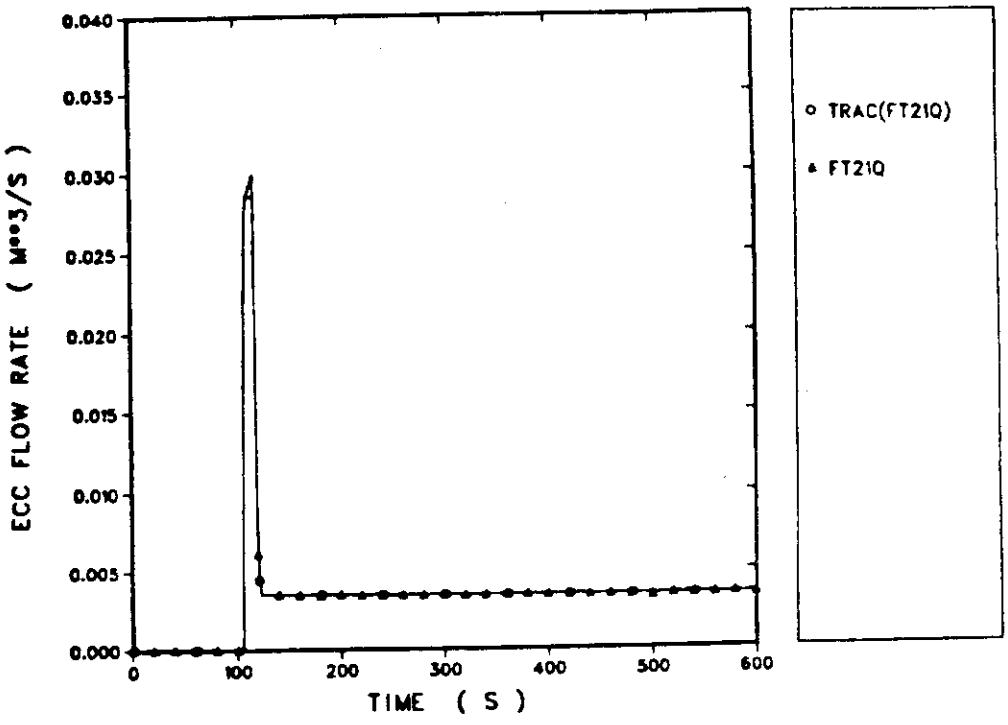

Fig. 5 ECC water flow rate through a cold leg ECC nozzle of CCTF test C1-19 (Run 38).

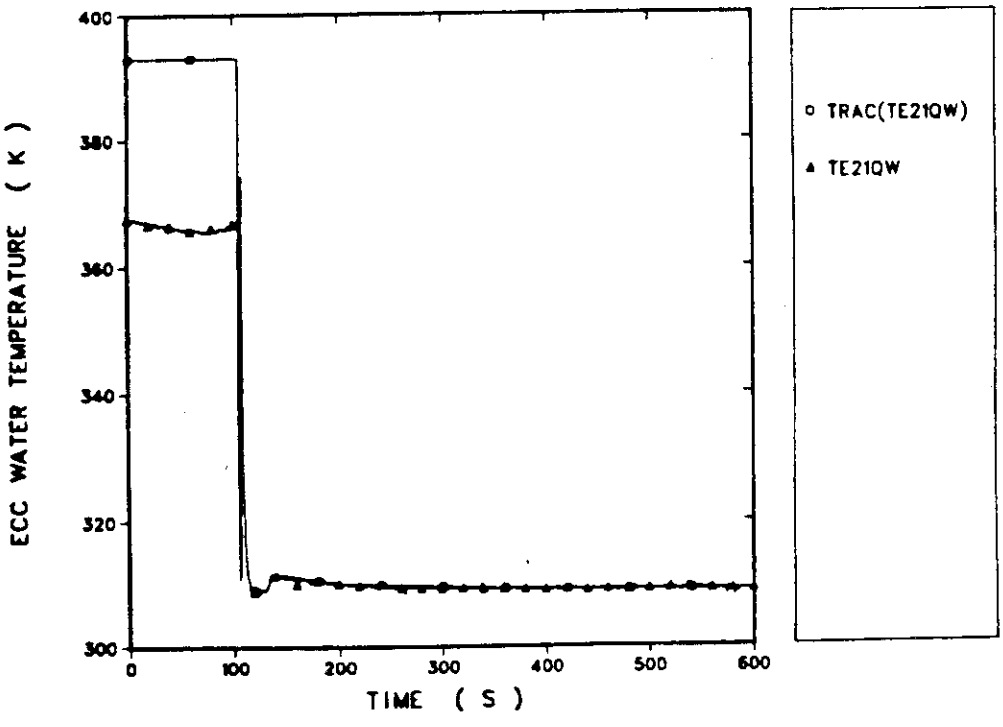

Fig. 6 ECC water temperature through a cold leg ECC nozzle of CCTF test C1-19 (Run 38).

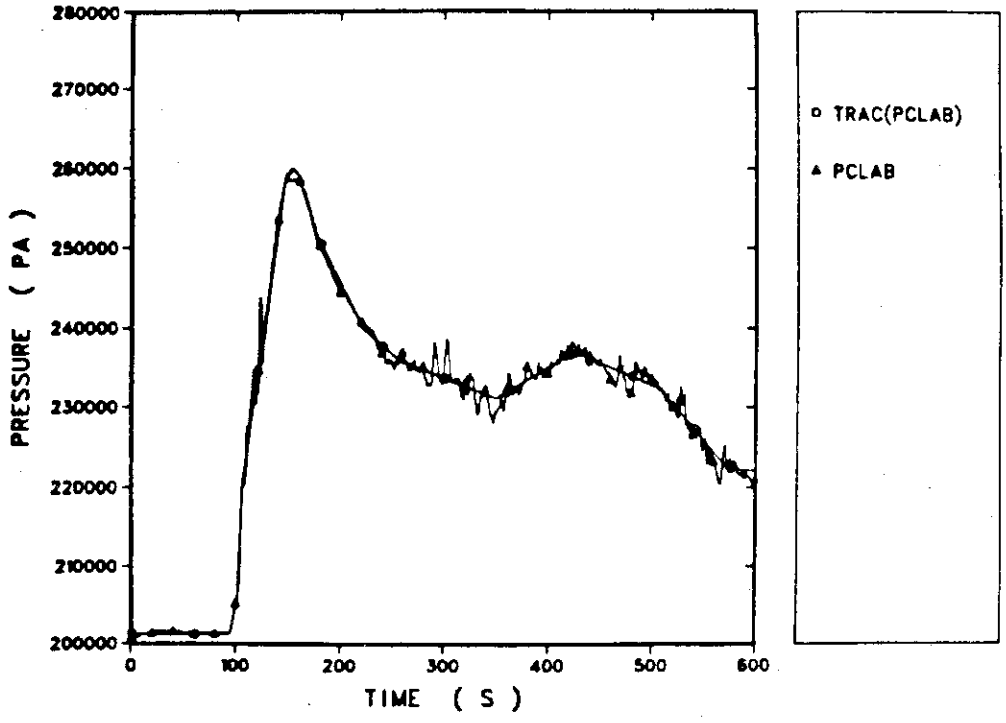

Fig. 7 Pressure transient of CCTF test C1-19 (Run 38) at the top of the downcomer.

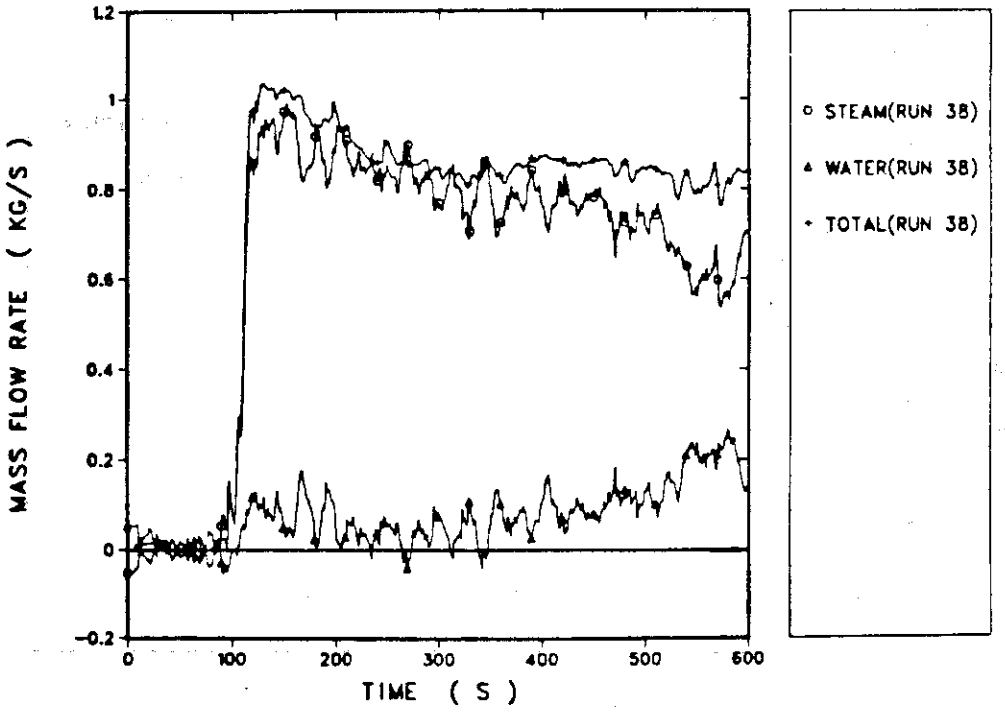

Fig. 8 Water, steam and total mass flow rate at the inlet plenum of the steam generator in CCTF test C1-19 (Run 38).

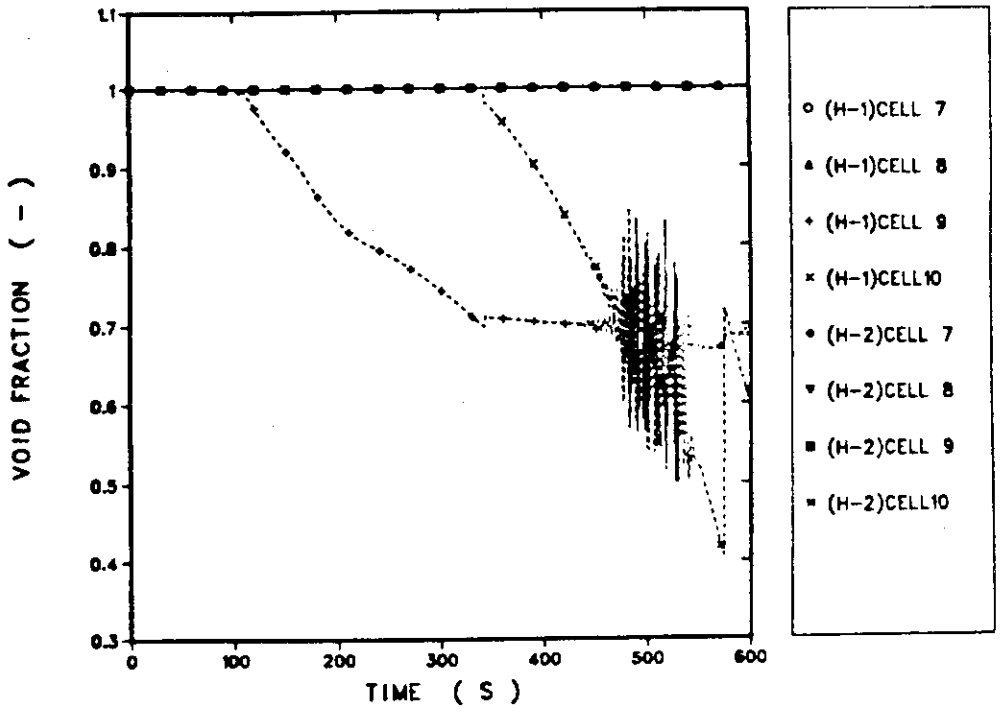

Fig. 9 Comparison of the calculated void fractions at cells 7 through 10 of the PIPE component between H-1 (with the inlet plenum) and H-2 (with the extension of pipe) calculations.

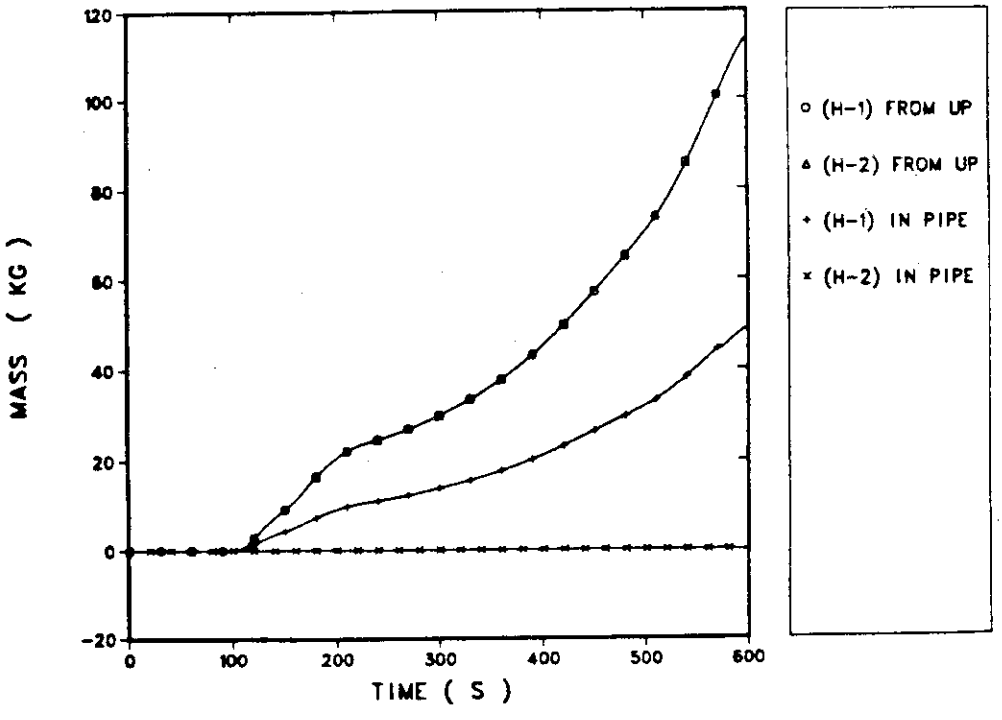

Fig. 10 Overall mass balance for the PIPE component in calculations H-1 (with the inlet plenum) and H-2 (with the extension of pipe).

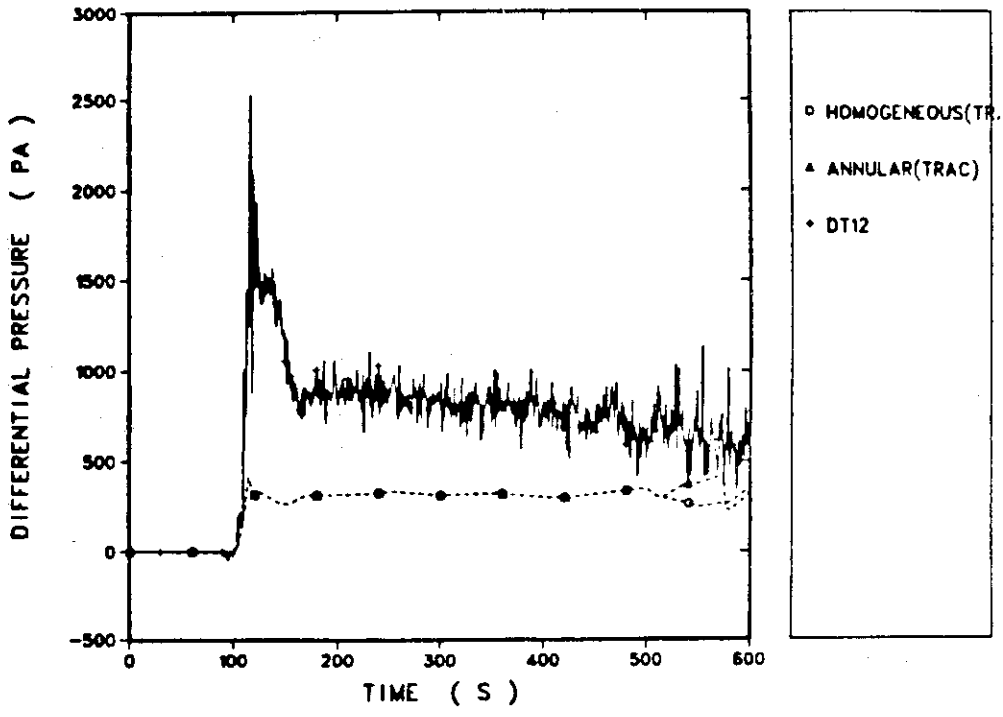

Fig. 11 Comparison of the calculated differential pressure between cell 1 and cell 4 of the PIPE component using the homogeneous or the annular wall friction model in the TRAC code with the CCTF result.

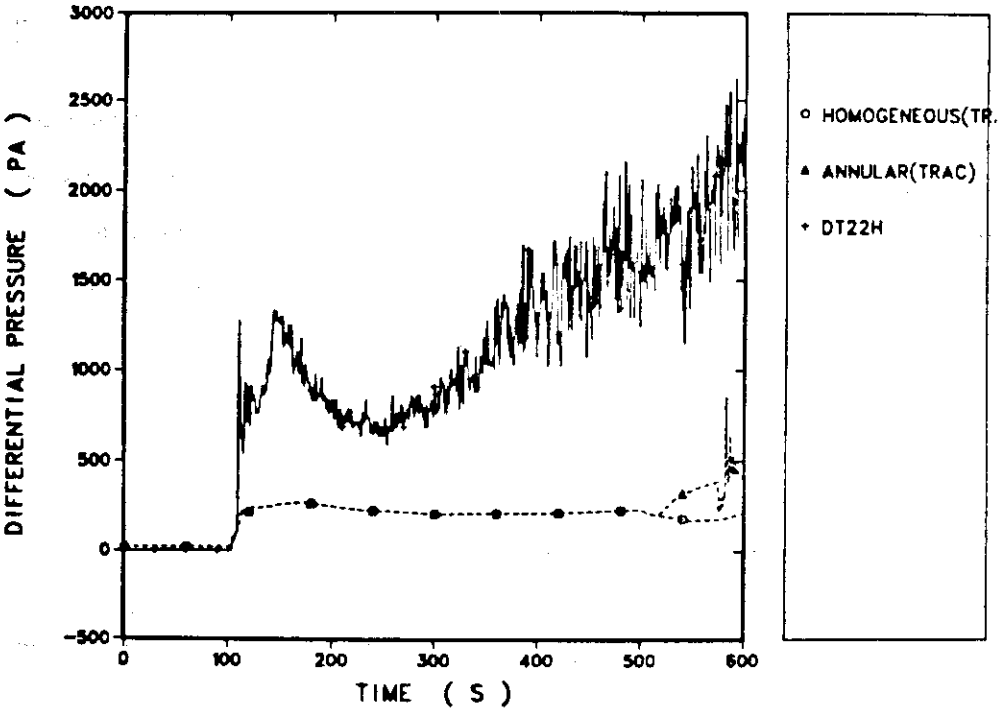

Fig. 12 Comparison of the calculated differential pressure between cell 4 and cell 10 of the PIPE component using the homogeneous or the annular wall friction model in the TRAC code with the CCTF result.

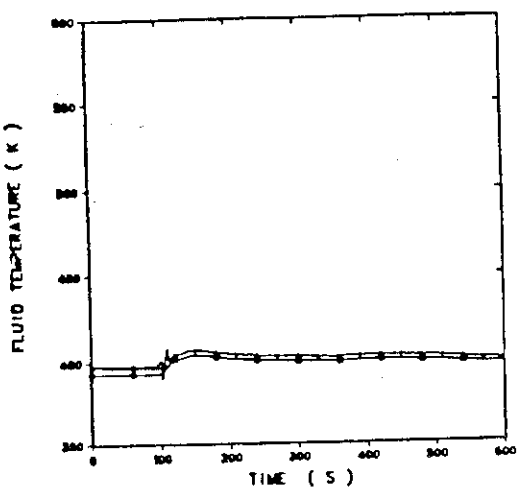

(a)Inlet fluid temperature

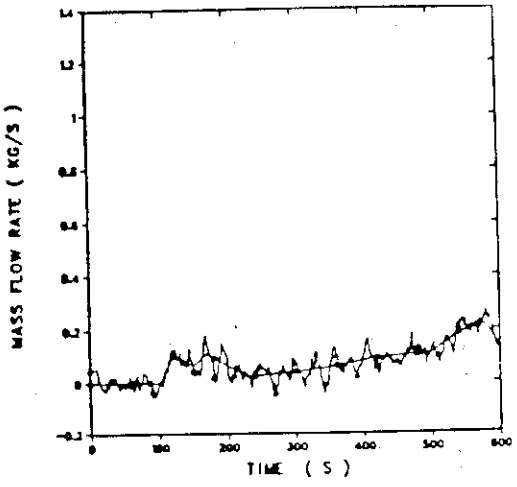

(b)Inlet water mass flow rate

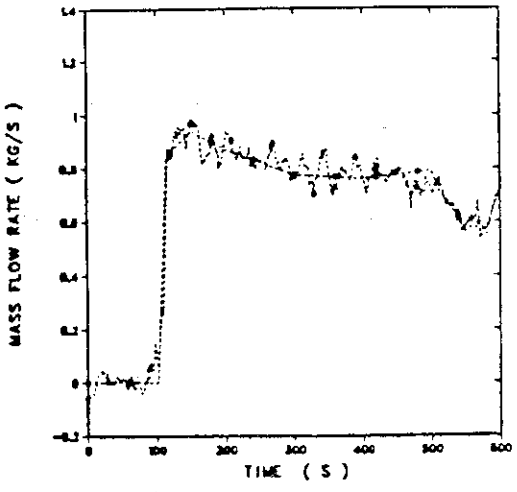

(c)Inlet steam mass flow rate

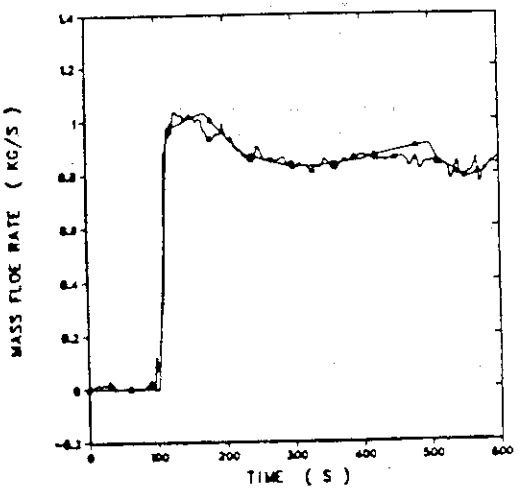

(d)Total mass flow rate at the inlet

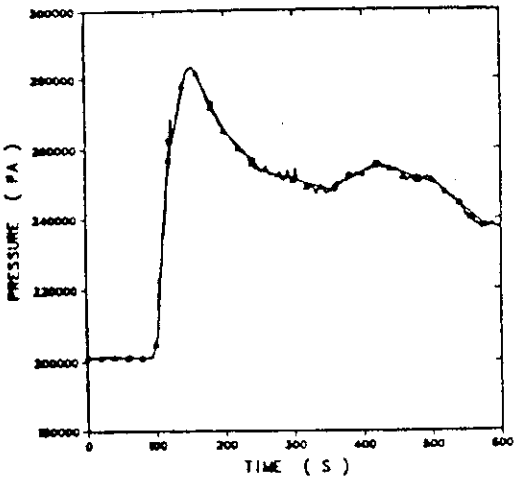

(e)Outlet pressure

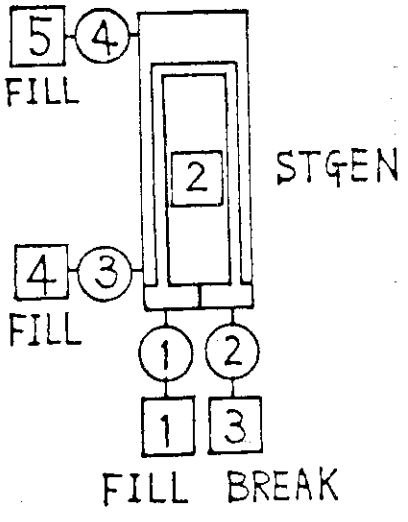

(f)TRAC input schematic.

Fig. 13 TRAC input schematic and boundary conditions assumed for the calculation S-1 (base case) of the steam generator study (a) Inlet fluid temperature (b) Inlet water mass flow rate (c) Inlet steam mass flow rate (d) Total mass flow rate at the inlet (e) Outlet pressure (f) TRAC input schematic.

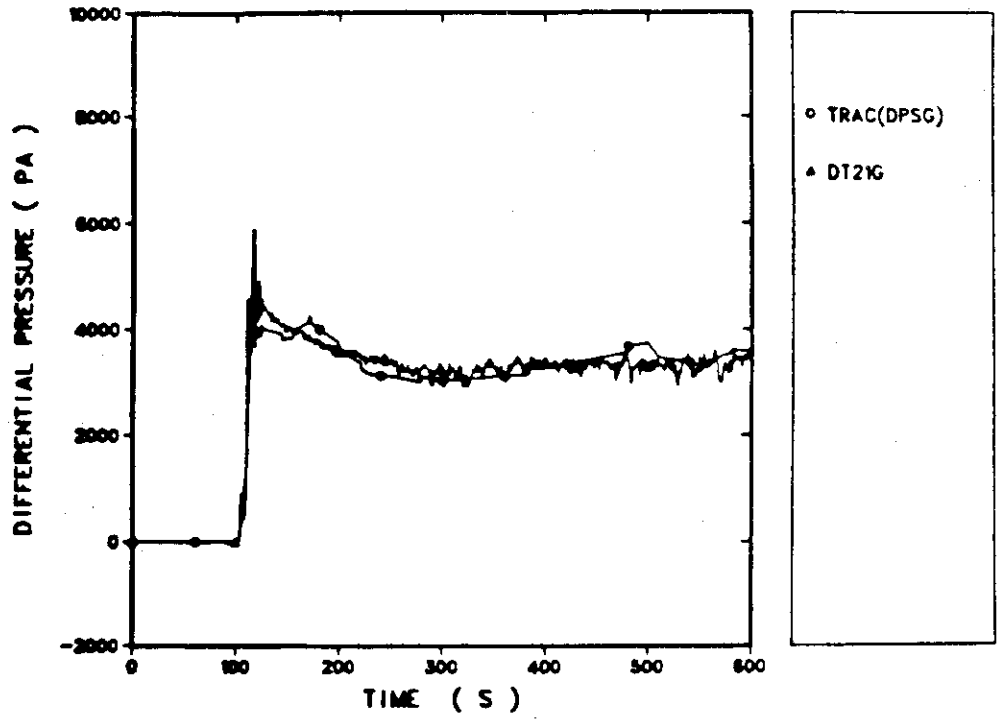

Fig. 14 Comparison of the differential pressure through the steam generator between CCTF and TRAC results.

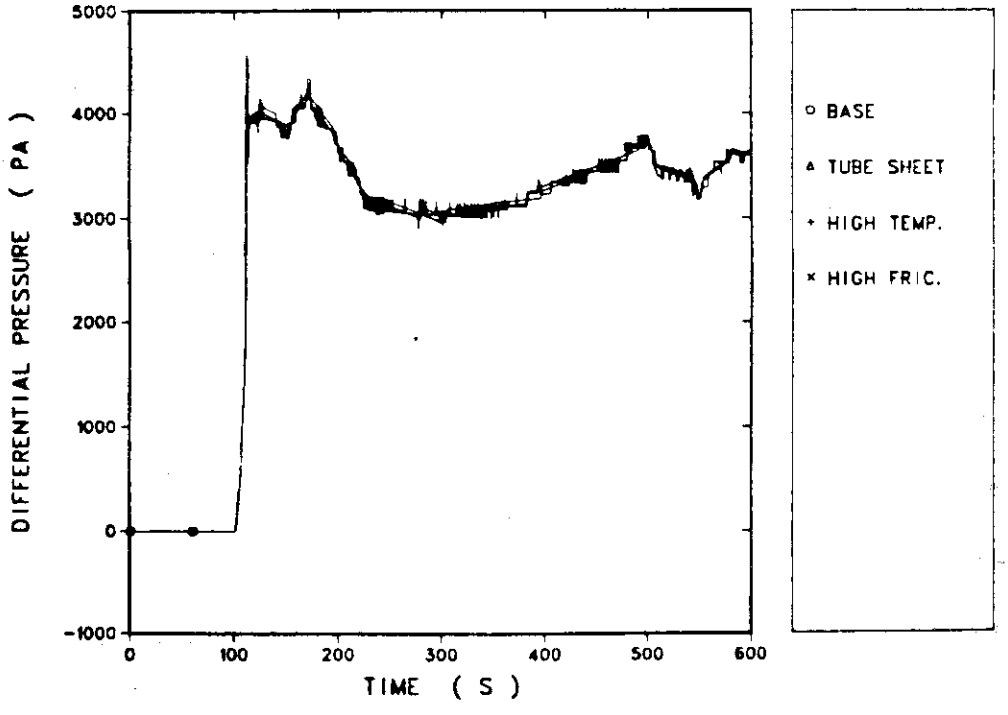

Fig. 15 Effect of the heat conduction through the tube sheet (S-2), the high liquid temperature at the bottom of the secondary side (S-3) and the friction factor in the secondary side (S-4) on the differential pressure through the primary side of the steam generator.

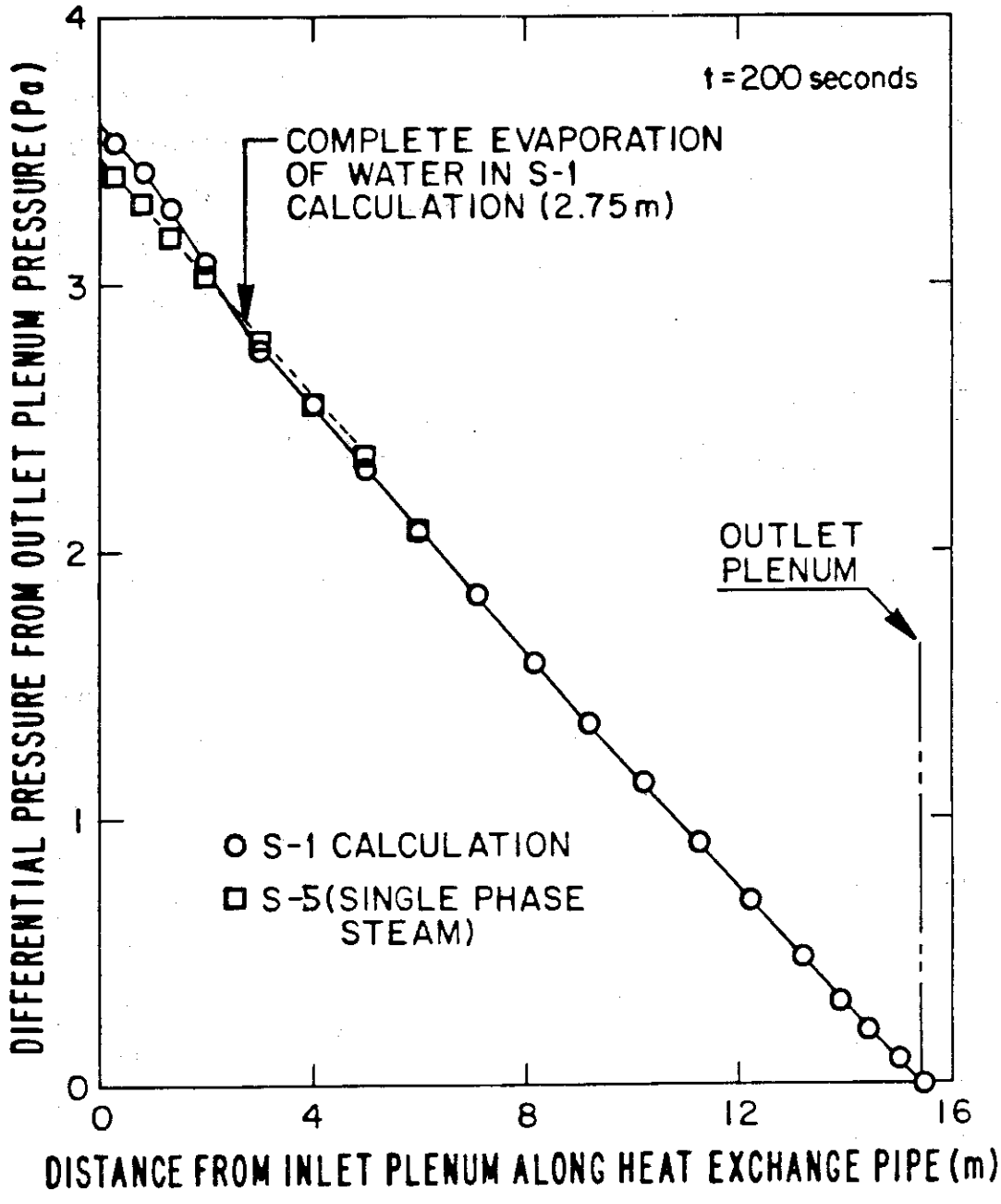

Fig. 16 Comparison of the pressure profile along the heat exchange pipe of the steam generator at 200 s between S-1 (base case) and S-5 (single phase water or steam flow at inlet) calculations.

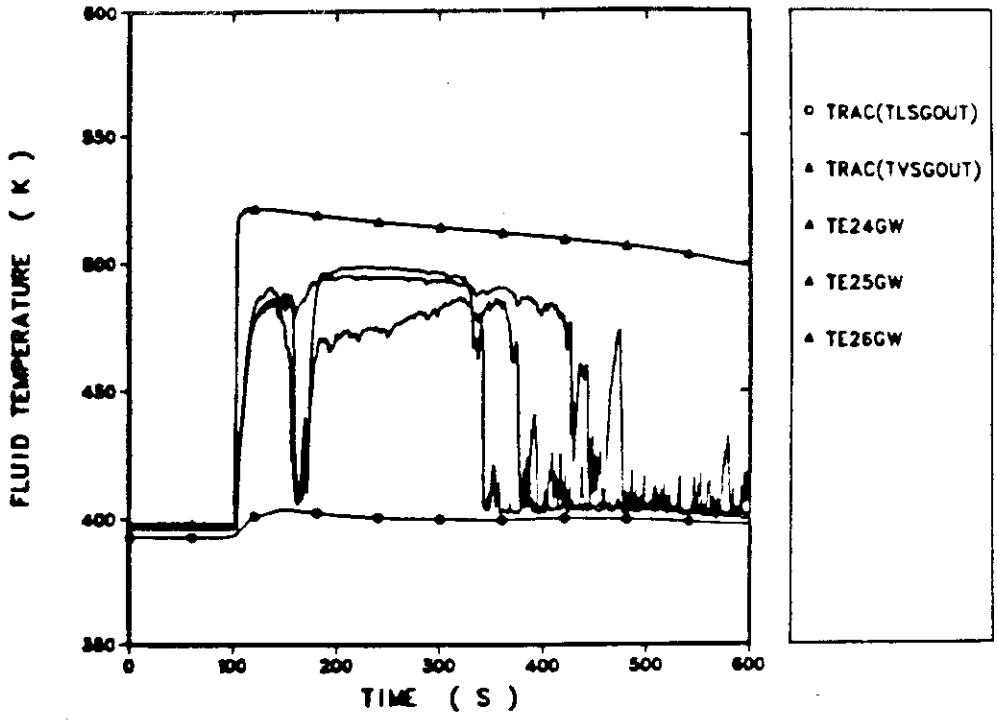

Fig. 17 Comparison of the fluid temperature at the outlet plenum of the steam generator between the CCTF and the TRAC results.

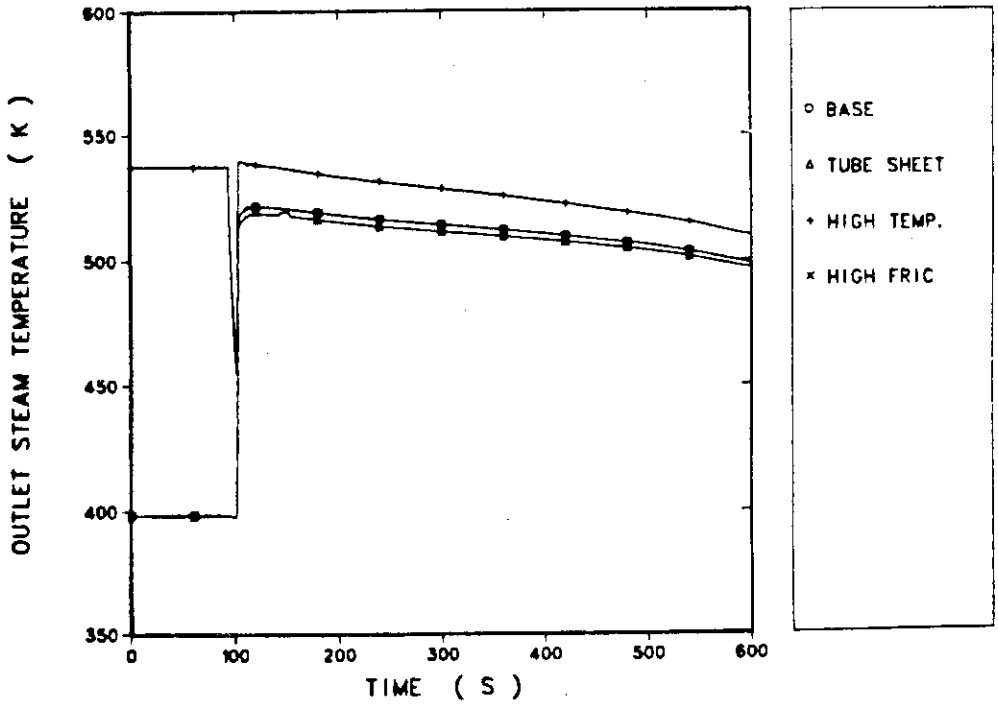

Fig. 18 Comparison of the calcualted steam temperature at the outlet plenum of the steam generator among the calculations S-1 (base case), S-2 (with the tube sheet model), S-3 (high initial liquid temperature at the bottom of the secondary side), and S-4 (high friction factor in the secondary side).

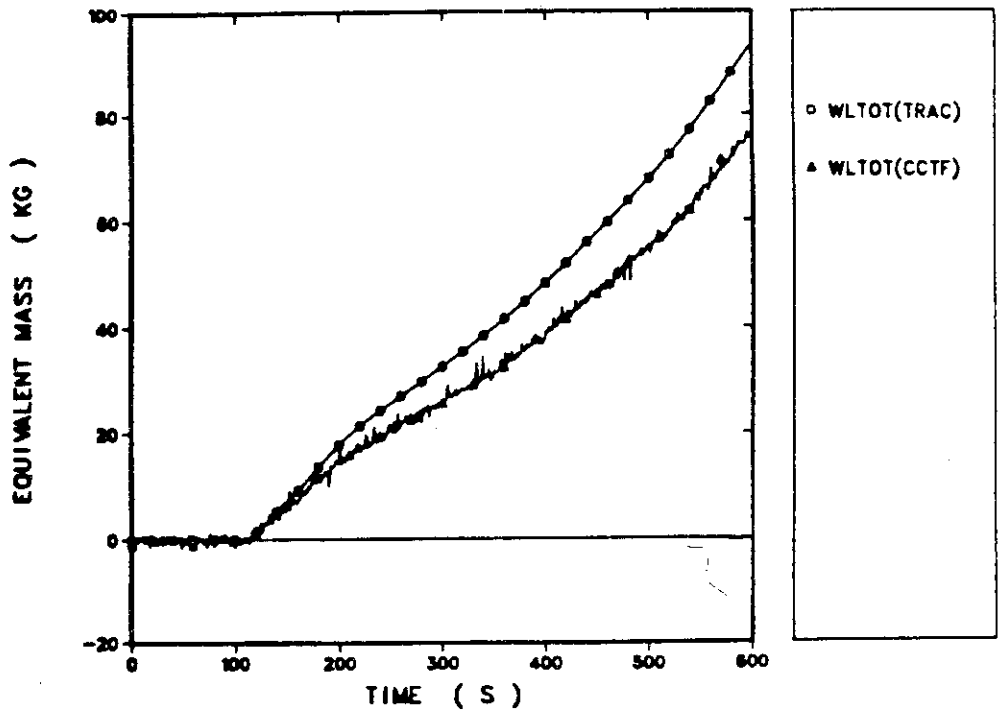

(a)Total energy

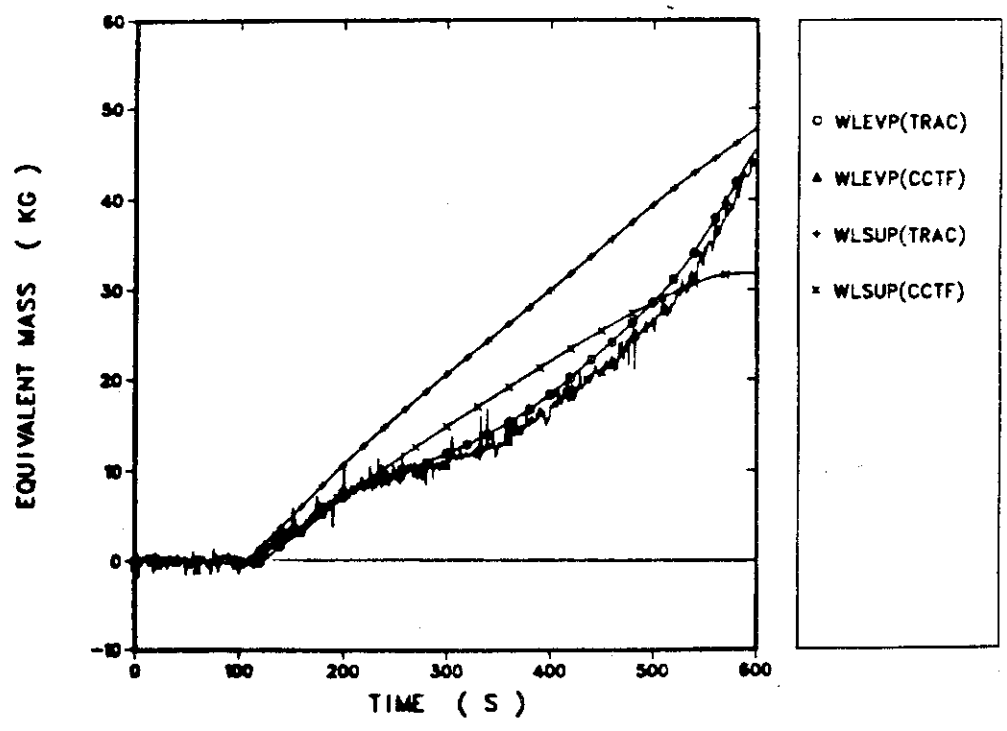

(b)Energy for evaporating water and superheating steam

Fig. 19 Comparison of the total energy transfer from the secondary side to the primary side of the steam generator between CCTF and TRAC results (a) Total energy (b) Energy for evaporating water and superheating steam.

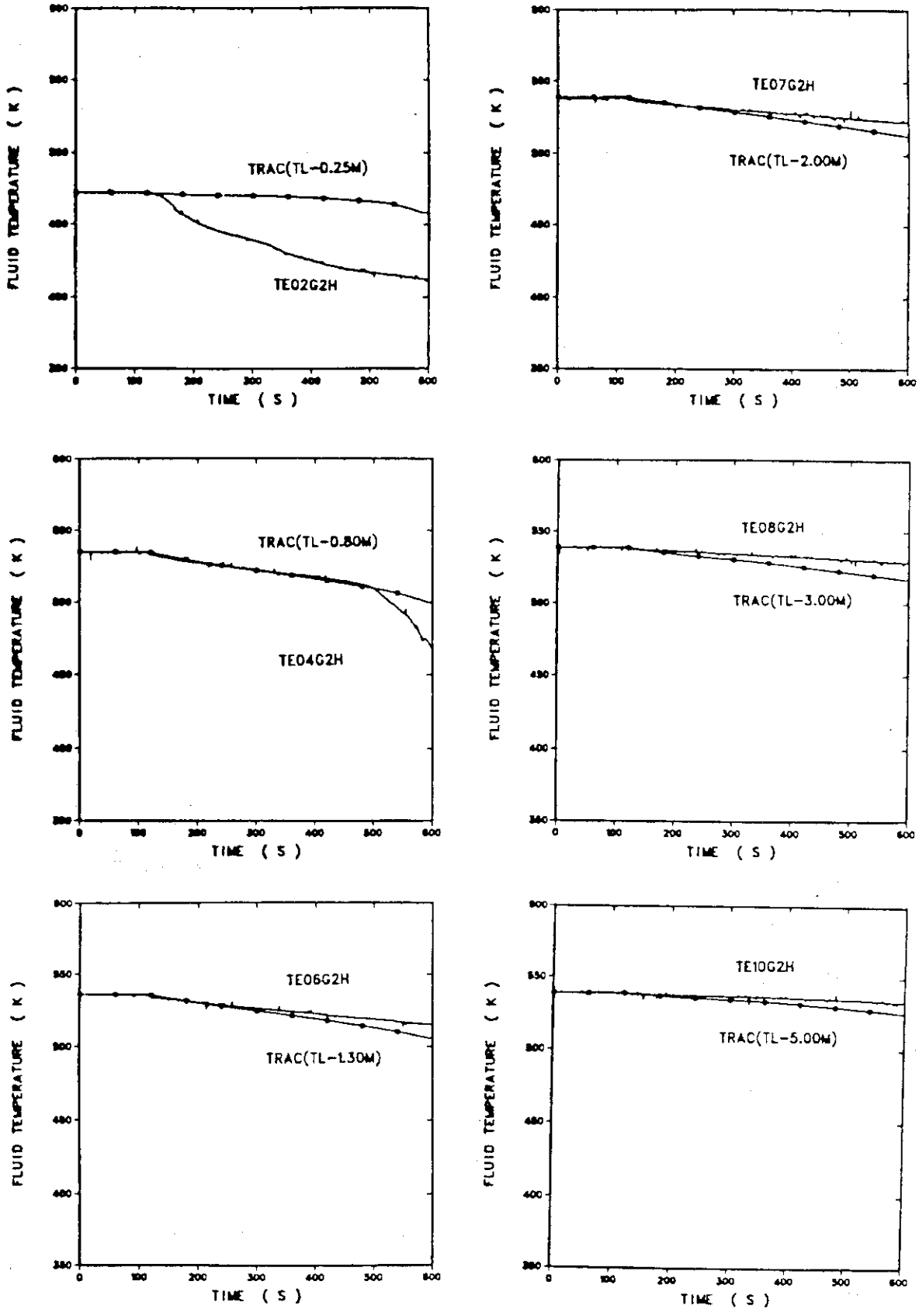

Fig. 20 Comparison of the liquid temperature transients at various elevations of the secondary side between CCTF and TRAC results.

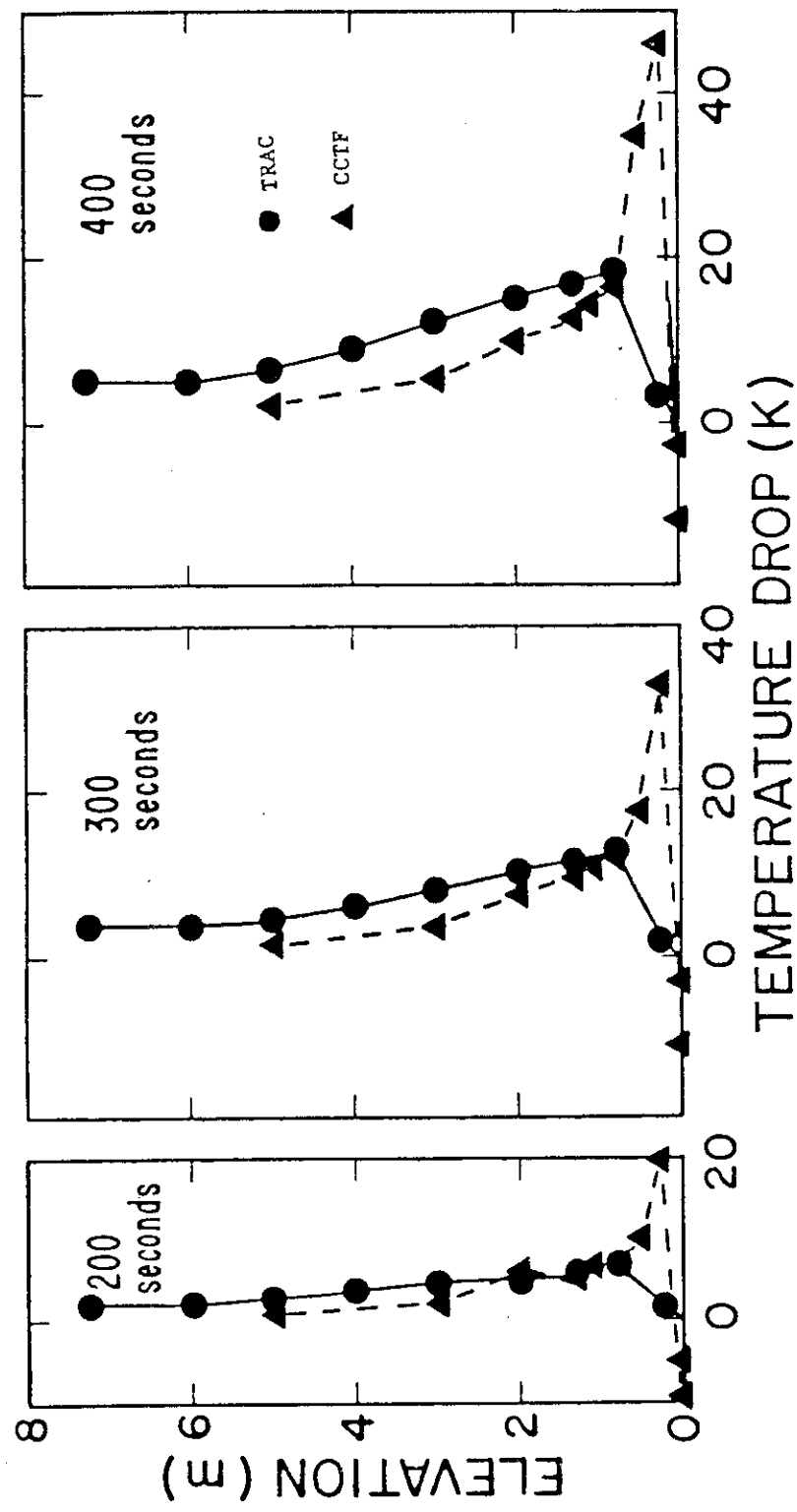

Fig. 21 Comarison of the liquid temperature drop from the initial temperature at 200, 300 and 400 s in the secondary side of the steam generator between CCTF and TRAC results.

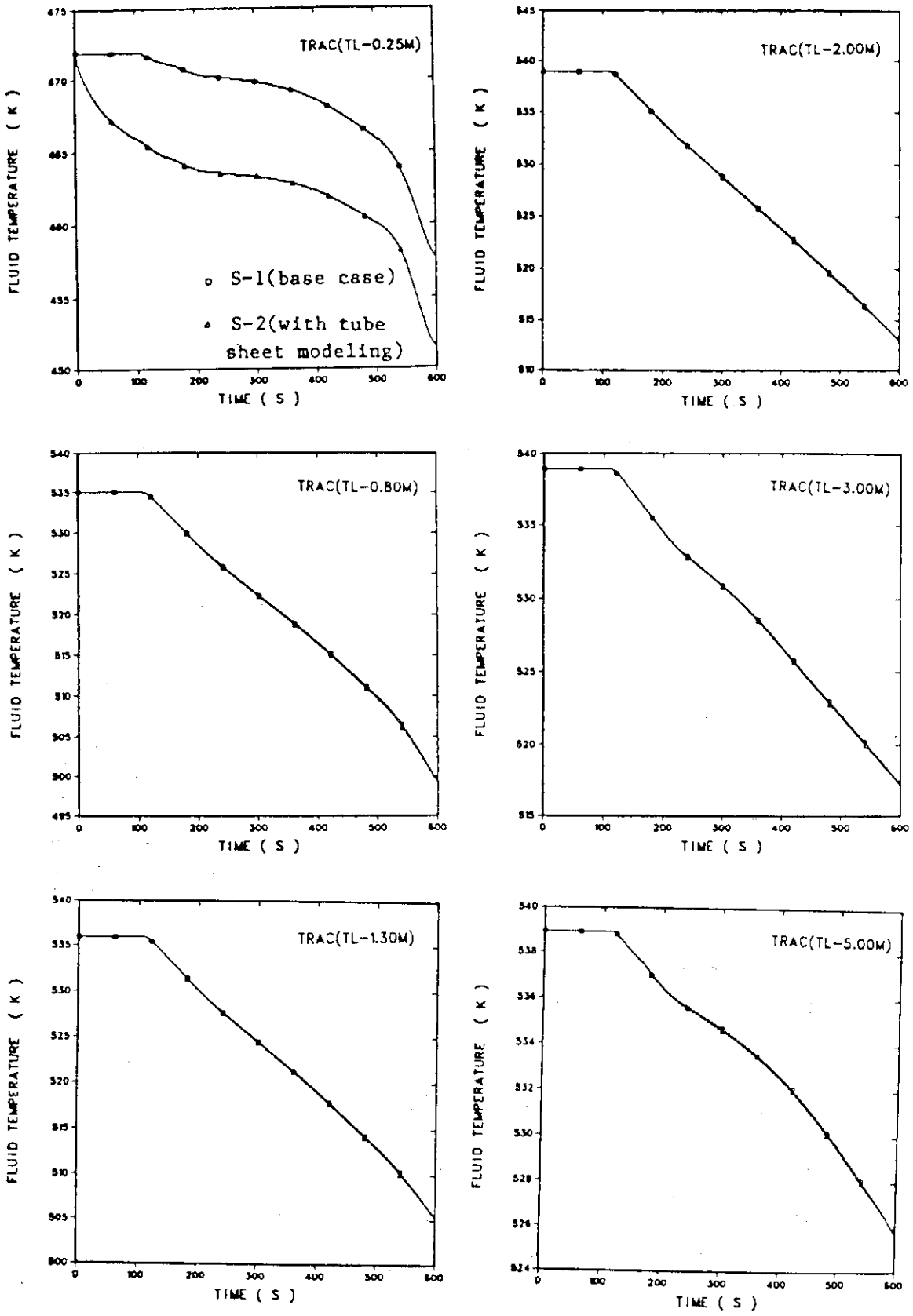

Fig. 22 Comparison of the liquid temperature transients at various elevations of the secondary side between S-1 (base case) and S-2 (with tube sheet modeling) calculations.

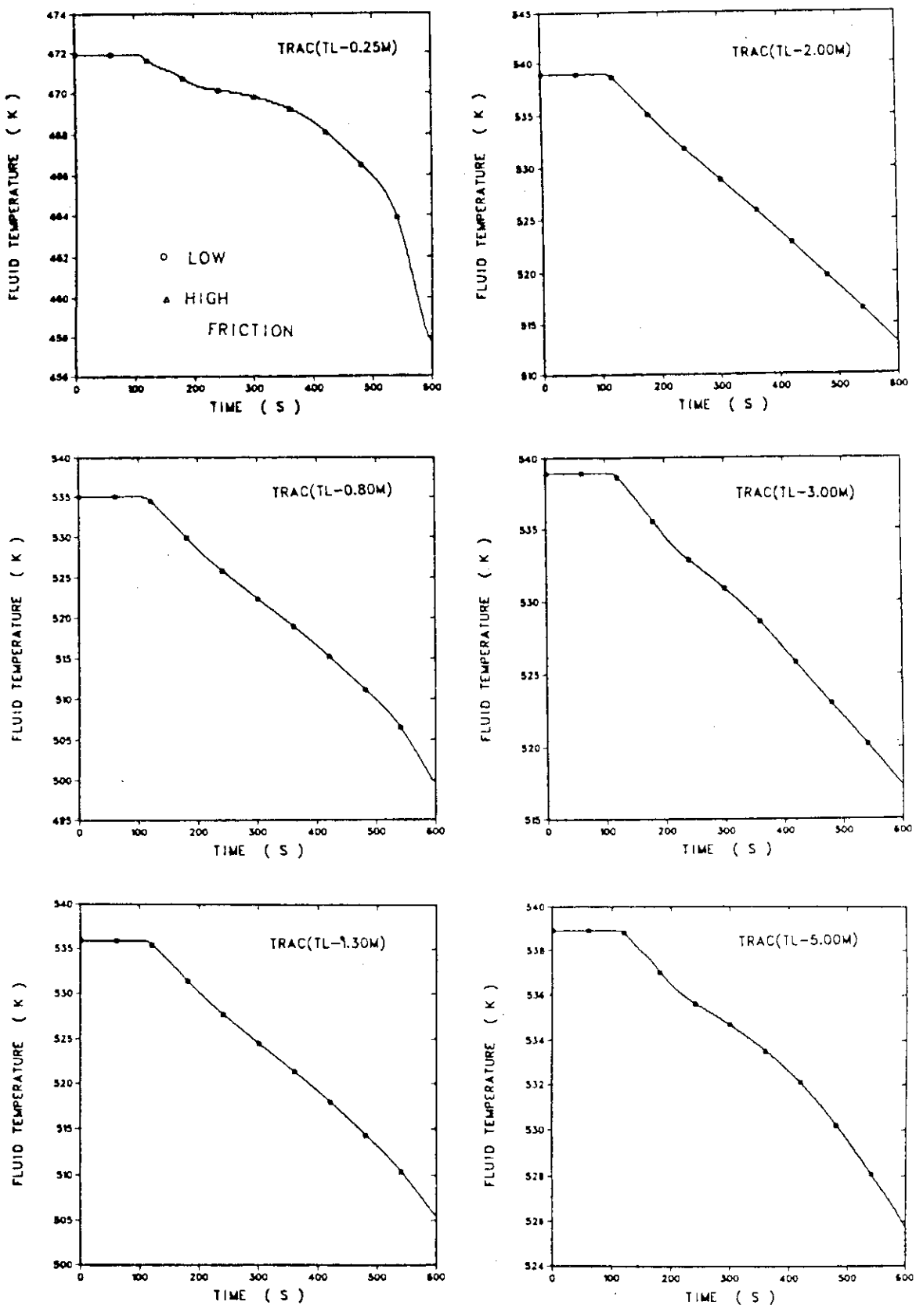

Fig. 23 Comparison of the liquid temperature transients at various elevations of the secondary side between S-1 (base case) and S-4 (with high friction factor in the secondary side) calculation.

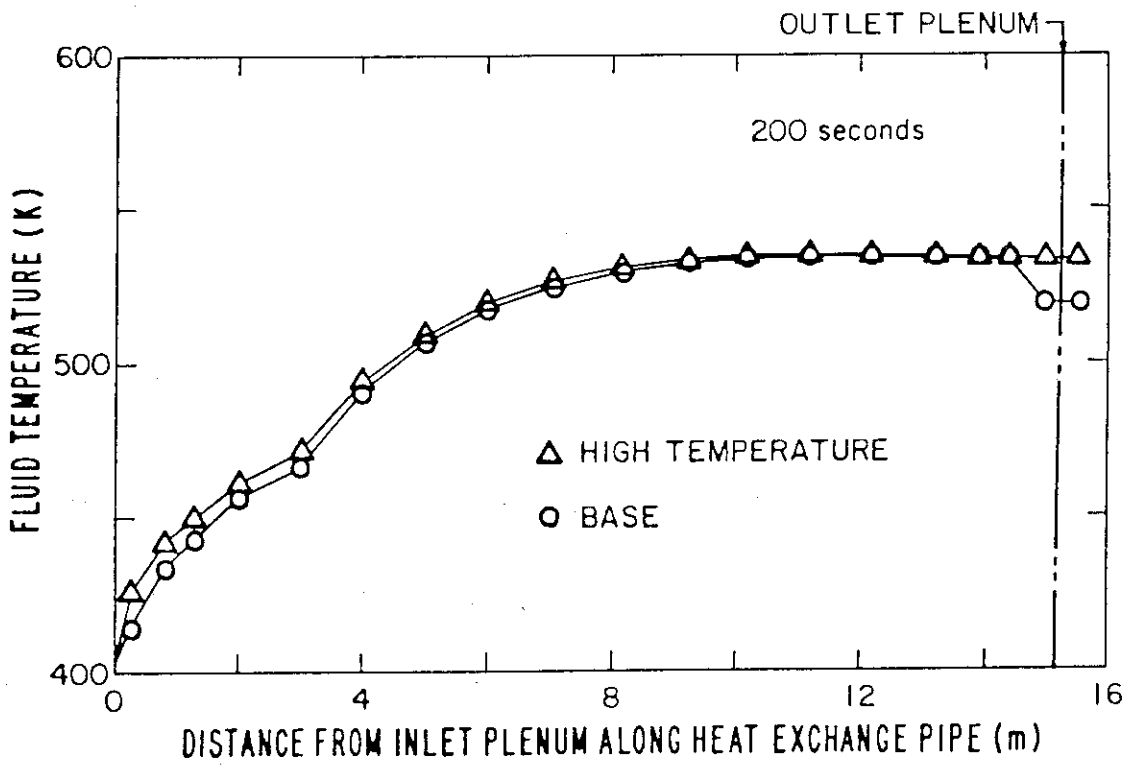

Fig. 24 Comparison of the steam temperature along the heat exchange pipe at 200 s between S-1 (base case) and S-3 (with high initial temperature at the bottom of the secondary side) calculations.

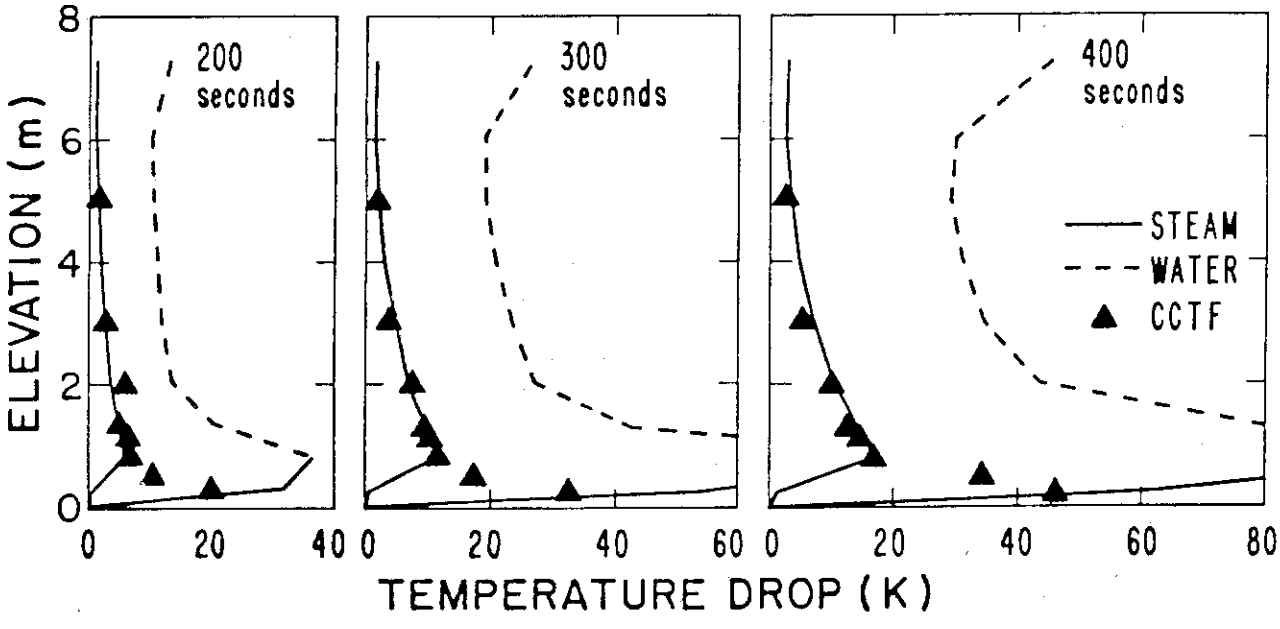

Fig. 25 Comparison of the liquid temperature drop from initial liquid temperature at 200, 300 and 400 s between CCTF results and S-5 (single phase water or steam flow at inlet) calculation.

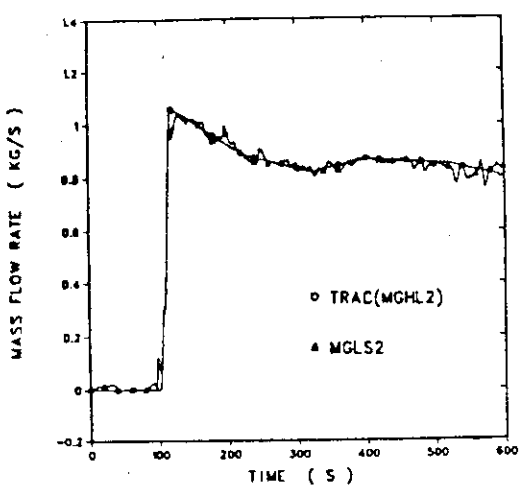

(a)Steam mass flow rate

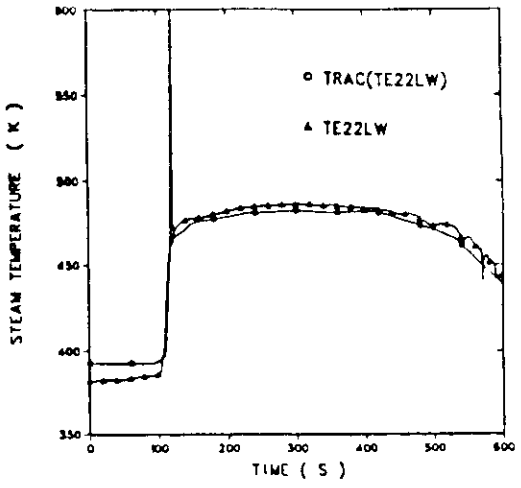

(b)Steam temperature

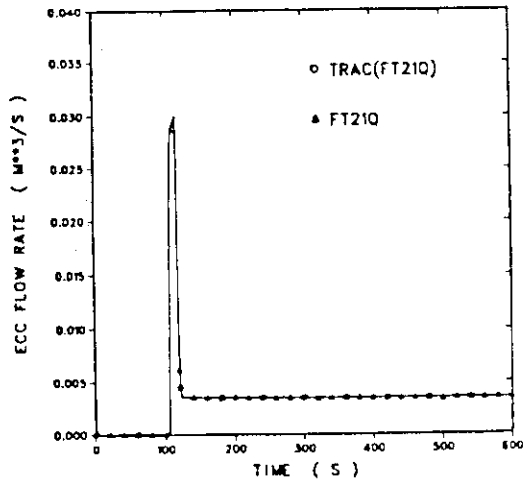

(c)ECC water flow rate

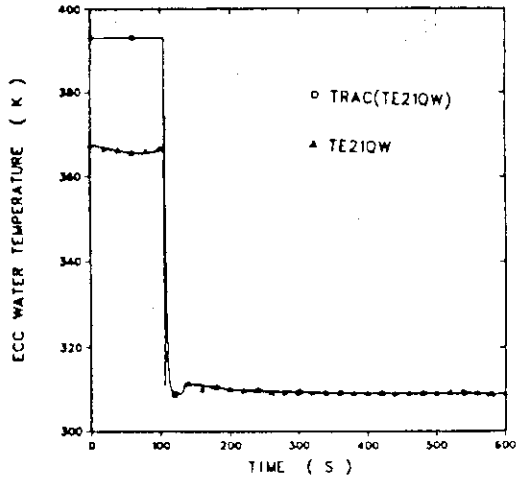

(d)ECC water temperature

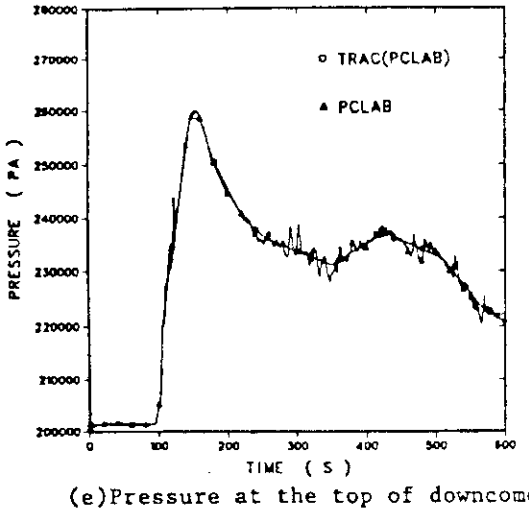

(e)Pressure at the top of downcomer

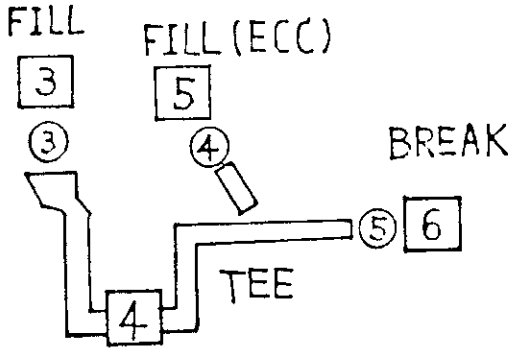

(f)TRAC input schematic

Fig. 26 TRAC input schematic and the boundary conditions for the cold leg study.

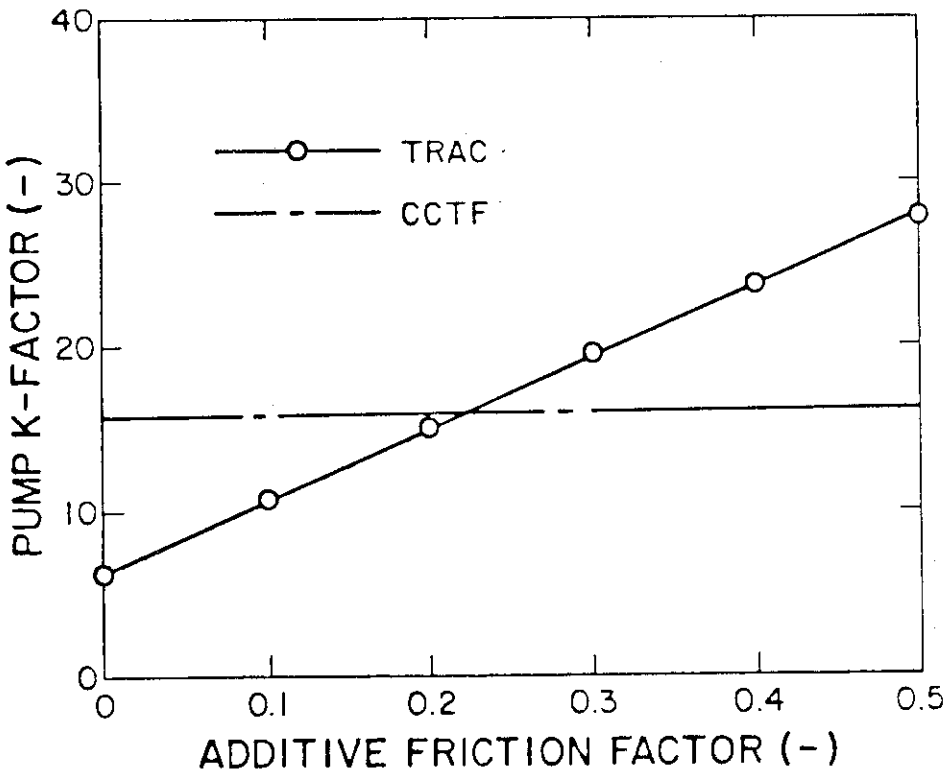

Fig. 27 Effect of additive friction factor on pump K-factor.

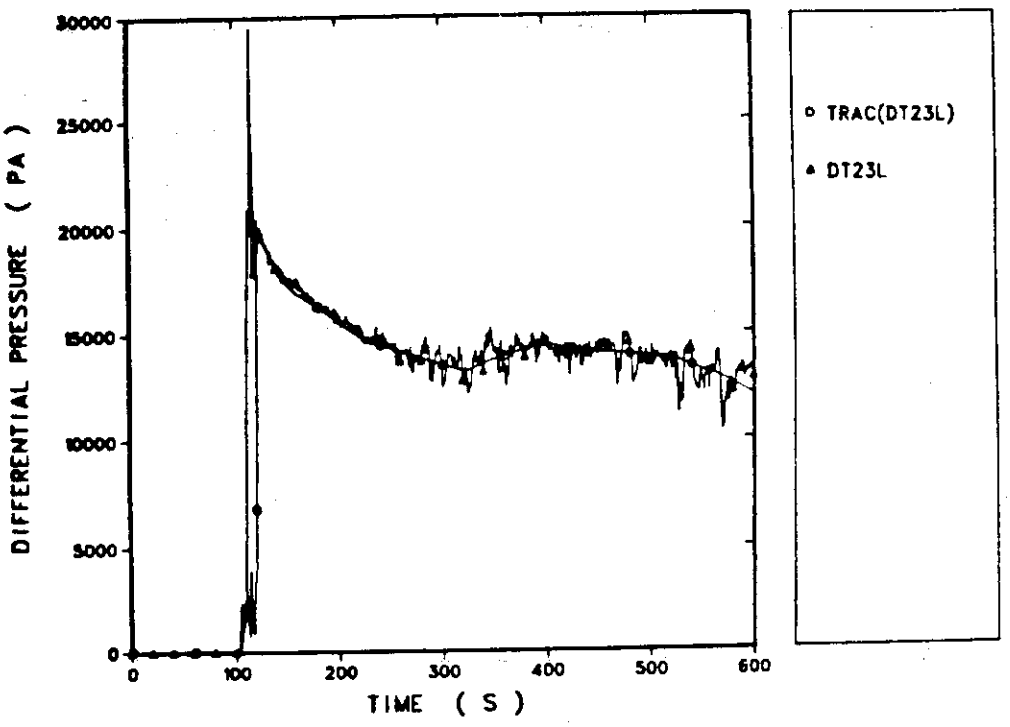

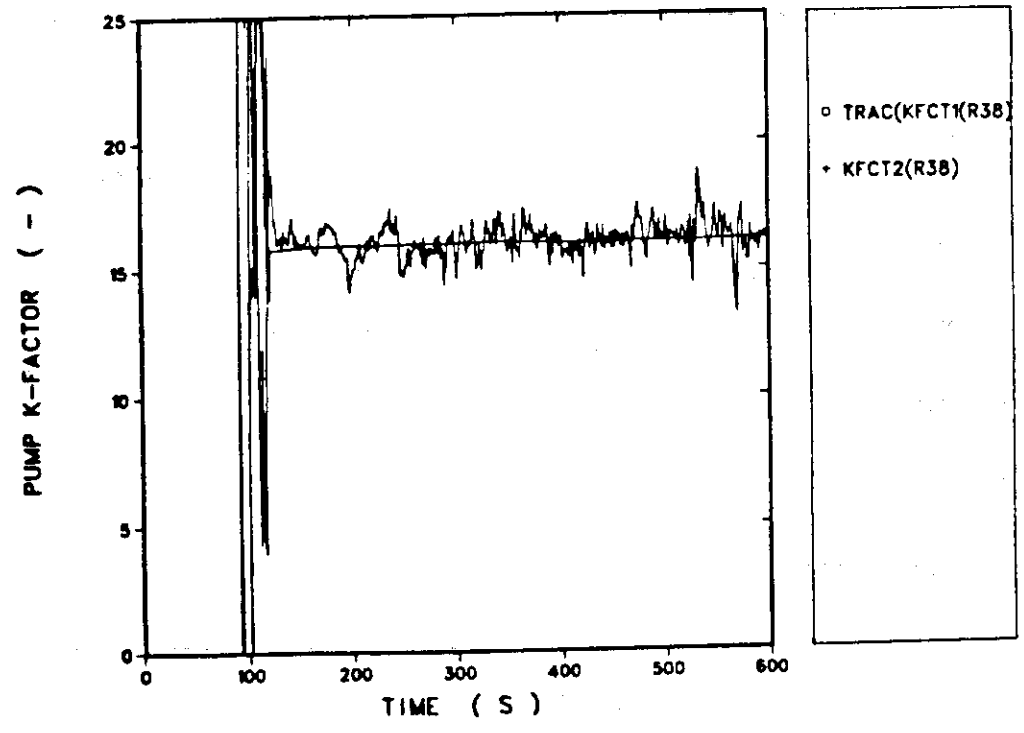

Fig. 28 Comparison of the differential pressure through the pump orifice part and the pump K-factor between CCTF and TRAC results.

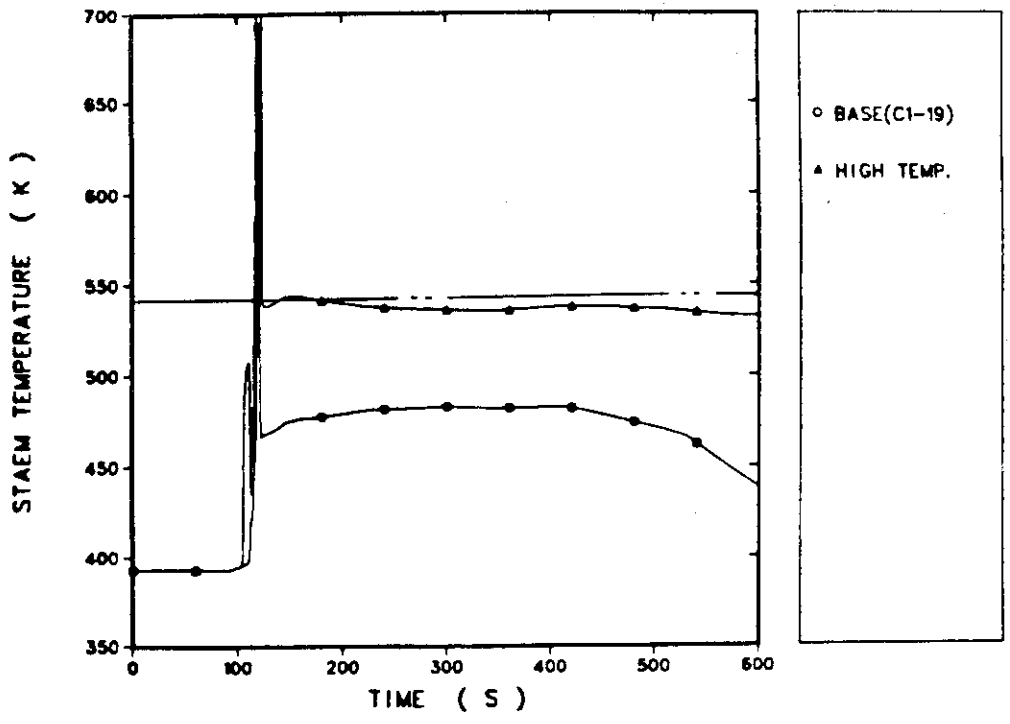

Fig. 29. Comparison of the steam temperature between C-2 (base case) and C-3 (high steam temperature)calculations.

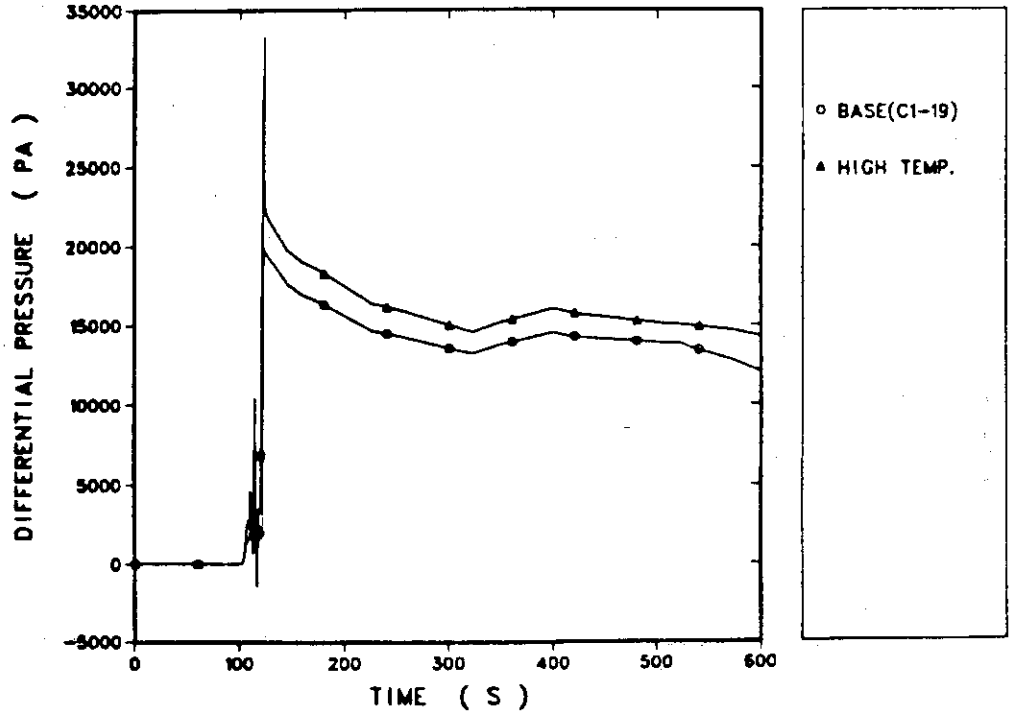

Fig. 30 Comparison of the differential pressure through the pump orifice part between C-2 (base case) and C-3 (high steam temperature) calculations.

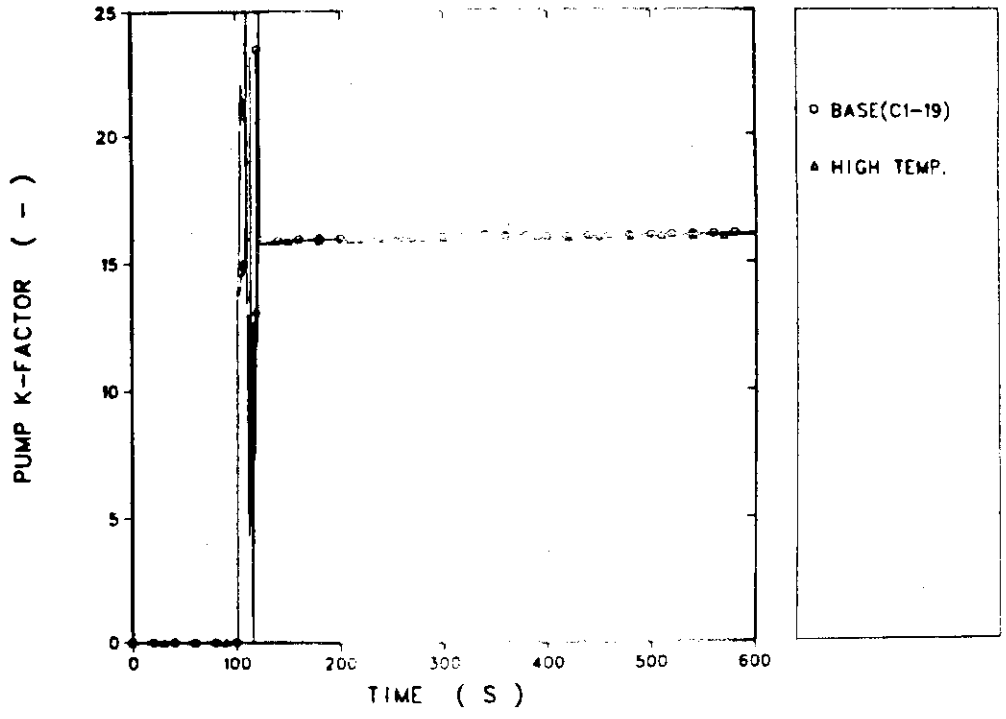

Fig. 31 Comparison of the pump K-factor between C-2 (base case) and C-3 (high steam temperature) calculations.

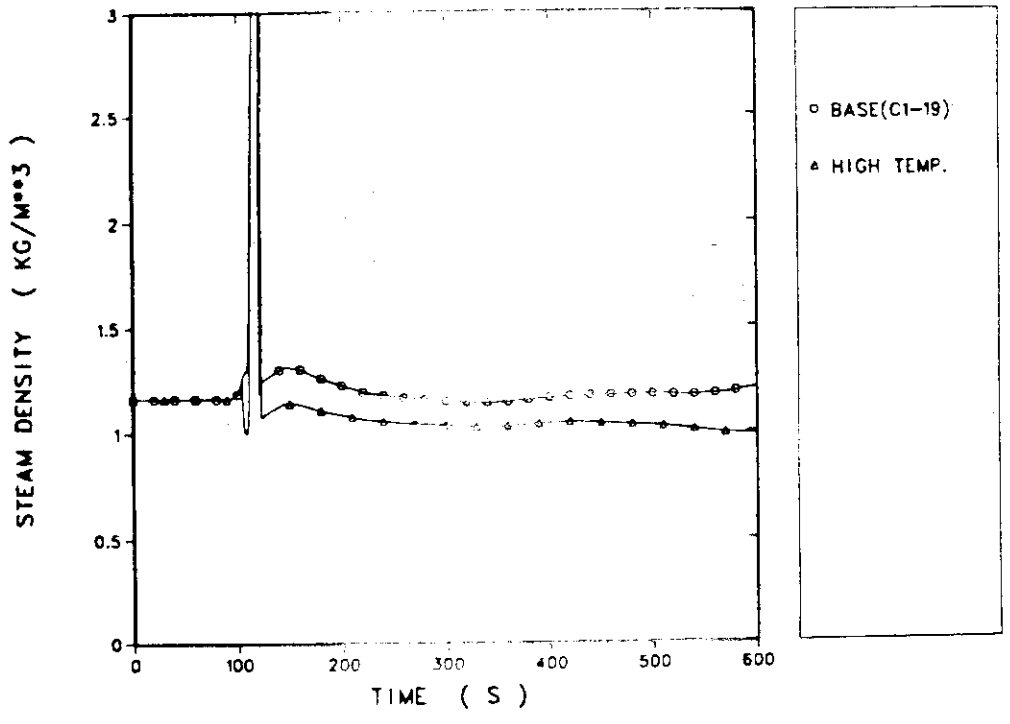

Fig. 32 Comparison of the steam density between C-2 (base case) and C-3 (high steam temperature) calculations.

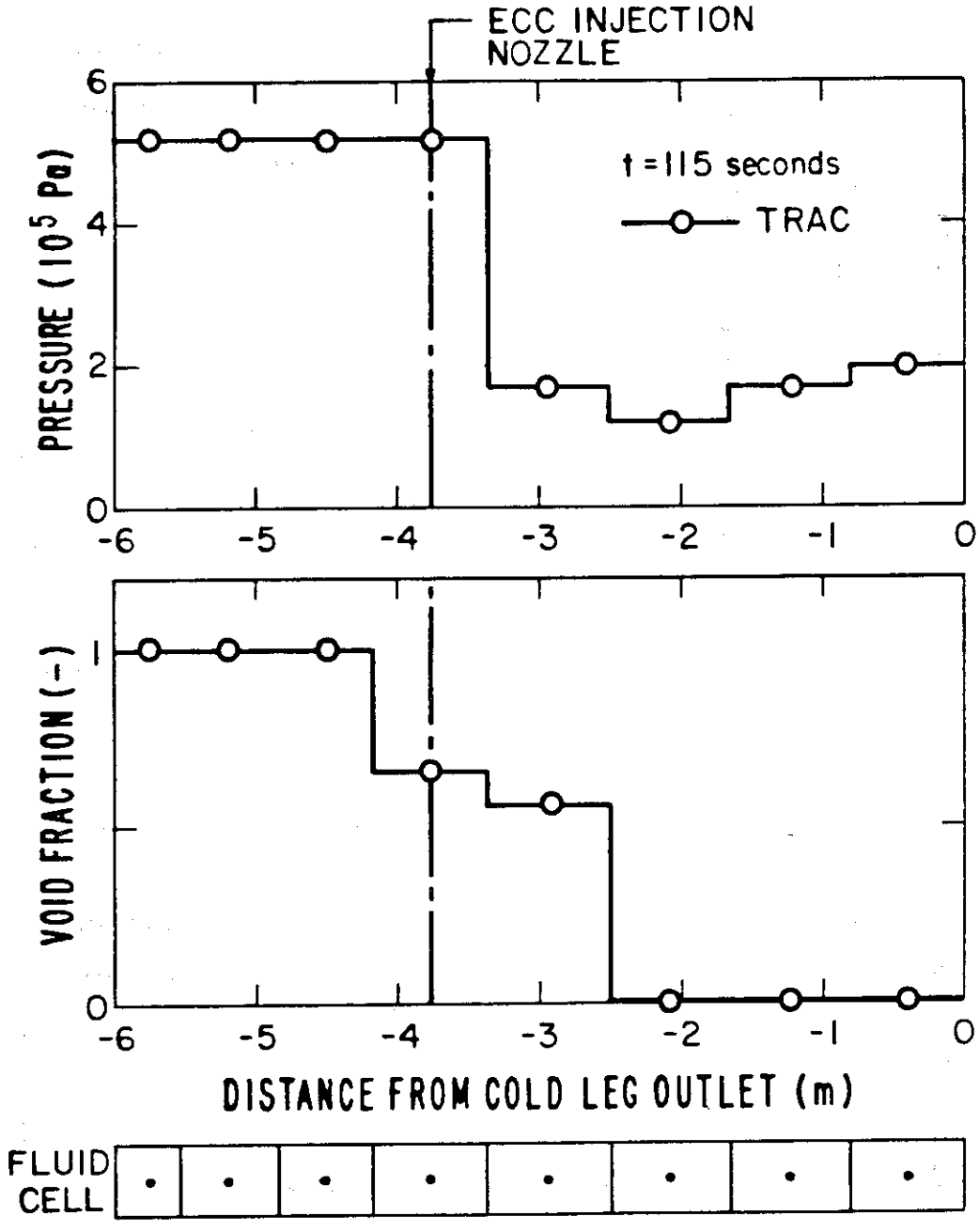

Fig. 33 Calculated pressure and void fraction profiles along the cold leg at 115 s.

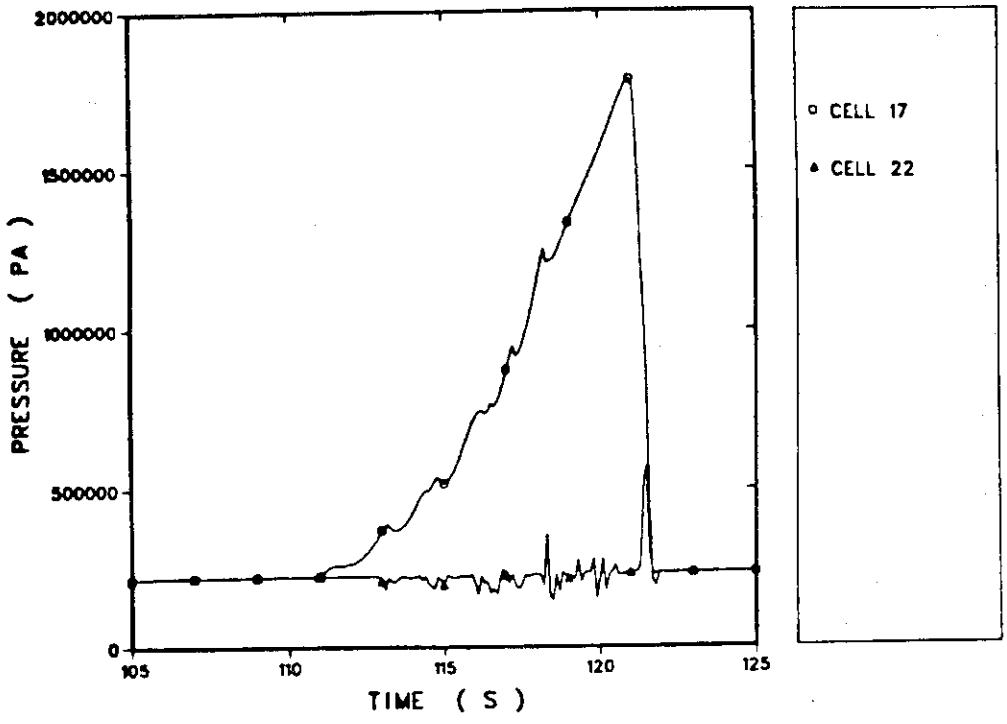

(a)Pressure transient at cells 17 and 22

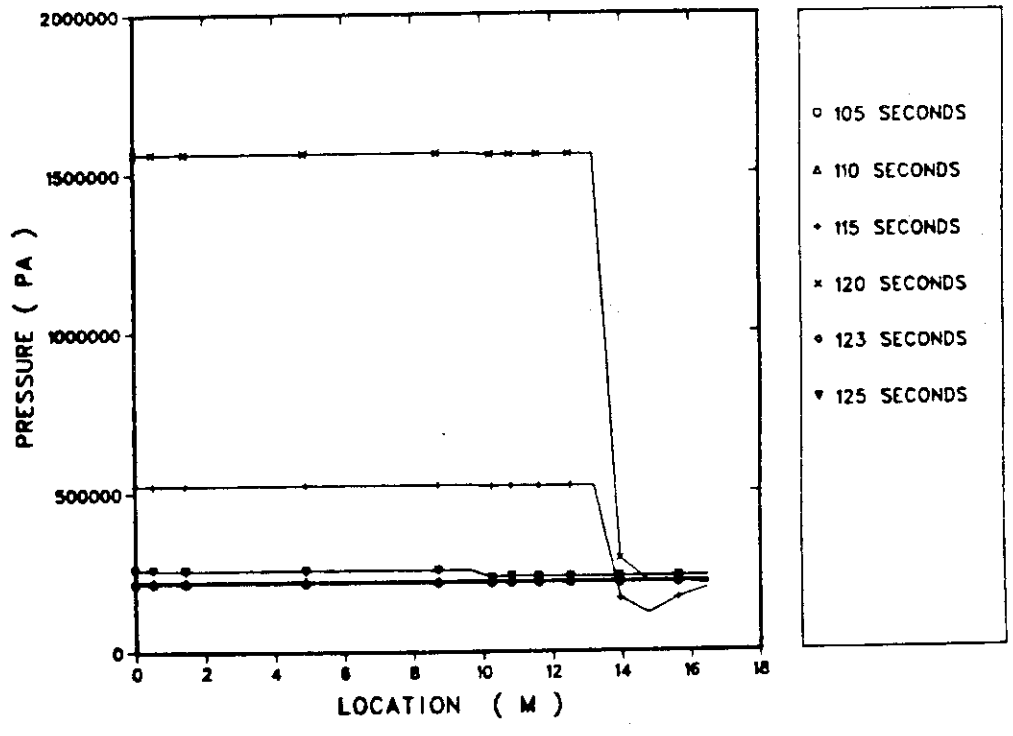

(b) Pressure profile along the TEE component

Fig. 34 Pressure transients and profiles during the accumulator injection (a) Pressure transients at cells 17 and 22 (b) Pressure profile along the cold leg.

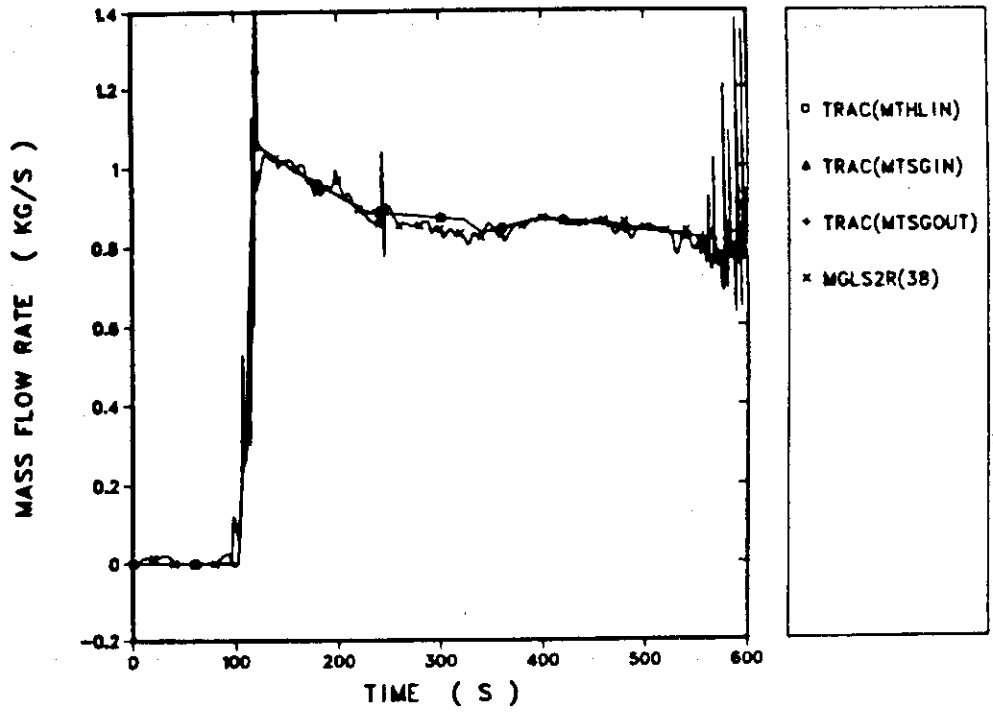

Fig. 35 Comparison of the mass flow rate through the loop between CCTF and TRAC results.

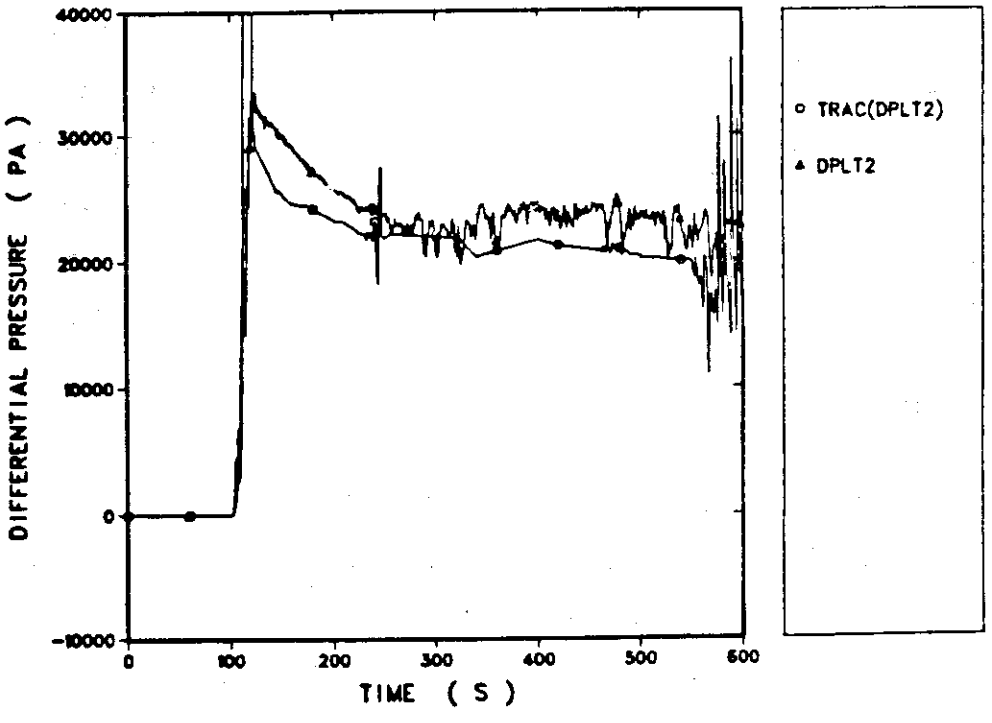

Fig. 36 Comparison of the total differential pressure through the loop between TRAC and CCTF results.

Appendix A

Source listing of the steam generator energy balance calculation program

```
$ftn (i=%me,cname=%mex,sym=^,short)
c
c       input for tidy
c        (tidy i="input" o="output")
c
*exempt
*nopack
*nostars
*nocollect
c       end tidy input
c       follow with program
c       this can be compiled and loaded under trix by:  run
c
       program sgcctf(tty,iin,twltot,twlsup,twlevp,
      1                tape6=tty
      2               ,tape5=iin
      3               ,tape55=twltot
      4               ,tape56=twlsup
      5               ,tape57=twlevp )
c
c  program for energy balance calculation of cctf sg
c
c
c      input file --- auxfile  made by trap ( format 3(1pe10.3) )
c         y(1,i)---fluid temp at sg secondary level 1
c         y(2,i)---fluid temp at sg secondary level 2
c           y(10,i)--fluid temp at sg secondary level 10
c           y(11,i)--total steam mass flow rate at sg exit(pitot data)
c           y(12,i)--fluid temp at sg outlet ( te231w )
c           y(13,i)--fluid temp at sg inlet  ( tesgin )
c
c      output file -- terminal
c           wltot(i)---total energy release from sg secondary in water mass
c           wlsup(i)---total energy to superheat steam
c           wlevp(i)---total energy used to evaporate incoming water
c
c
       dimension x(1000),y(13,1000),title(13)
        dimension q(10),dt(10),cp(10),dt0(10),dz(10),dz1(10)
       dimension qt(1000),wltot(1000),wlsup(1000),wlevp(1000)
       dimension tini(13)
c
       data (dz(i),i=1,10)/0.003,0.247,0.25,0.3,0.3,0.2,0.7,1.0,2.0,
      1                    2.4/
c
       data (dz1(i),i=1,10)/0.003,0.247,0.25,0.3,0.3,0.2,0.7,1.0,2.0,
      1                    2.6/
c
c
c  constant to estimate sectional heat release
c             924.0=( heat capacity of unit volume water at 240 c and 50 ata)
c            0.6301=( flow area of cctf sg-ii secondary side )
c             922.76=( heat capacity of unit volume tube  )
c            0.064776=( tube area of cctf sg-ii  )
c
         do 95 i=1,10
       cp(i)=924.0*0.3151*dz(i)+922.76*0.064776*dz1(i)
    95 continue
c
c
c
       read(5,8000) nc1
 8000 format(i5)
c
```

```
      write(6,8100) nc1
 8100 format(1h ///1h ,10x,16hecho of sgcctf  //1h ,10x,
     1   4hnc1=,i5///)
c
c
      do 1000 j=1,nc1
c
c   read title etc.
c
      read(5,*) xn
      npts=int(xn)
      read(5,8300) title(j)
 8300 format(a10)
c
      write(6,8400) title(j),npts
 8400 format(//1h ,5x,6htitle=,a10,5x,6h npts=,i5)
c
c  read data
c
      do 100 i=1,npts
c
      read(5,8500) x(i),y(j,i)
 8500 format(2(1pe10.3))
c
  100 continue
c
c  initial temperature
c
      tini(j)=0.0
c
      do 200 i=1,20
      tini(j)=tini(j)+y(j,i)
c
  200 continue
c
      tini(j)=tini(j)/20.0
c
      write(6,8600) tini(j)
 8600 format(1h ,5x,5hinit=,f10.2)
c
c
c
 1000 continue
c
c  average initial temp.  (each section)
c
      do 300 j=1,9
      dt0(j)=(tini(j+1)+tini(j))/2.0
  300 continue
      dt0(10)=tini(10)
c
c  heat release from secondary side
c
      dtime=1.0
      wlsup(1)=0.0
c
      do 2000 i=1,npts
c
c
c  heat release (each section)
c
      do 400 j=1,9
      dt(j)=-(y(j+1,i)+y(j,i))/2.0+dt0(j)
      q(j)=cp(j)*dt(j)
```

```
129   400 continue
130       dt(10)=dt0(10)-y(10,1)
131       q(10)=cp(10)*dt(10)
132 c
133 c  total heat release ( qt )
134 c
135       qt(1)=0.0
136       do 500 j=1,10
137       qt(1)=qt(1)+q(j)
138   500 continue
139 c
140 c  data print
141 c
142 c
143 c  calculate equivalent water m.f.r. to qt
144 c
145       wltot(1)=qt(1)/535.0
146 c
147       if(1.le.1) go to 550
148       sup1=y(11,1-1)*0.53*(y(12,1-1)-y(13,1-1))/535.0
149       sup2=y(11,1  )*0.53*(y(12,1  )-y(13,1  ))/535.0
150       sup=(sup1+sup2)/2.0
151       wlsup(1)=wlsup(1-1)+sup*dtime
152   550 continue
153       wlevp(1)=wltot(1)-wlsup(1)
154 c
155 c
156 c
157       k=mod(1-1,50)
158       if(k.ne.0) go to 10
159 c
160       10=1-1
161       write(6,8700) 10
162  8700 format(////2x,5htime=,14,4h sec//1h ,14htitle,dt0,dt,q)
163       do 600 j=1,10
164       write(6,8800) title(j),dt0(j),dt(j),q(j)
165  8800 format(1h ,10x,a10,2x,f10.2,2x,f10.2,2x,f10.2)
166   600 continue
167 c
168       write(6,8900) qt(1),wltot(1),wlsup(1),wlevp(1)
169  8900 format(/1h ,5x,6h   qt=,f12.2,2x,6hwltot=,f12.4/
170      1       /1h ,5x,6hwlsup=,f12.4,2x,6hwlevp=,f12.4///)
171 c
172    10 continue
173 c
174  2000 continue
175 c
176 c
177 c
178       write(55,9000)
179  9000 format(5h    1)
180       write(55,9100) npts
181  9100 format(15)
182       write(55,9200)
183  9200 format(11hwltot(cctf))
184       do 3000 1=1,npts
185       ti=float(i-1)
186       write(55,9300) ti,wltot(1)
187  9300 format(2(1pe10.3))
188  3000 continue
189 c
190 c
191 c
192       write(56,9000)
```

```
193         write(56,9100) npts
194         write(56,9400)
195    9400 format(1ihwlsup(cctf))
196         do 4000 i=1,npts
197         ti=float(i-1)
198         write(56,9300) ti,wlsup(i)
199    4000 continue
200 c
201 c
202 c
203         write(57,9000)
204         write(57,9100) npts
205         write(57,9500)
206    9500 format(1ihwlevp(cctf))
207         do 5000 i=1,npts
208         ti=float(i-1)
209         write(57,9300) ti,wlevp(i)
210    5000 continue
211         stop
212         end
```

Appendix B

TRAC input listing for loop calculation

```
trac
          5              0              0
cctf loop calculation
cctf test c1-19 transients
 com 1---fill(upper plenum)  com 2---pipe(hot leg)  com 3---stgen(steam gen.)
 com 4---tee(ls,pump,cold leg)  com 5---fill(ecc inj.)  com 6---break(dc top)
 com 7,com 8---fill(stgen secondary - zero fill)
            0              0                                              *  mccd 1
            0              1              8              7               1*  mccd 7
         .001         .00001         .0001          .001               0*  mccd 3
           10              0             10              0               0*  mccd 4
            1              0              0              0               0*  mccd 5
            1              2              3              4               5*  iorder
            6              7             8e
          101              0              0              0               0*  idsd
fill                       1              1 hot leg boundary cond.           card 1
            1              6            101              0              21*  card 6
            0              0              0              0            100.*  card 3
        0.800        .015135        1.00000        0.00000           392.9*  card 4
      3.000e5            0.0           0.00          0.000           392.9*  card 5
       2.5196                                                            *  vmsc1
          0.0            0.0          102.0           0.0s               *  vmtb
        120.0         0.2384          150.0         0.1522s
        170.0         0.2527          230.0         0.0521s
        340.0         0.1209          420.0         0.2125s
        500.0         0.2508          540.0         0.4121s
        580.0         0.4854          610.0         0.2018s
        870.0         0.2018          920.0         0.0000s
        930.0           0.00          940.0           0.00s
        950.0           0.00          960.0           0.00s
        970.0           0.00          980.0           0.00s
       1000.0         0.0000e
       1.0000            1.0            1.0            1.0          1.0*  vvsc1
          0.0         0.0000          102.0         0.0000s
        107.0         8.0820          110.0         8.6890s
        118.0         29.918          120.0         29.540s
        123.0         29.615          150.0         29.440s
        170.0         26.950          225.0         26.660s
        230.0         26.768          323.0         25.312s
        340.0         24.125          400.0         24.326s
        420.0         23.819          500.0         22.530s
        523.0         20.994          540.0         19.787s
        580.0         18.202          600.0         20.528s
        610.0         21.822e
          0.0          392.9          102.0          394.5s
        105.0          394.8          110.0          405.5s
        113.0          398.2          123.0          402.8s
        125.0          401.8          145.0          404.5s
        153.0          404.8          199.5          402.3s
        266.0          400.5          505.0          400.5s
        570.0          398.5          600.0          398.5s
        910.0          398.5          920.0          398.5s
        930.0          398.5          940.0          398.5s
        950.0          398.5          960.0          398.5s
       1000.0          398.5e
          0.0          392.9          102.0          394.5s
        105.0          394.8          110.0          405.5s
        113.0          398.2          123.0          402.8s
        125.0          401.8          145.0          404.5s
        153.0          404.8          199.5          402.3s
        266.0          400.5          505.0          400.5s
        570.0          398.5          600.0          398.5s
        910.0          398.5          920.0          398.5s
        930.0          398.5          940.0          398.5s
        950.0          398.5          960.0          398.5s
       1000.0          398.5e
```

```
 67            0.0          0.99          50.0          0.99s
 68          100.0          0.99         150.0          0.99s
 69          200.0          0.99         250.0          0.99s
 70          300.0          0.99         350.0          0.99s
 71          400.0          0.99         450.0          0.99s
 72          500.0          0.99         550.0          0.99s
 73          600.0          0.99         650.0          0.99s
 74          910.0          0.99         920.0          0.99s
 75          930.0          0.99         940.0          0.99s
 76          950.0          0.99         960.0          0.99s
 77         1000.0          0.99e
 78            0.0       3.00e5          50.0       3.00e5s
 79          100.0       3.00e5         150.0       3.00e5s
 80          200.0       3.00e5         250.0       3.00e5s
 81          300.0       3.00e5         350.0       3.00e5s
 82          400.0       3.00e5         450.0       3.00e5s
 83          500.0       3.00e5         550.0       3.00e5s
 84          600.0       3.00e5         650.0       3.00e5s
 85          910.0       3.00e5         920.0       3.00e5s
 86          930.0       3.00e5         940.0       3.00e5s
 87          950.0       3.00e5         960.0       3.00e5s
 88         1000.0       3.00e5e
 89            0.0         0.00          50.0          0.00s
 90          100.0         0.00         150.0          0.00s
 91          200.0         0.00         250.0          0.00s
 92          300.0         0.00         350.0          0.00s
 93          400.0         0.00         450.0          0.00s
 94          500.0         0.00         550.0          0.00s
 95          600.0         0.00         650.0          0.00s
 96          910.0         0.00         920.0          0.00s
 97          930.0         0.00         940.0          0.00s
 98          950.0         0.00         960.0          0.00s
 99         1000.0         0.00e
100 pipe                     2              2 hot leg--intact loop        *  card 1
101              10          2              1              2             6*  card 2
102               1          0              0              0             0*  card 3
103         .07760        .005             0.             0.         293.*  card 4
104           293.           0.
105          0.8000       0.9456         0.9456         1.0176       0.4500*  dx
106          0.9320       0.7765         0.2131         0.4400       0.3000e
107       0.015134     0.017889       0.017889       0.019251     0.008513*  vol
108       0.017631     0.014690       0.004032       0.008325     0.005676e
109 r08     .01892       .01892        0.01892        0.01892e             *  fa
110 f          0.0e                                                       *  fric
111 r 6     0.0r 2      0.766r 3         1.0e                             *  grav
112 r 8     0.1552       0.1552        0.1552         0.1552e              *  hd
113 f            1e                                                       *  nff
114 f           1.e                                                       *  alp
115 f          0.0e                                                       *  vl
116 f          0.0e                                                       *  vv
117 f         392.9e                                                      *  tln
118 f         392.9e                                                      *  tvn
119 f       2.012e5e                                                      *  p
120 f          0.0e                                                       *  pa
121 f          0.0e                                                       *  qppp
122 f            6e                                                       *  material
123 f         392.9e                                                      *  tw
124 stgen                    3              3 steam generator-intact loop*  card 1
125              20          2              2              3             7*  card 2
126               1          0              1              1             *  card 3
127         .009800      .002900                                         *  card 4
128               9             6           7                            *  card 5
129 r 2     0.500r 1       0.60        0.40r 5       1.000r 2      1.100*  dx
130 r 5       1.000        0.400       0.600r 2       0.500e
131 r 1   0.00946r 1     0.02384        0.02860      0.01907r 5   0.04767*  vol
132 r 2   0.05244r 5     0.04767        0.01907        0.02860    0.023840
133         0.07093e
134         0.01892r19      .04767      0.16604e                          *  fa
135 f            0.e                                                      *  fric
136 r10          1.0          0.0r10       -1.0e                          *  grav
137           .15520r19        .0196        .3957e                        *  hd
138                1             1r17          1              1          1e*  nff
139 f           1.e                                                       *  alp
140 f           0.e                                                       *  vl
141 f          0.0e                                                       *  vv
142           392.9         471.88         534.96       535.89r12    538.90s*  tv
143          535.89         534.96         471.88         392.90e
144           392.9         471.88         534.96       535.89r12    538.90s*  tl
145          535.89         534.96         471.88         392.90e
146 f       2.012e5e                                                      *  p
147 f          0.0e                                                       *  pa
```

```
148 f          7e                                                          *  material
149 r02     392.90r02     471.88r02     534.96r02     535.89r24     538.90s*  tv
150 r02     535.89r02     534.96r02     471.88r02     392.90e
151          0.50          0.60          0.40r 5          1.00          1.50e*  dx
152         0.1575         0.1890        0.1260r 5       0.3151        0.6960e*  vol
153           0.r 8          .3151           0.e                             *  fa
154 f        0.000e
155 f          1.e                                                           *  grav
156           0.0r 8     0.019054           0.0e                             *  hd
157 f          1e                                                            *  nff
158 r 8         0.           .600e                                          *  alp
159 f          0.e                                                           *  vl
160 f          0.0e                                                          *  vv
161         471.88        534.96        535.89        538.90        538.90s*  tl
162         538.90        538.90        538.90        538.90e
163         471.88        534.96        535.89        538.90        538.90s*  tv
164         538.90        538.90        538.90        538.90e
165        5.200e6       5.195e6       5.191e6       5.185e6       5.177e6s*  pf
166        5.169e6       5.161e6       5.153e6       5.150e6e
167 f          0.0e                                                          *  pa
168            0.0          4.8644        5.8373        3.8916r 5     9.7289*  wa-pri
169 r 2    10.7018r 5       9.7289        3.8916        5.8373        4.8644
170            0.0e
171           6.3039        7.5647        5.0431r 5     12.6078       13.8686e*  waa-sec
172 tee                          4                4 cold leg--intact loop          card 1
173              18              2                6          -.707          1*  card 2
174               0             22                3              5          0*  card 3
175          0.0776         0.005                0              0       293.*  card 4
176            293.              0                0              0          0*  card 5
177               0              1                4              0          0*  card 6
178           .02350           .004                0              0       293.*  card 7
179            293.              0                0              0          0*  card 8
180          0.3000         0.4400        0.2131        0.9914        1.8866*  dx
181          2.1400         2.2800        0.9400        0.9000        0.3290
182          0.2750         0.2520        0.5240        0.2600        0.4400
183          0.6850         0.6850        0.8000        0.8573        0.8573
184          0.8573         0.8000e
185        0.046595       0.057256      0.029039      0.018755      0.035691*  vol
186        0.040484       0.043133      0.017783      0.017026      0.010129
187        0.018796       0.007607      0.015818      0.095500      0.008324
188        0.012956       0.012956      0.015134      0.016218      0.016218
189        0.016218       0.015134e
190         0.16604        0.14471     0.11607r 7      0.01892     0.0070882*  fa
191 r 3  0.030187r 9       0.01892e
192 r10         0.           0.215f          0.e                             *  fric
193 r 3        -1.       -0.76604r 2        -1.r 2          0.r 6         1.*  grav
194 r 9         0.e
195          0.3957         0.3688        0.3294r 7       0.1552        0.0950*  hd
196 r 3    0.04734r 9       0.1552e
197 f          1e                                                            *  nff
198 f          1.e                                                           *  alp
199 f          0.e                                                           *  vl
200 f          0.0e                                                          *  vv
201 f         392.9e                                                         *  tln
202 f         392.9e                                                         *  tvn
203 f        2.012e5e                                                        *  p
204 f          0.0e                                                          *  pa
205 f          0.e                                                           *  qppp
206 f           6e                                                           *  material
207 f         392.9e                                                         *  tw
208 f        3.0000e                                                         *  dx
209 f        .115450e                                                        *  vol
210 f        .001735e                                                        *  fa
211 f          0.e                                                           *  fric
212 f         .707e                                                          *  grav
213 f         .047e                                                          *  hd
214 f            0e                                                          *  nff
215             1.0e
216 f          0.e                                                           *  vl
217 f          0.0e                                                          *  vv
218 f        392.90e                                                         *  tvn
219 f         392.9e                                                         *  tln
220 f        2.012e5e                                                        *  p
221 f          0.0e                                                          *  pa
222 f          0.e                                                           *  qppp
223 f           6e                                                           *  material
224 f        392.90e                                                         *  tw
```

```
fill                 5             5 cold leg ecc injection           card 1
           4         6           101            0             15*  card 6
           0         0             0            0            100.* card 3
       3.000   .011545       1.00000      0.00000          392.9*  card 4
     6.000e5       0.0          0.00        0.000          392.9*  card 5
      576.37                                                   *  vmscl
         0.0       0.0         105.0         0.0s              *  vmtb
       108.0   0.02531         109.0     0.02800s
       110.0   0.02860         117.0     0.03000s
       119.0   0.00917         121.0     0.00440s
       123.0  0.003524         150.0    0.003520s
       200.0  0.003480         300.0    0.003460s
       400.0  0.003460         500.0    0.003460s
       700.0  0.003460e
      1.0000       1.0           1.0          1.0             1.0*  vvscl
         0.0      0.00          50.0        0.00s
       100.0      0.00         150.0        0.00s
       200.0      0.00         250.0        0.00s
       300.0      0.00         350.0        0.00s
       400.0      0.00         450.0        0.00s
       500.0      0.00         550.0        0.00s
       600.0      0.00         650.0        0.00s
      1000.0     0.00e
         0.0     392.9         105.0       392.9s
       106.0     310.8         107.0       316.6s
       108.0     374.3         109.0       338.4s
       111.0     316.6         113.0       311.5s
       117.0     308.9         131.0       309.1s
       136.0     311.4         150.0       311.4s
       200.0     310.0         400.0       309.0s
       700.0    309.0e
         0.0     392.9         105.0       392.9s
       106.0     310.8         107.0       316.6s
       108.0     374.3         109.0       338.4s
       111.0     316.6         113.0       311.5s
       117.0     308.9         131.0       309.1s
       136.0     311.4         150.0       311.4s
       200.0     310.0         400.0       309.0s
       700.0    309.0e
         0.0      0.00          50.0        0.00s
       100.0      0.00         150.0        0.00s
       200.0      0.00         250.0        0.00s
       300.0      0.00         350.0        0.00s
       400.0      0.00         450.0        0.00s
       500.0      0.00         550.0        0.00s
       600.0      0.00         650.0        0.00s
      1000.0     0.00e
         0.0    6.00e5          50.0      6.00e5s
       100.0    6.00e5         150.0      6.00e5s
       200.0    6.00e5         250.0      6.00e5s
       300.0    6.00e5         350.0      6.00e5s
       400.0    6.00e5         450.0      6.00e5s
       500.0    6.00e5         550.0      6.00e5s
       600.0    6.00e5         650.0      6.00e5s
      1000.0   6.00e5e
         0.0      0.00          50.0        0.00s
       100.0      0.00         150.0        0.00s
       200.0      0.00         250.0        0.00s
       300.0      0.00         350.0        0.00s
       400.0      0.00         450.0        0.00s
       500.0      0.00         550.0        0.00s
       600.0      0.00         650.0        0.00s
      1000.0     0.00e
```

```
break                    6          6 cold leg break-vessel side     card 1
          5              1         14              3              0*  card 2
      0.800       .015134         1.          392.9       2.012e5*  card 3
         0.             0          0              0              0*  pain
        1.0                                                      *  pscl
        0.0      2.012e5       94.0       2.012e5s
      102.0      2.065e5      106.0       2.201e5s
      146.0      2.586e5      160.0       2.586e5s
      177.0      2.515e5      221.0       2.400e5s
      257.0      2.358e5      350.0       2.311e5s
      425.0      2.370e5      508.0       2.323e5s
      573.0      2.223e5      900.0       2.199e5e
fill                     7          7 st. gen. sec.-intact loop      card 1
          6              1          0              0              0*  card 2
          0              0        0.9            0.0          100.0*  card 3
        1.1         0.1980         0.             0.            400.*  card 4
    5.20e6             0.          0              0            400.*  card 5
fill                     8          8 st. gen. sec.-intact loop      card 1
          7              1          0              0              0*  card 2
          0              0        0.9            0.0          100.0*  card 3
        1.1         1.1051         0.             0.            535.*  card 4
    5.15e6             0.          0              0            535.*  card 5
    1.0e-6          0.200      102.0
       25.0           0.50       25.0
    1.0e-6          0.050      106.0
        1.0           0.10        1.0
    1.0e-6          0.020      112.0
        1.0           0.10        1.0
    1.0e-6          0.010      116.0
        1.0           0.10        1.0
    1.0e-6          0.005      120.0
        1.0           0.10        1.0
    1.0e-6          0.020      124.0
        1.0           0.10        1.0
    1.0e-6          0.050      125.0
        1.0           0.10        1.0
    1.0e-6          0.100      200.0
       10.0           0.10       10.0
    1.0e-6          0.500      600.0
       25.0           0.50       25.0
       -1.
```

Appendix C

Main result of loop calculation for CCTF test C1-19 (Run 38)

List of figures for Appendix C

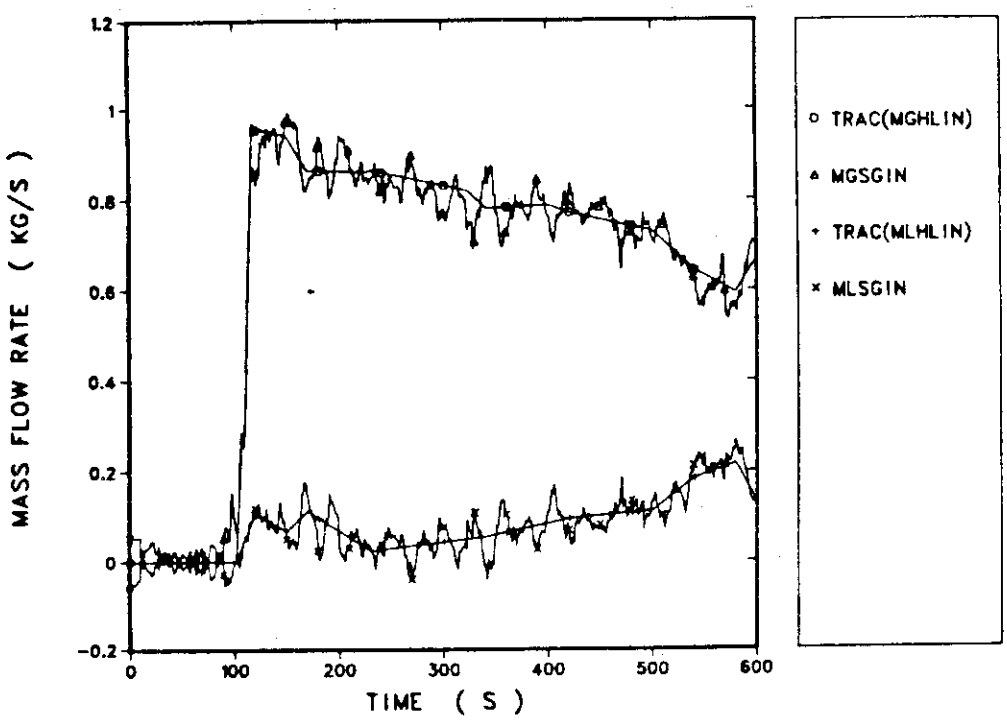

Fig. C.1 Water and steam mass flow rate.

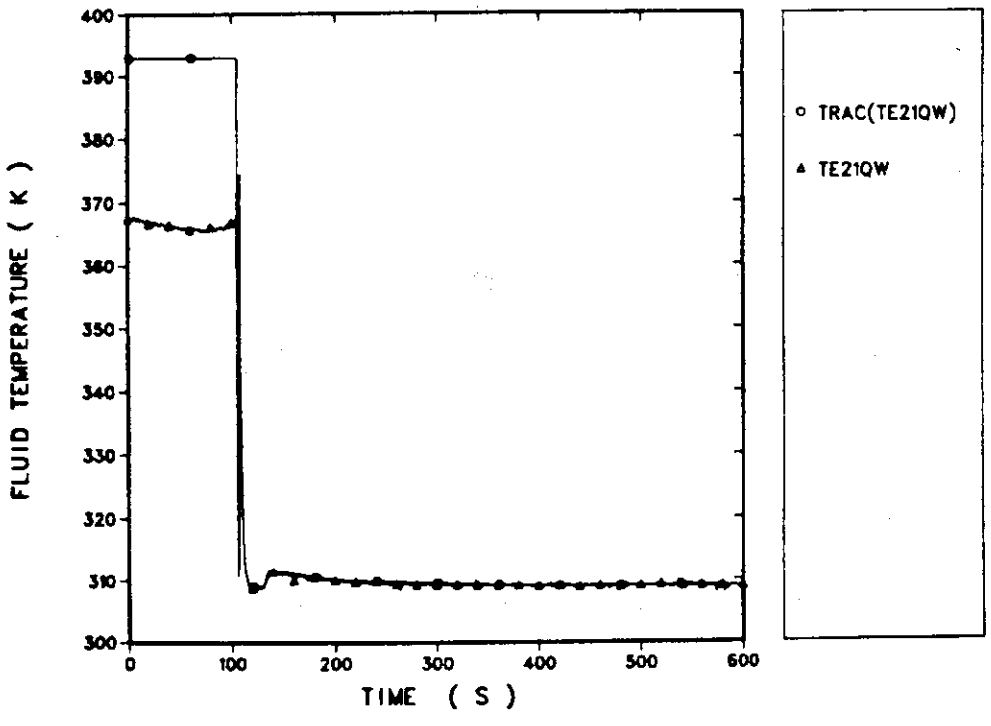

Fig. C.2 ECC water temperature.

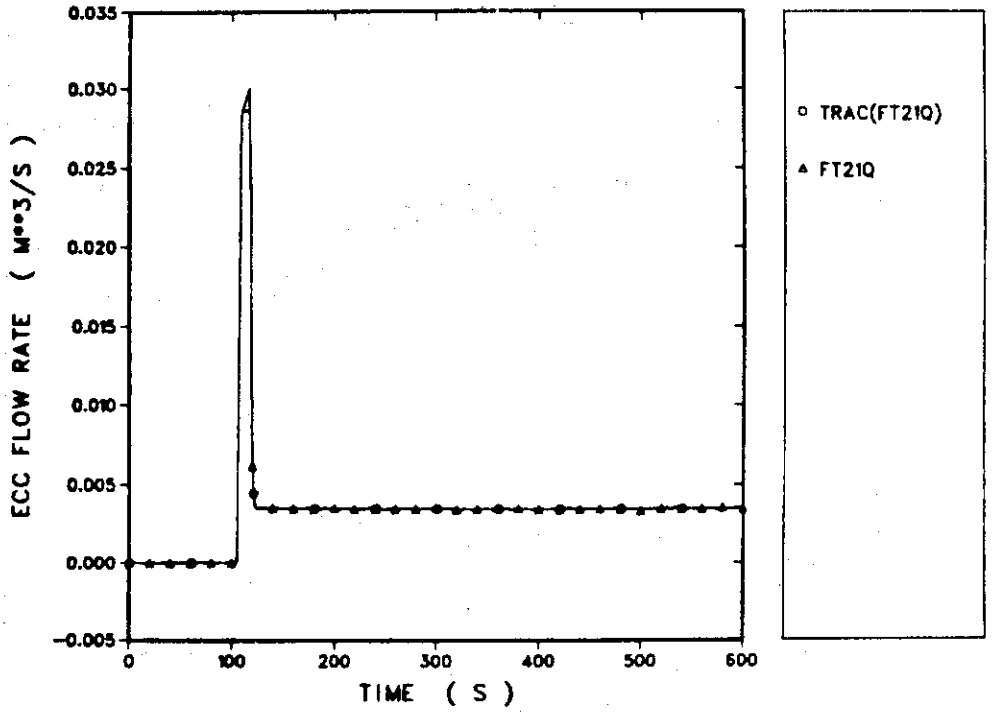

Fig. C.3 ECC flow rate.

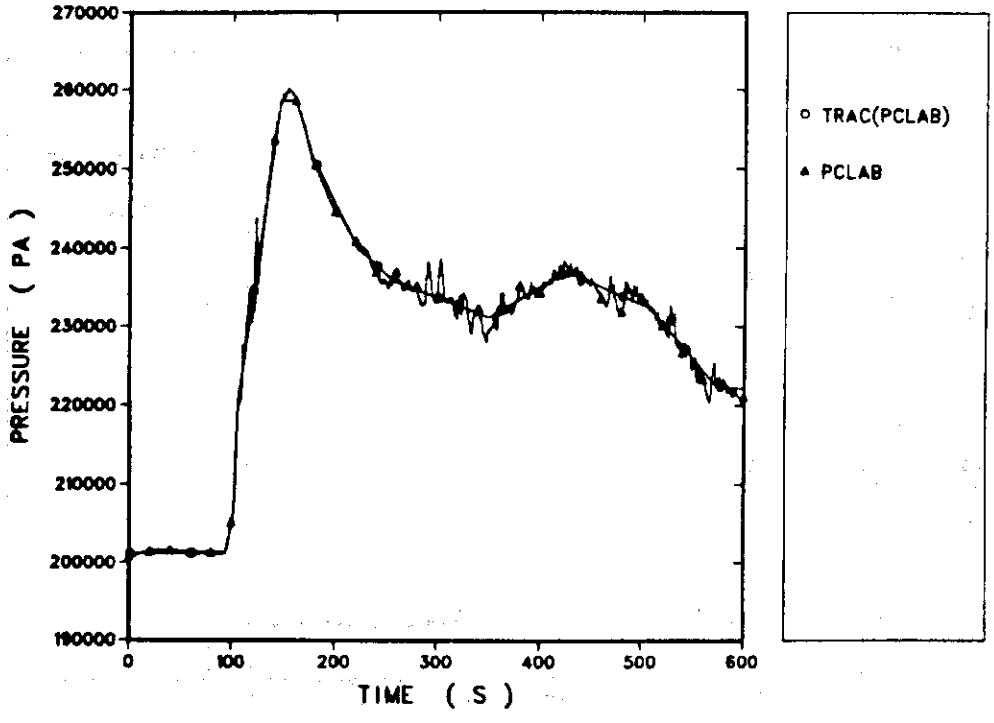

Fig. C.4 Pressure at the top of the downcomer.

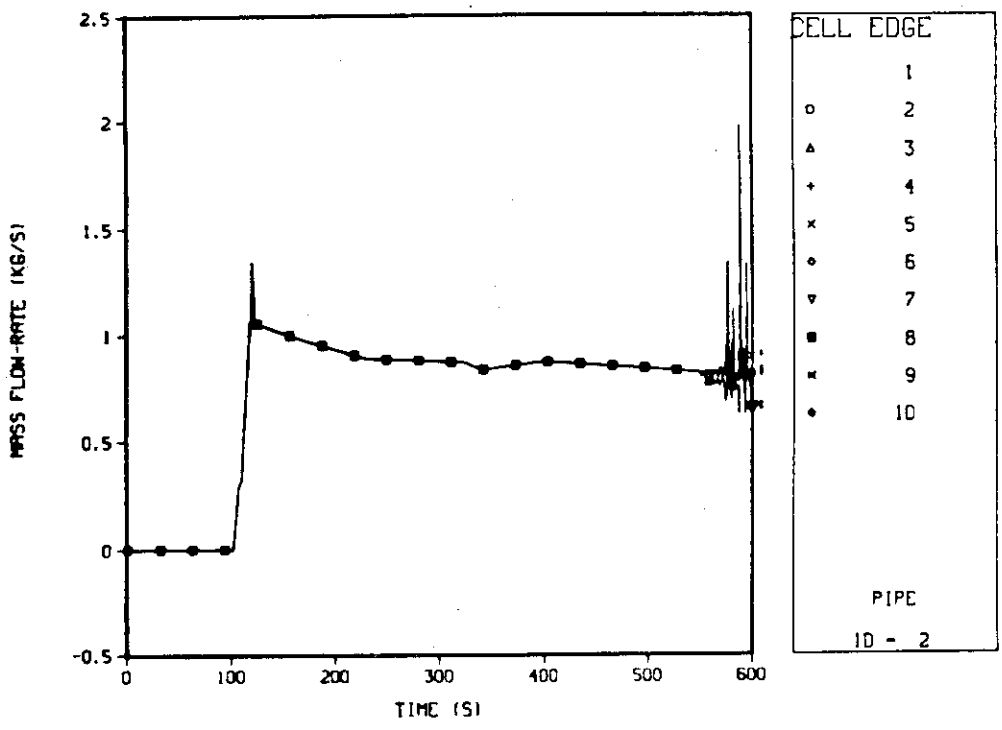

Fig. C.5 Mass flow rate along the PIPE component.

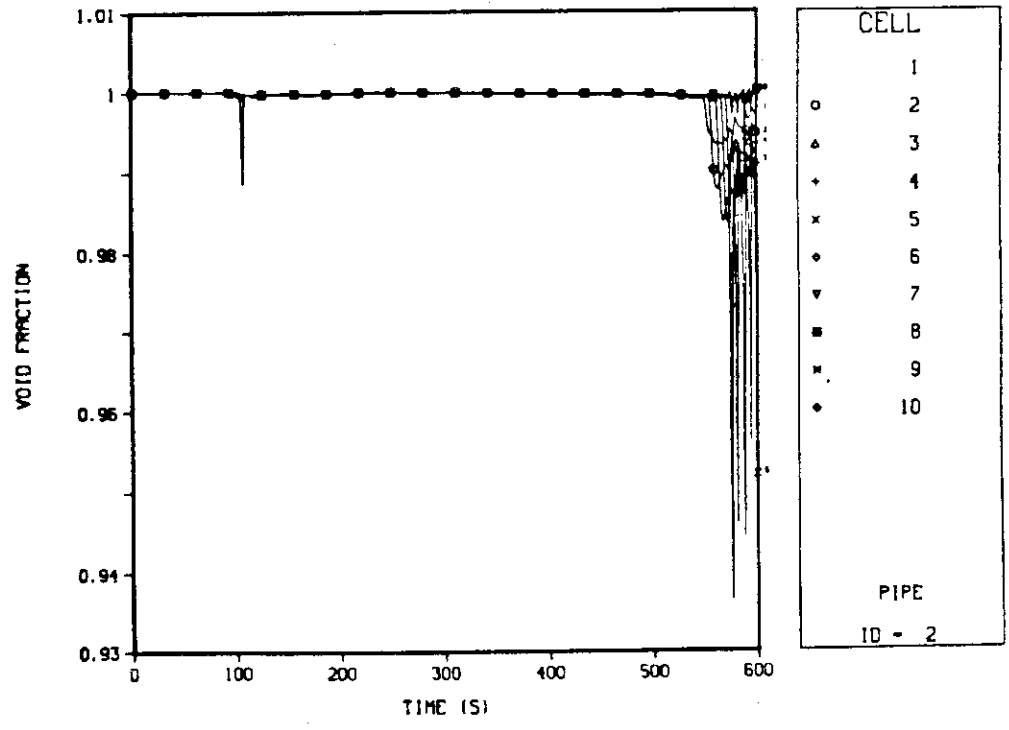

Fig. C.6 Void fraction along the PIPE component.

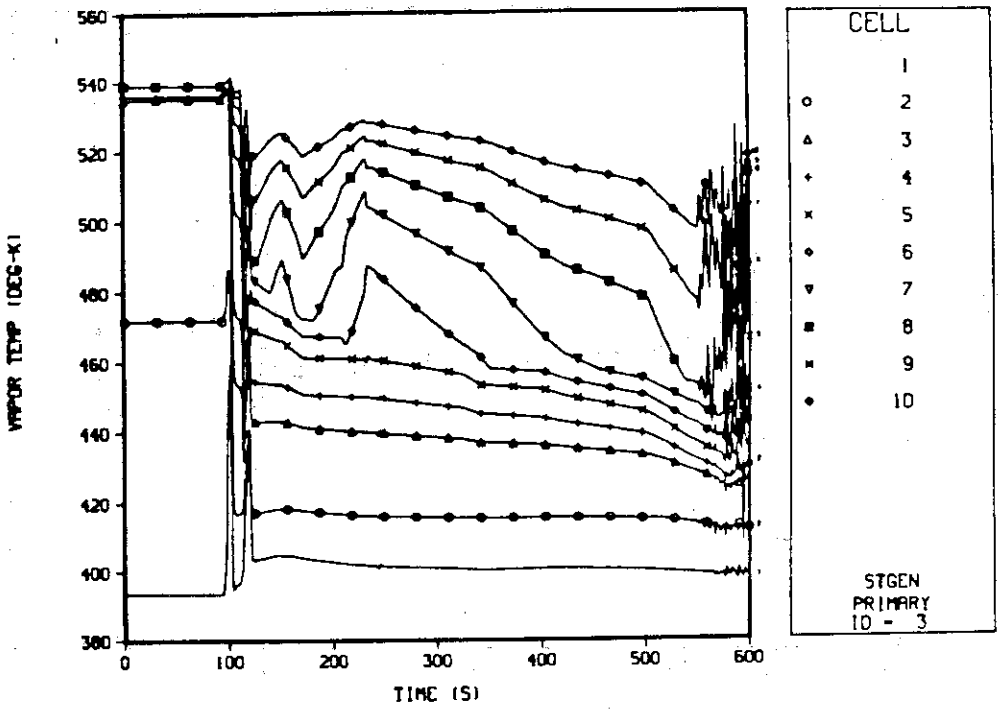

Fig. C.7 Steam temperature at cell 1 through cell 10 of the primary side of the STGEN component.

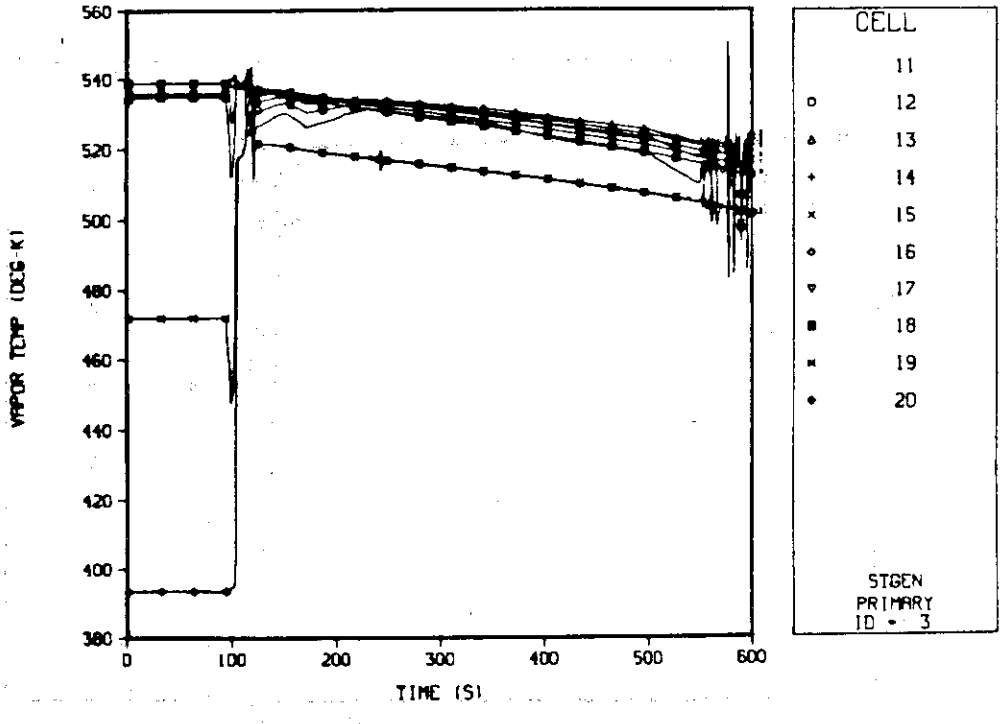

Fig. C.8 Steam temperature at cells 11 through 20 of the primary side of the STGEN component.

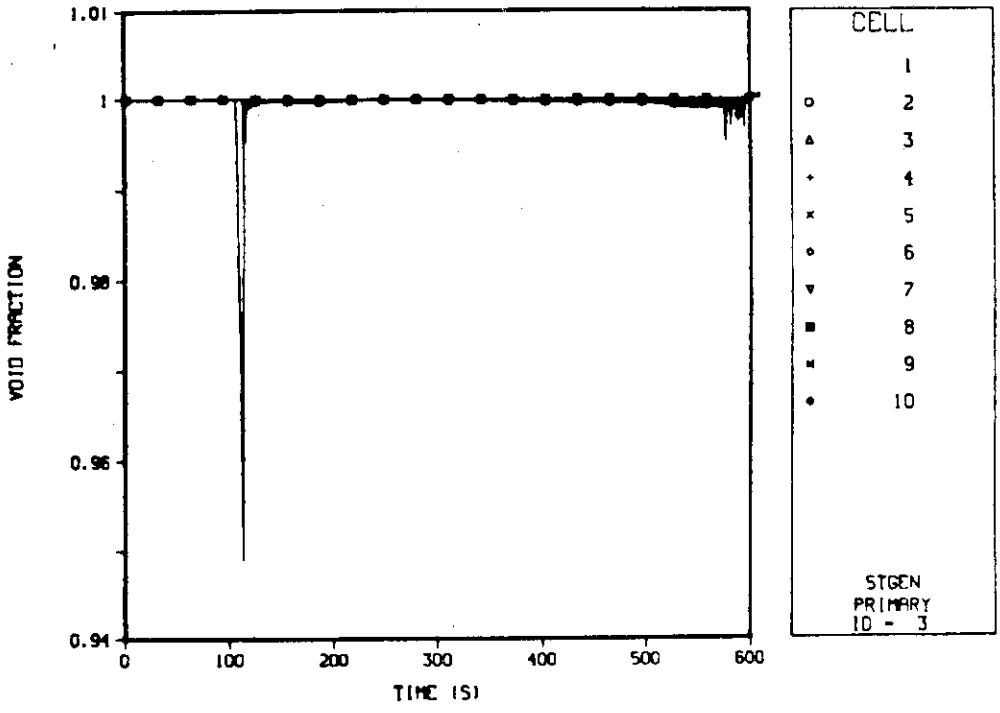

Fig. C.9 Void fraction at cells 1 through 10 of the primary side of the STGEN component.

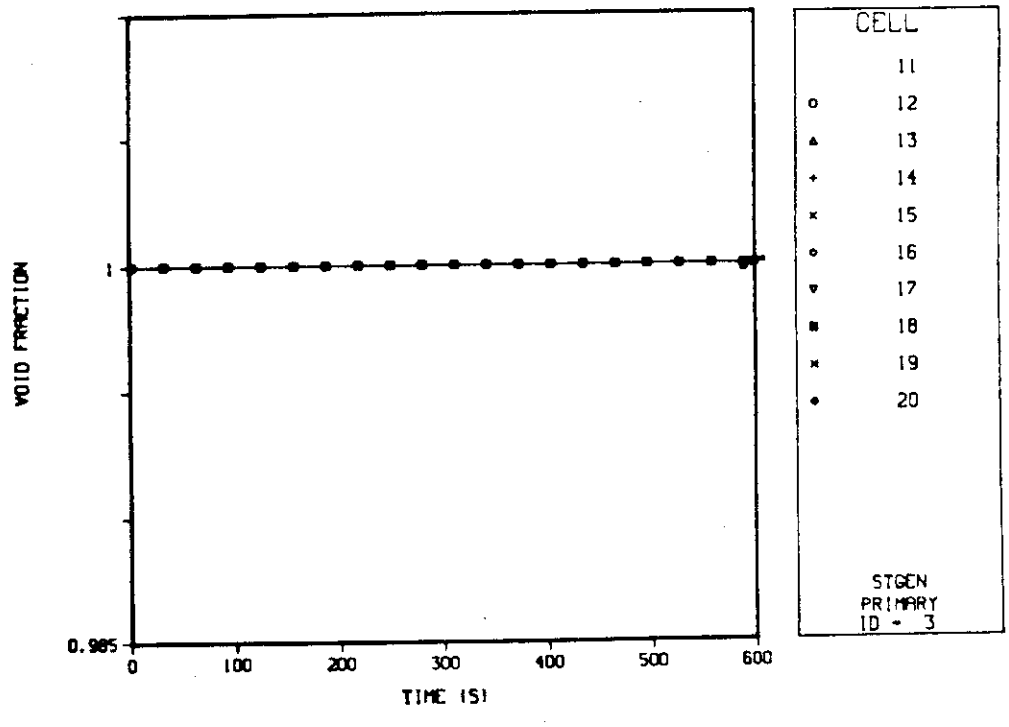

Fig. C.10 Void fraction at cells 11 through 20 of the primary side of the STGEN component.

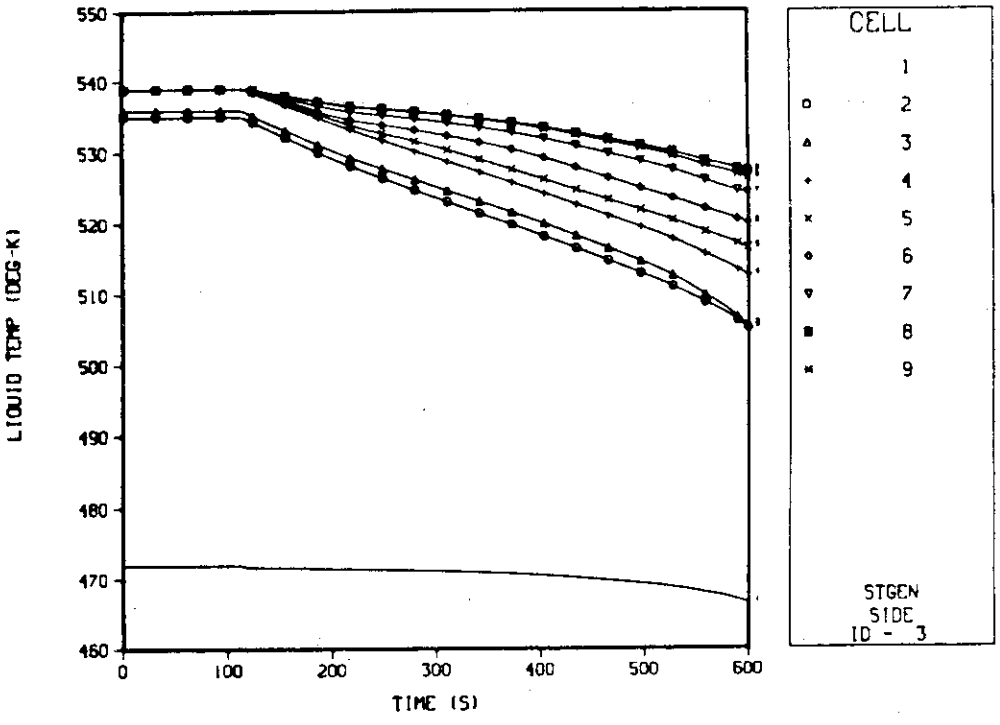

Fig. C.11 Liquid temperature in the secondary side of the STGEN component.

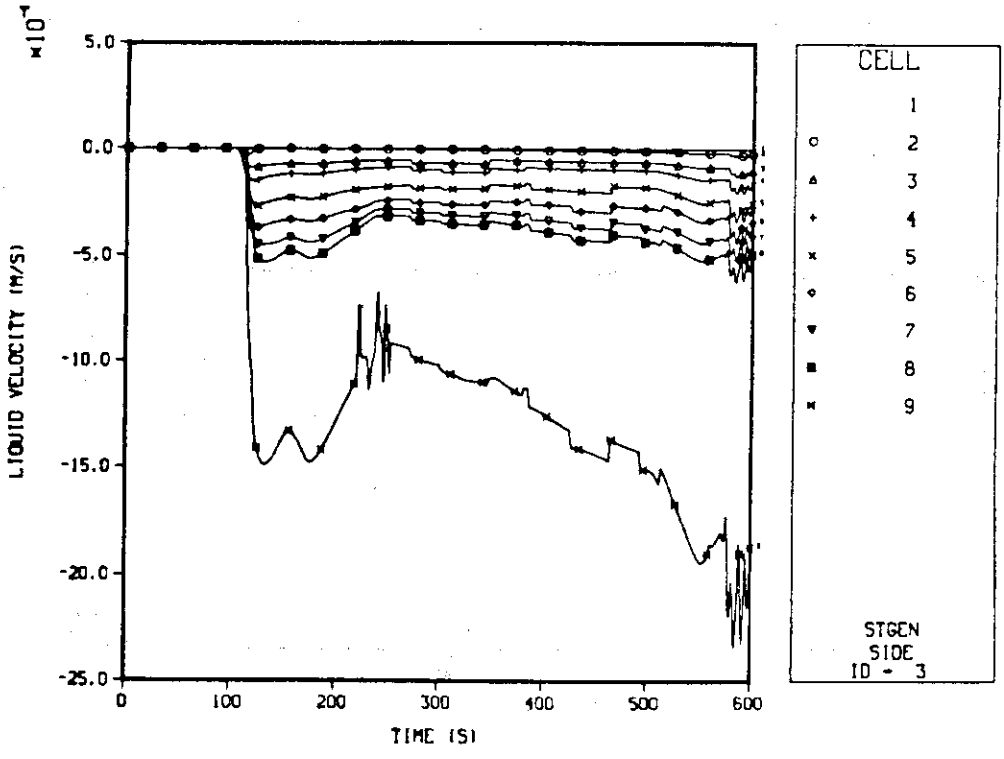

Fig. C.12 Liquid velocity in the secondary side of the STGEN component.

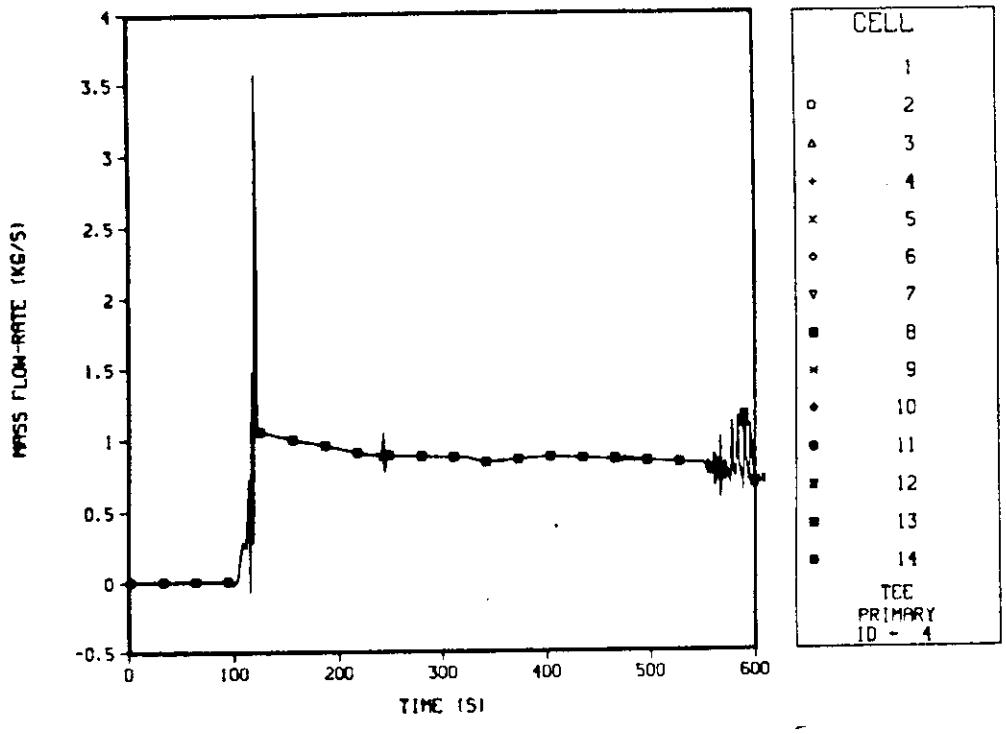

Fig. C.13 Mass flow rate along the TEE componemt at cells 1 through 14.

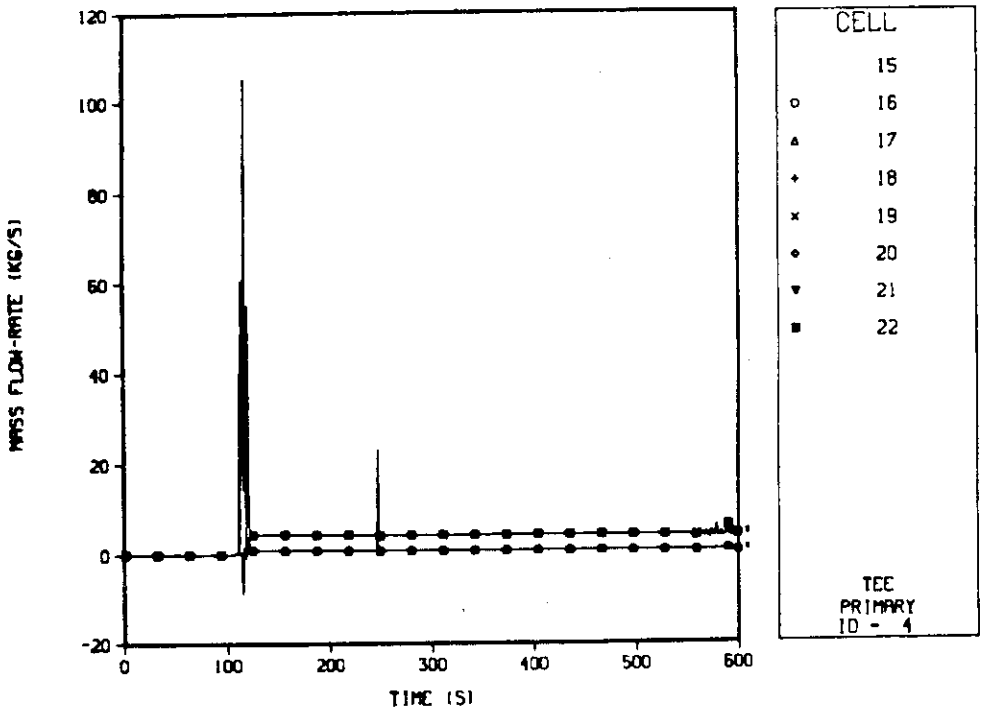

Fig. C.14 Mass flow rate along the TEE componemt at cells 15 through 22.

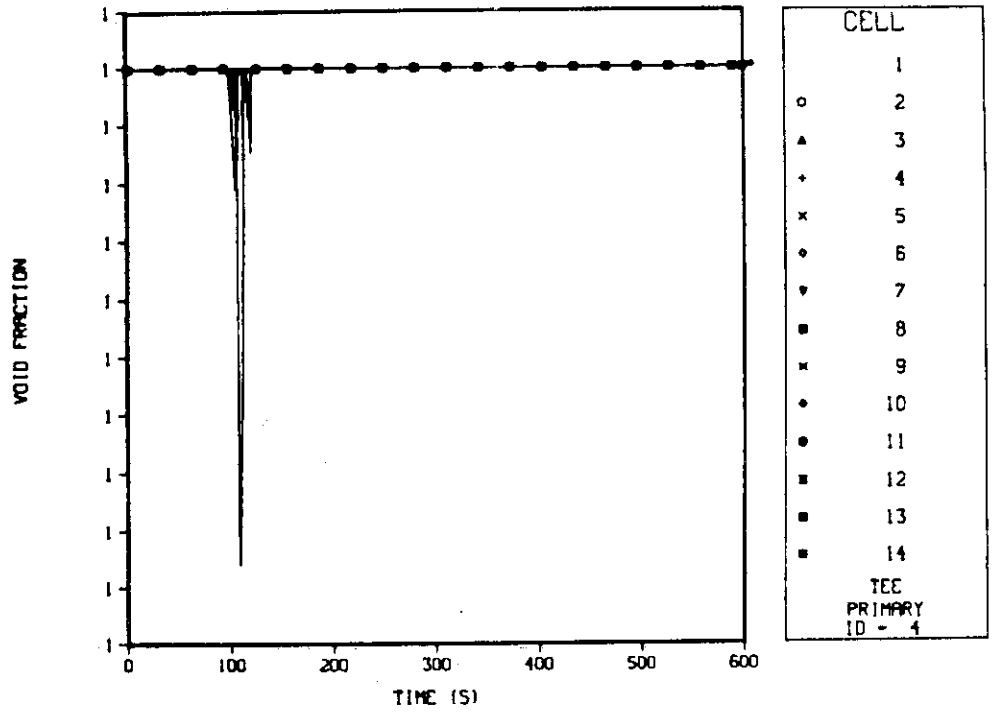

Fig. C.15 Void fraction along the TEE componemt at cells 1 through 14.

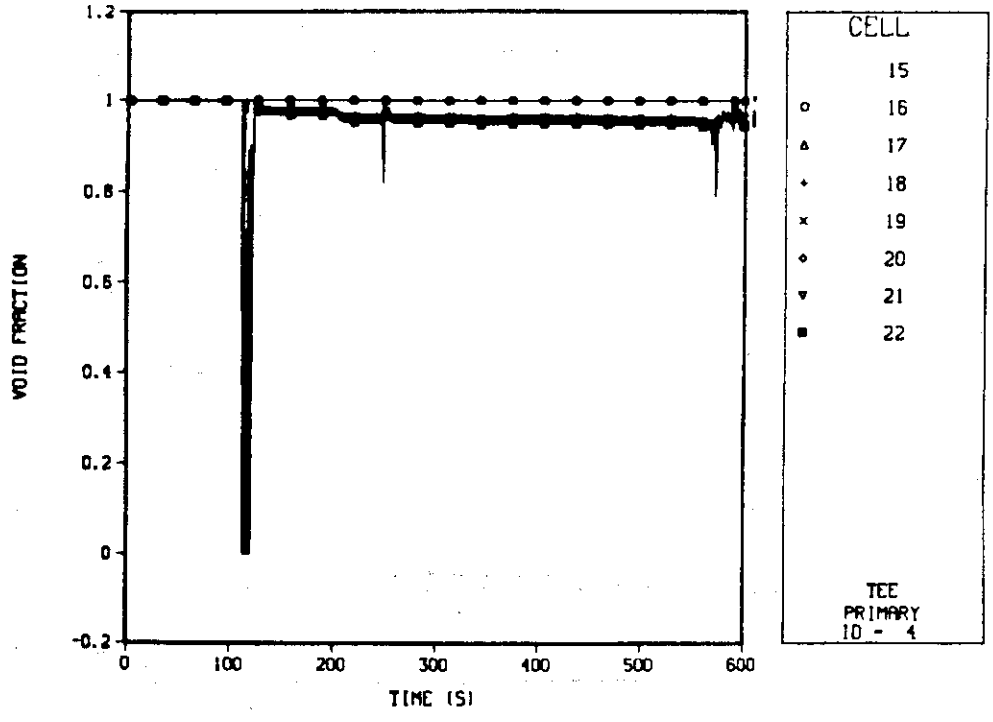

Fig. C.16 Void fraction along the TEE componemt at cells 15 through 22.

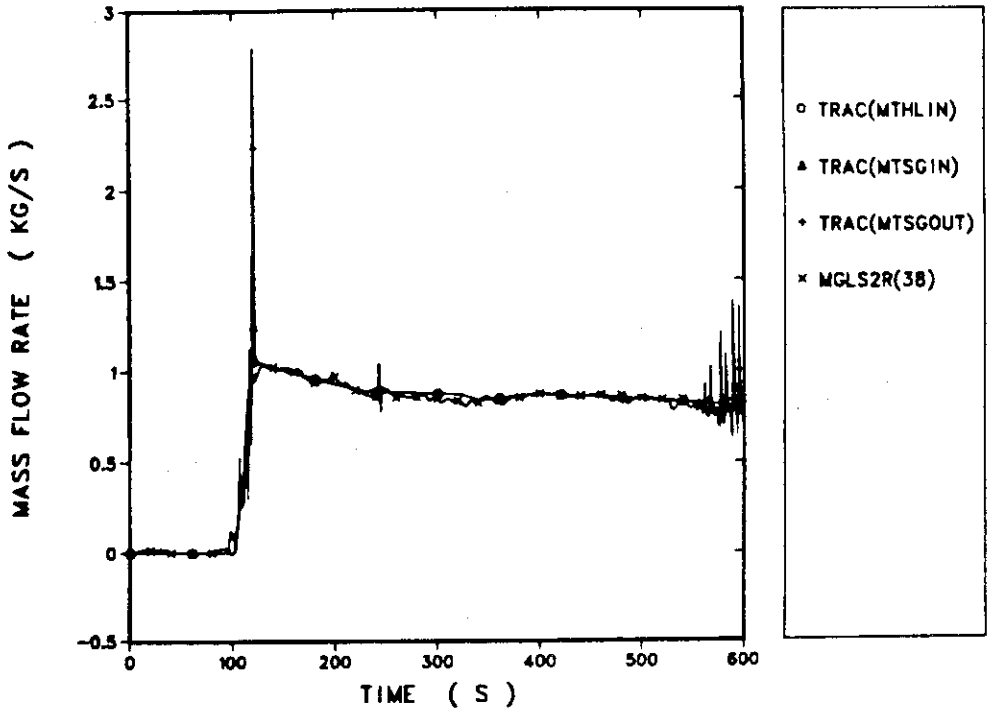

Fig. C.17 Mass flow rate through loop.

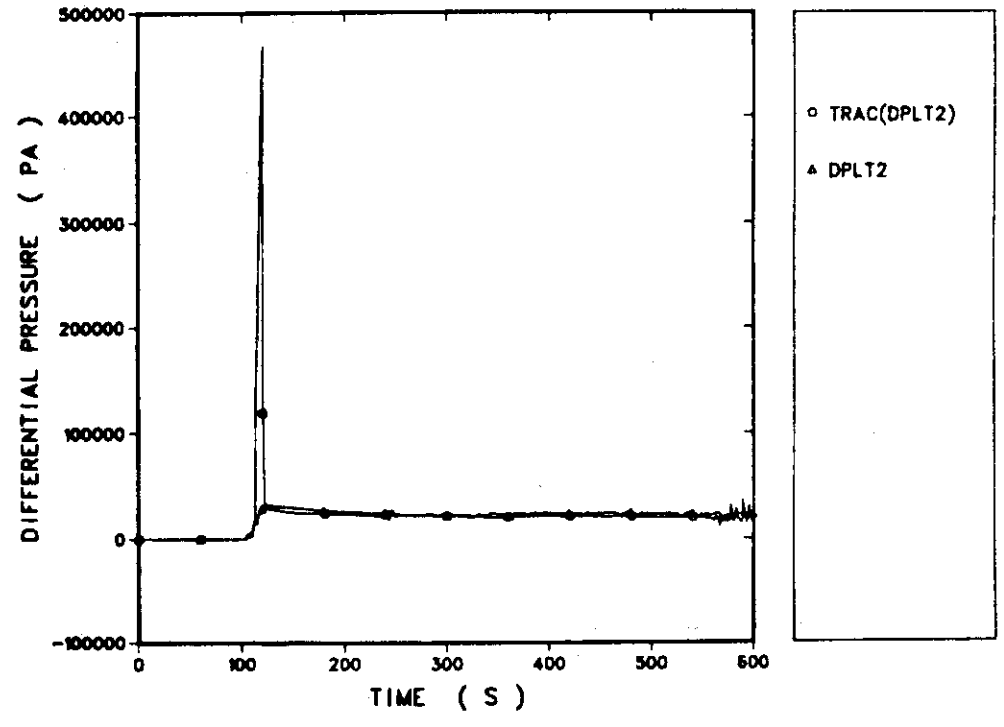

Fig. C.18 Total differential pressure through the loop.

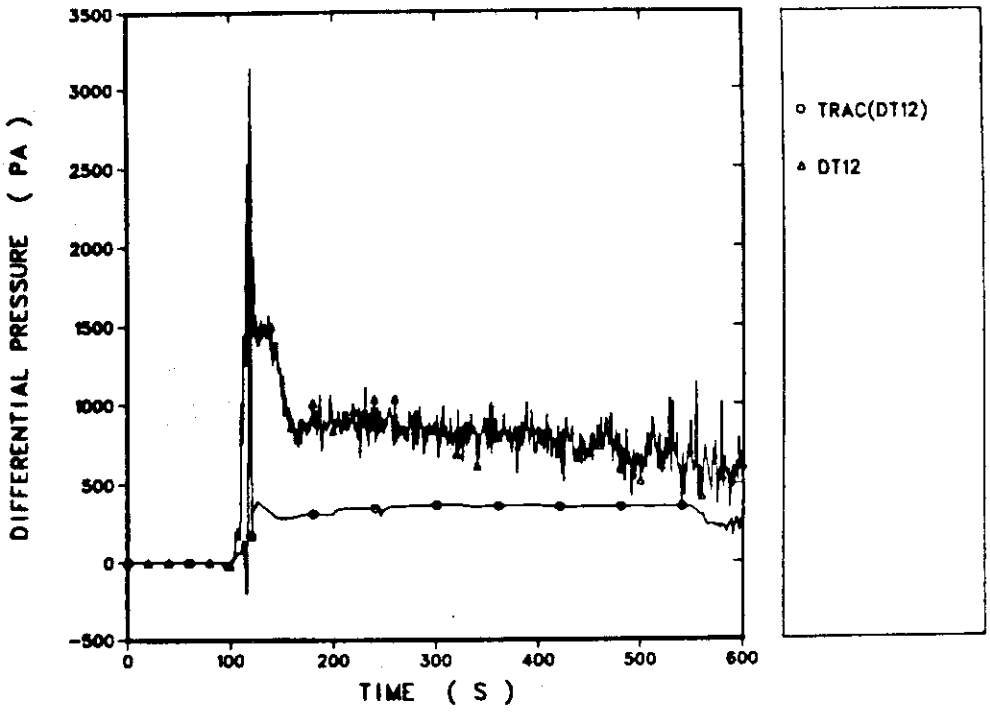

Fig. C.19 Differential pressure between cell 1 and cell 4 of the PIPE component.

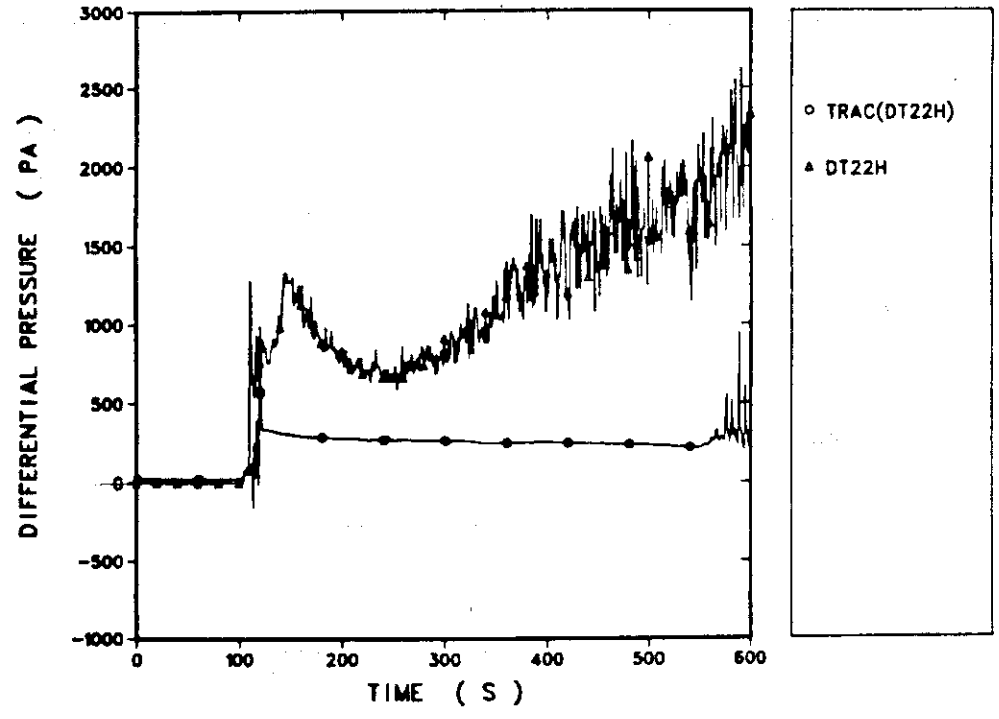

Fig. C.20 Differential pressure between cell 4 of the PIPE component and cell 1 of the STGEN component.

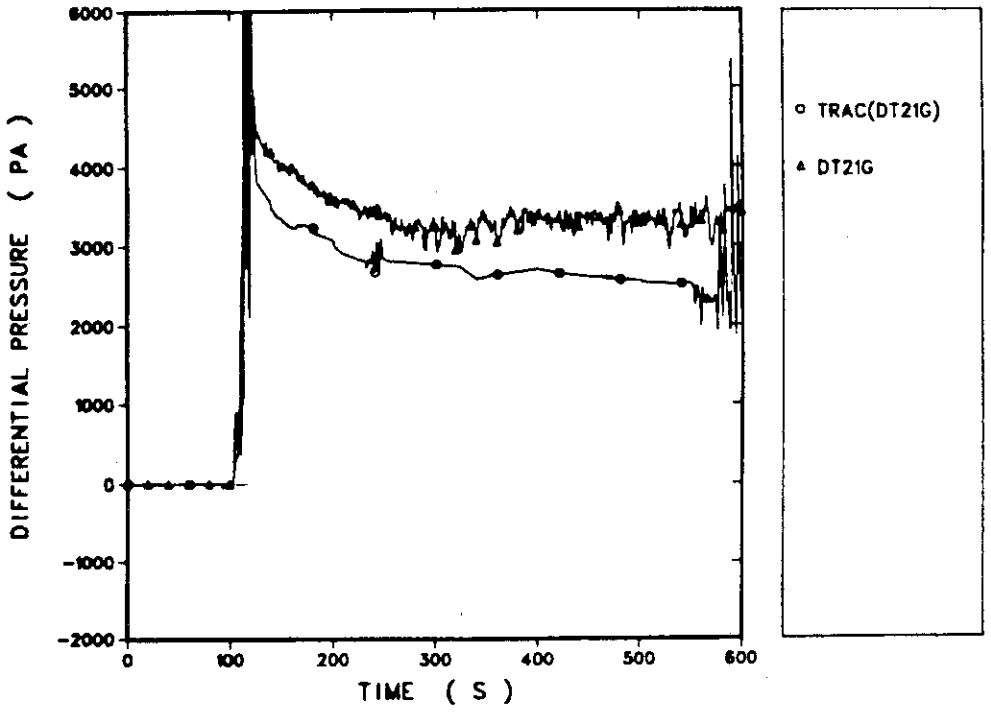

Fig. C.21 Differential pressure between cell 1 and cell 20 of the STGEN component

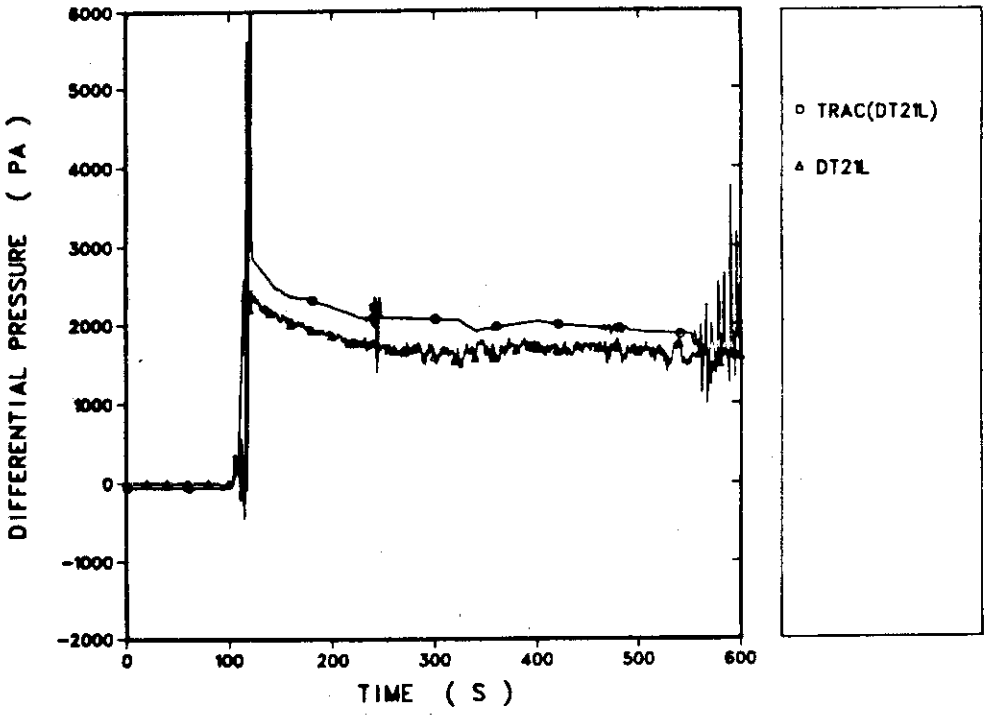

Fig. C.22 Differential pressure between cell 20 of the STGEN component and cell 7 of the TEE component.

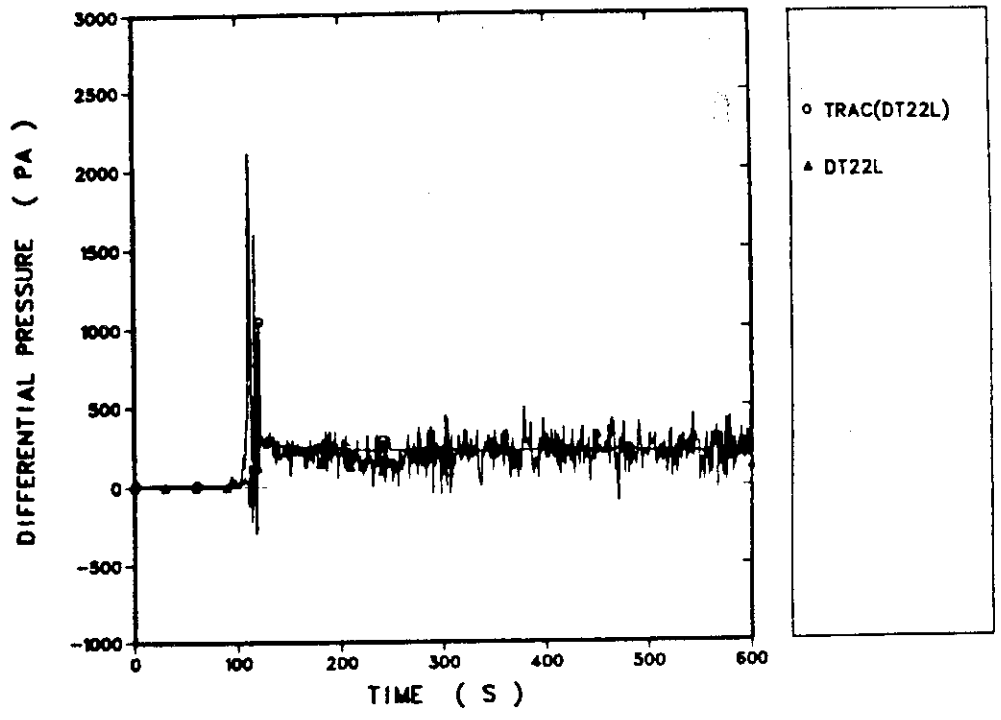

Fig. C.23 Differential pressure between cell 7 and cell 9 of the TEE componenet.

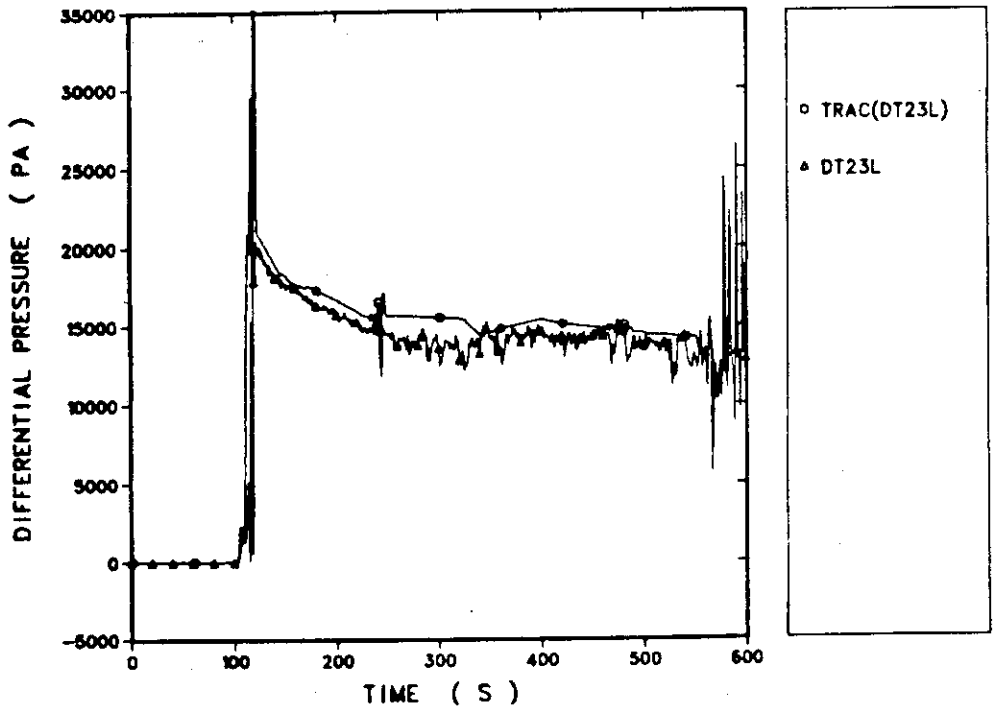

Fig. C.24 Differential pressure between cell 9 and cell 12 of the TEE componenet.

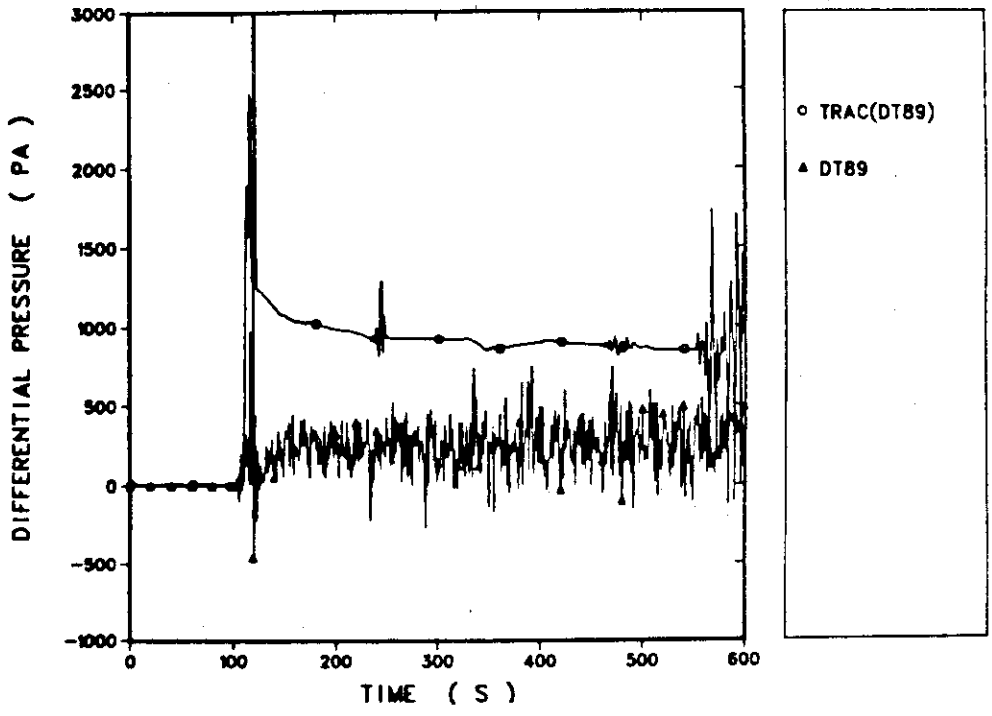

Fig. C.25 Differential pressure between cell 12 and cell 15 of the TEE componenet.

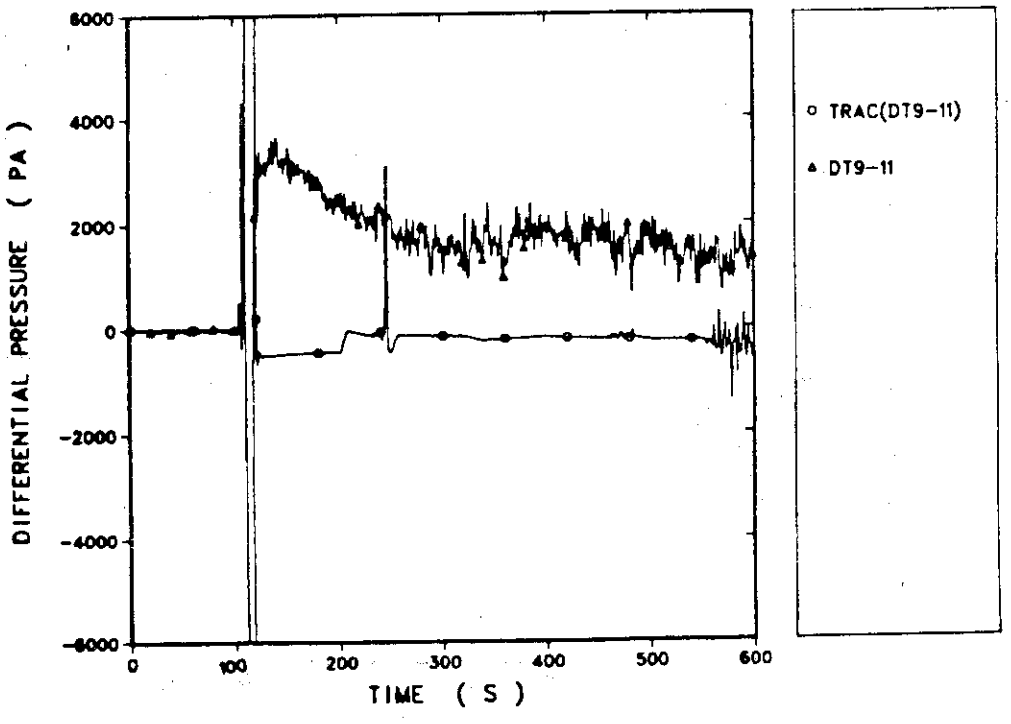

Fig. C.26 Differential pressure between cell 15 and cell 22 of the TEE componenet.

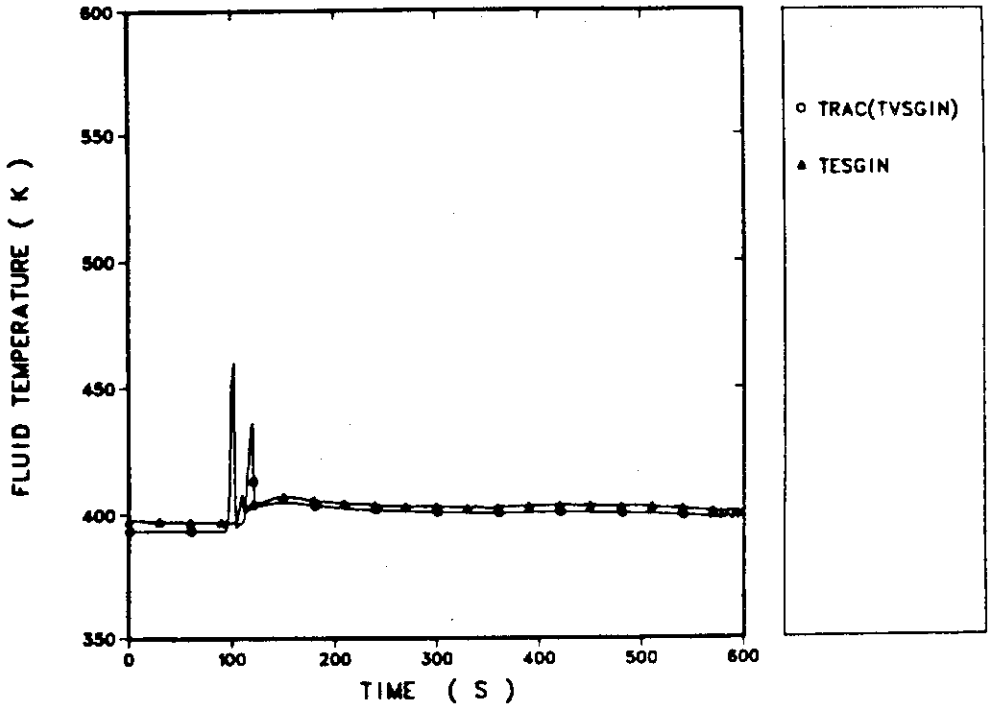

Fig. C.27 Steam temperature at the inlet plenum of the steam generator.

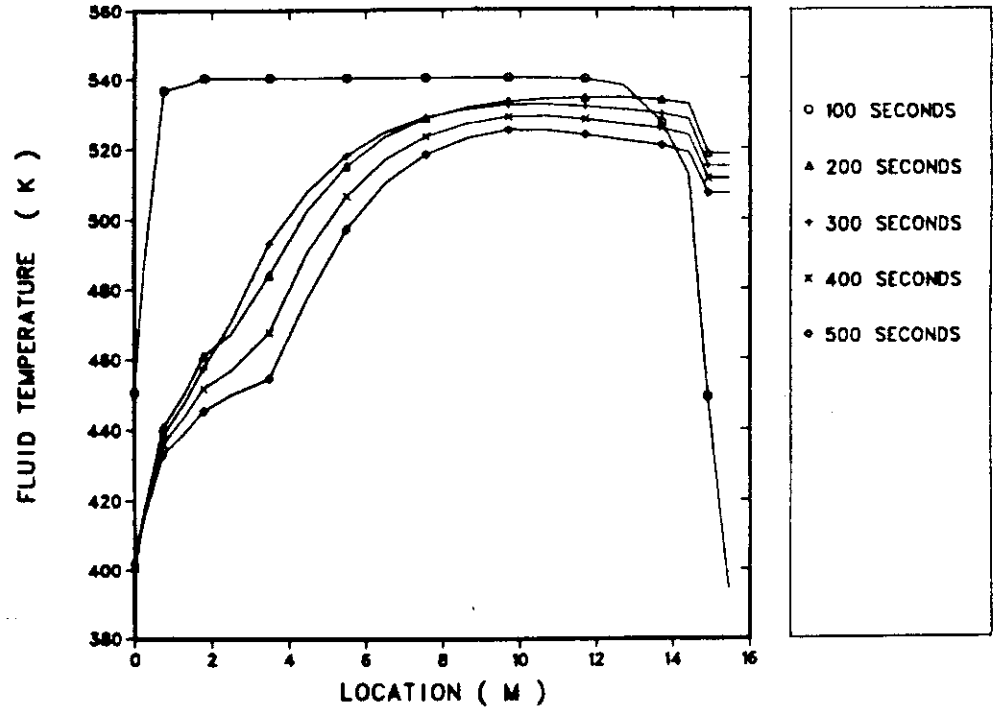

Fig. C.28 Steam temperature profile along the heat exchange pipe of the steam generator.

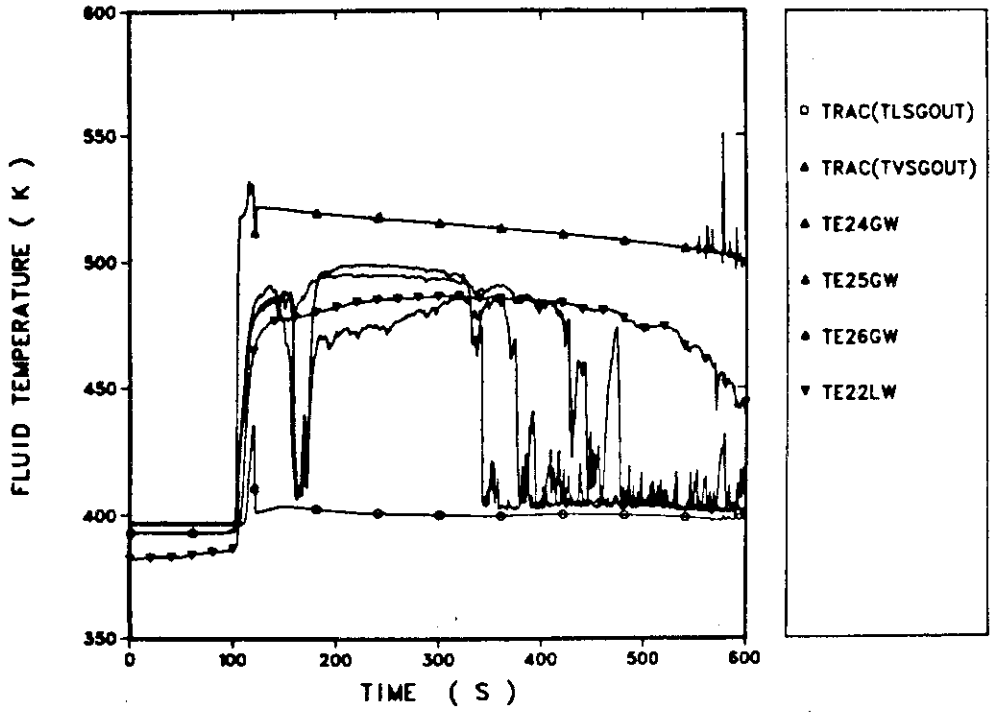

Fig. C.29 Fluid temperature at the outlet plenum of the steam generator.

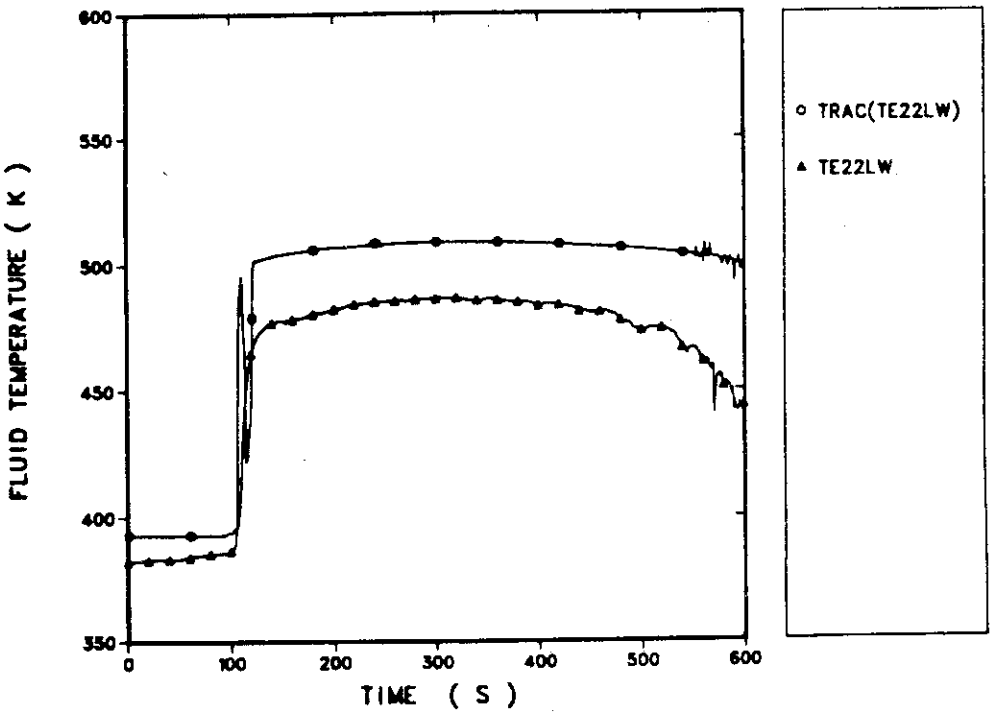

Fig. C.30 Steam temperature at the loop seal section.

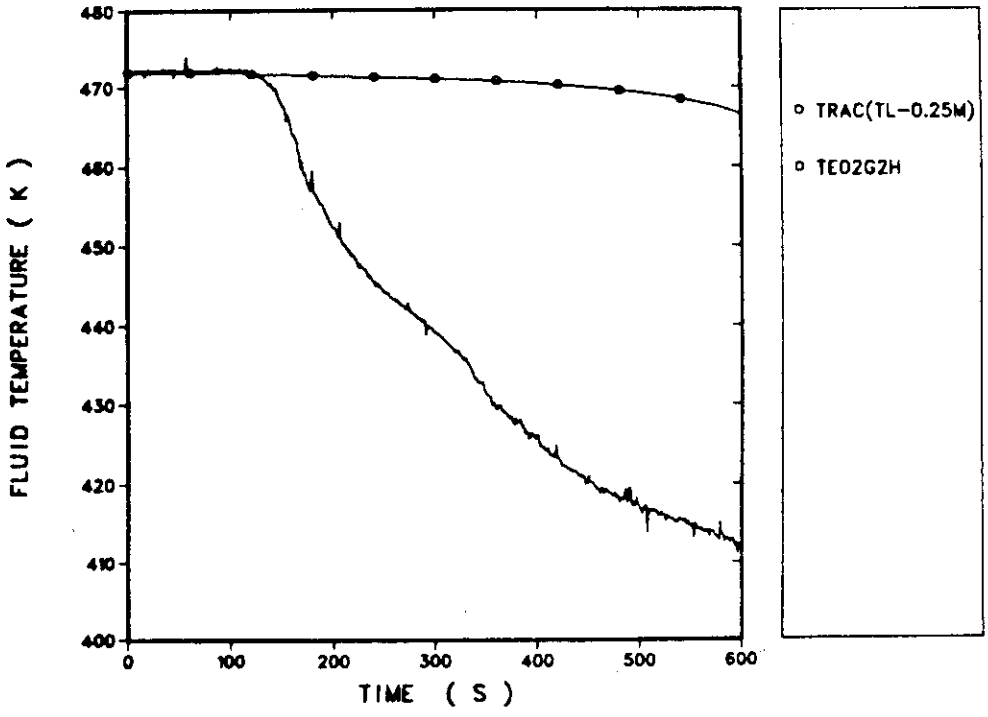

Fig. C.31 Liquid temperature in the secondary side of the steam generator (0.25 m).

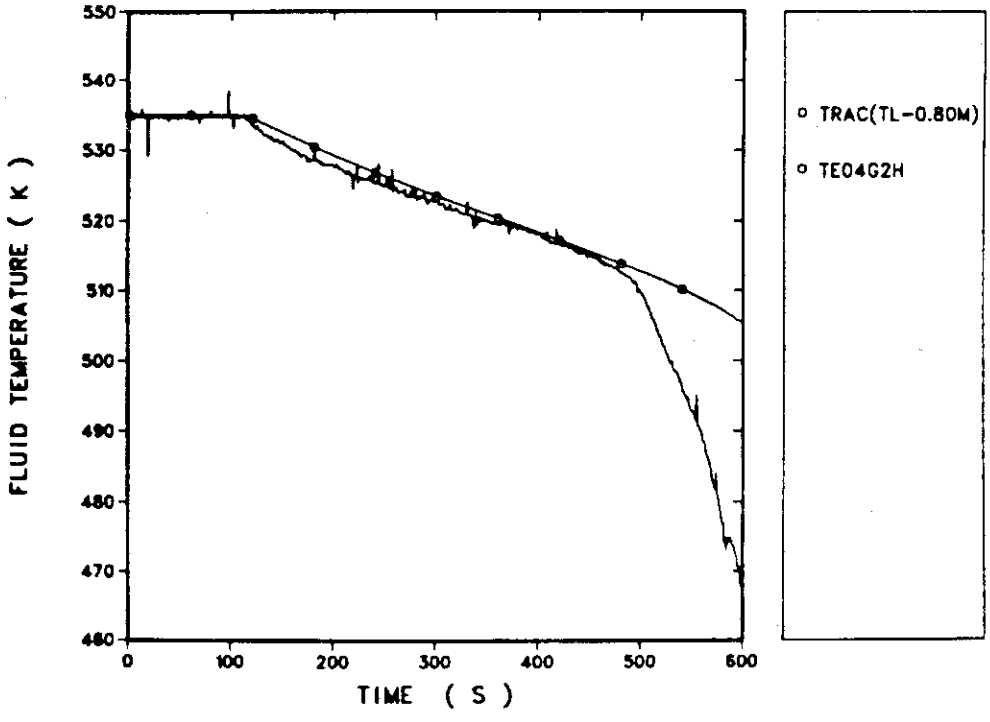

Fig. C.32 Liquid temperature in the secondary side of the steam generator (0.80 m).

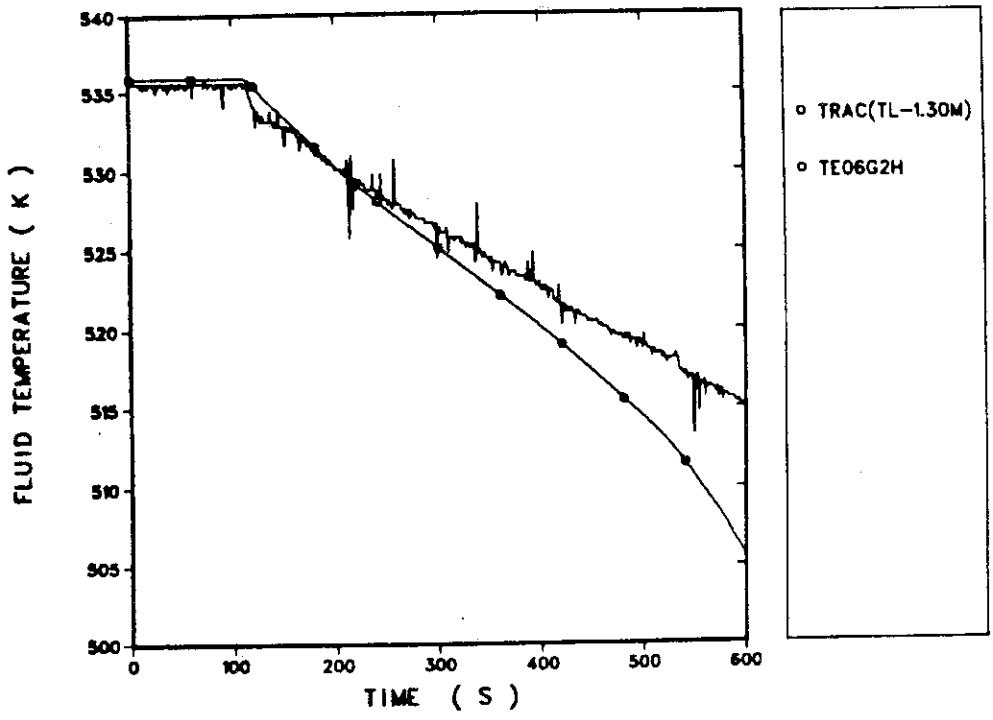

Fig. C.33 Liquid temperature in the secondary side of the steam generator (1.30 m).

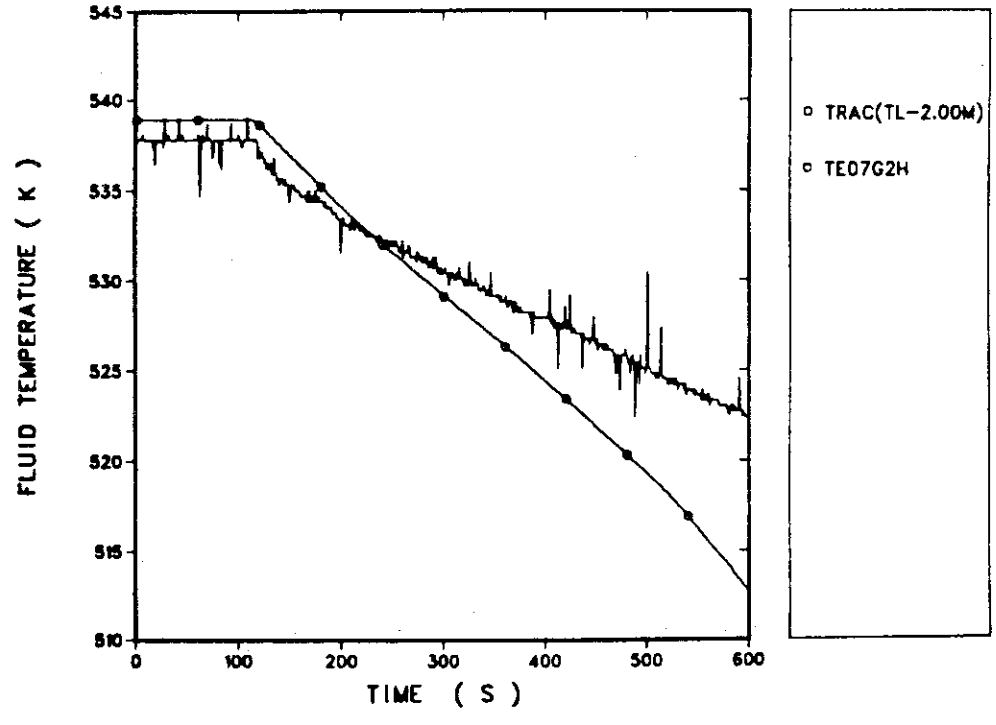

Fig. C.34 Liquid temperature in the secondary side of the steam generator (2.00 m).

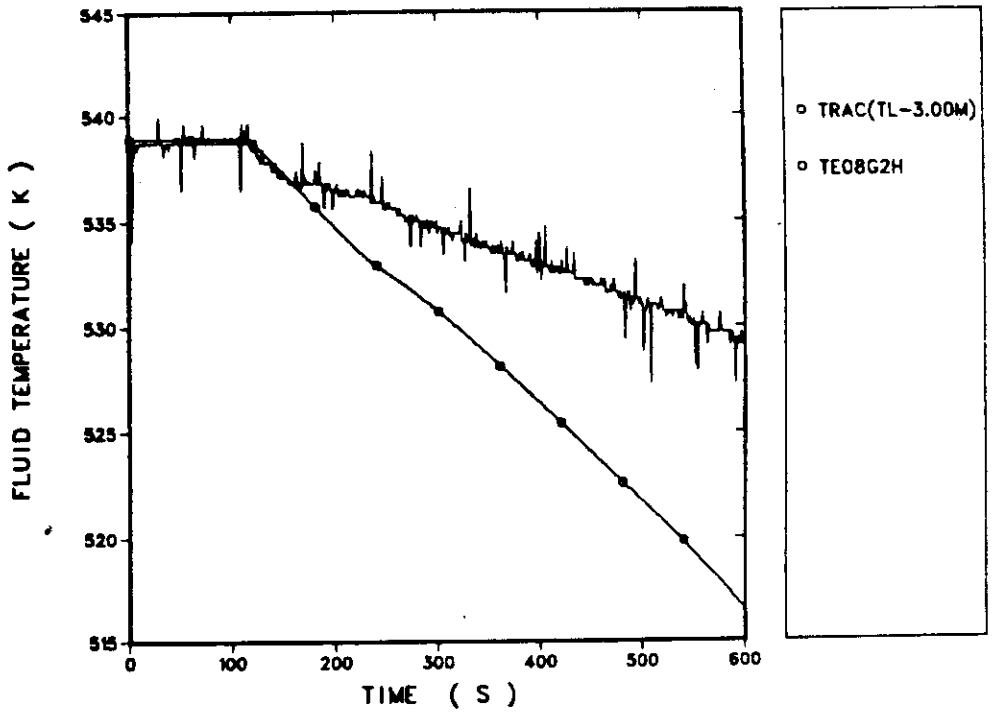

Fig. C.35 Liquid temperature in the secondary side of the steam generator (3.00 m).

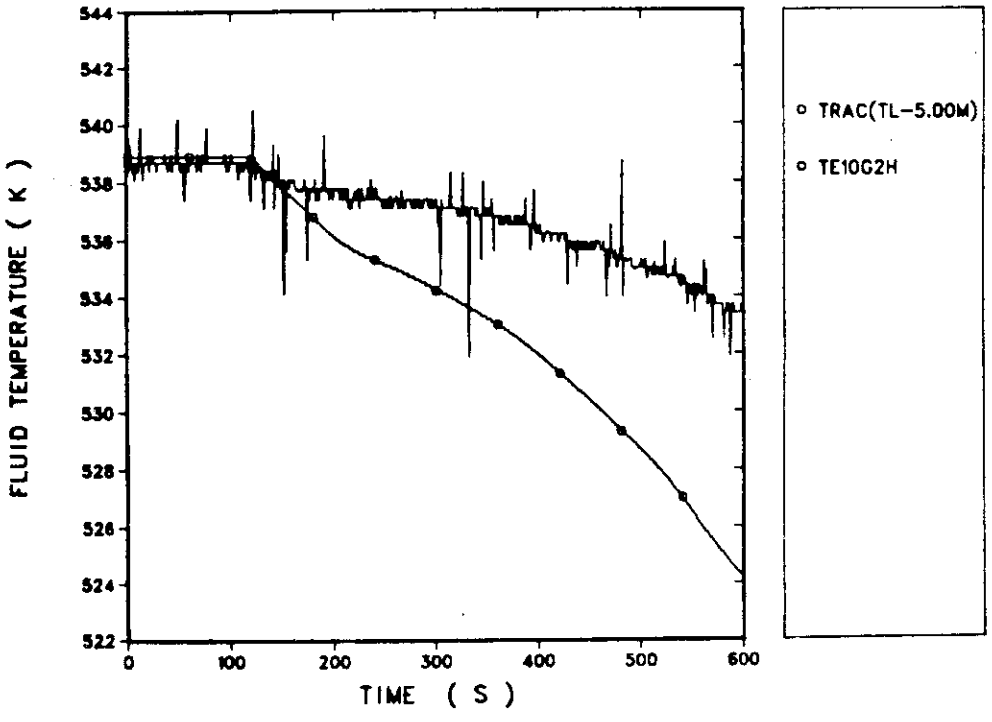

Fig. C.36 Liquid temperature in the secondary side of the steam generator (5.00 m).